Ph.D. DISSERTATION

Negative Capacitance Phenomena in Dielectric/Ferroelectric Bi-layer Structures

by

Yu Jin Kim

August 2016

DEPARTMENT OF MATERIALS SCIENCE AND ENGINEERING

COLLEGE OF ENGINEERING

SEOUL NATIONAL UNIVERSITY

Negative Capacitance Phenomena in Dielectric/Ferroelectric Bi-layer Structures

Advisor : Prof. Cheol Seong Hwang

by

Yu Jin Kim

A thesis submitted to the Graduate Faculty of Seoul National University in partial fulfillment of the requirements for the Degree of Doctor of Philosophy

Department of Materials Science and Engineering

August 2016

Approved

by

Chairman of Advisory Committee :	Hyeong Joon Kim
Vice-chairman of Advisory Committee :	Cheol Seong Hwang
Advisory Committee :	Ho Won Jang
Advisory Committee :	Sung-Min Yoon
Advisory Committee :	Seong Keun Kim

Abstract

The capacitor is an essential component in many electronic devices, which all essentially require a large charge storage density. Conventional methods implemented to increase the charge storage density usually include increasing the capacitor area, decreasing the dielectric thickness, using higher dielectric constant materials. However, this approach is no longer compatible with the miniaturization and lower operation voltage trends found in futuristic electronic devices, and, therefore, an alternative but fundamentally disparate method is necessary. The negative capacitance (NC) effect found in ferroelectrics (FE) can be an intriguing contender to solve this problem. However, the NC effect can be expected in the FE only when they are near the FE instability. Recently, it was found that the NC effect in a FE layer in dielectric (DE)/FE stacked materials can be stabilized if the polarizations of the DE and FE layers are strongly coupled to form a single domain structure along the lateral and perpendicular directions of the films. Under this circumstance, the FE layer in the DE/FE structure can show the NC, and several studies demonstrated that the NC effect can be observed in the hetero-epitaxial DE/FE bi-layer system. Up to now, the NC effect from the DE/FE bi-layer structure has been explained based on the linear combination of the free energies with respect to polarization of DE and FE

layers, which were described by the phenomenological expression of Landau-Khalatnikov (LK). However, there were conceptual difficulties in using the displacement equation within the bi-layer structure.

In this work, therefore, the authors suggest an alternative approach to the possible NC mechanism in general DE/FE bi-layer structures adopting the depolarization theory. In this model, the Landau-Devonshire (LD) theory is extended to encompass the case where the high depolarization field is present due to an imperfect polarization compensation by the interposed thin DE layer between the FE and the metal electrode. When an external bias voltage is applied to the DE/FE system to polarize the FE layer, the FE bound charge of the FE layer at the interface between the FE layer and metal electrode can be fluently compensated by free carriers in the metal electrode. However, the FE bound charge at the DE/FE interface cannot be fully compensated by the presence of the DE layer between the FE layer and the opposite metal electrode. This induces depolarization field across the FE layer, and the direction of overall field across the FE layer is opposite to the applied field direction. In order to make the total applied voltage over the DE/FE layer equal to the external voltage, a voltage which is even higher than the applied voltage must be applied to the DE layer. This corresponds to the NC phenomena, leading to the capacitance boosting effect.

This work also discusses the conditions that have hindered the operation of the NC phenomena in general DE/FE systems. The charge injection across the thin DE layer during voltage sweep can largely mitigate the depolarization effect, leading to decrease in the voltage and capacitance boosting. Under this circumstance, the spontaneous polarization of the FE layer can be irreversibly switched as it is the case for a single layer FE, which may correspond to the frustration of the NC phenomena in the DE/FE layer.

Next, the polarization-voltage (P-V) characteristic of Al_2O_3/$Pb(Zr,Ti)O_3$ (AO/PZT) structure was examined by comparing the NC model. The specific thicknesses of the amorphous AO films were varied from 2 nm to 10 nm, where the thicknesses of PZT layer were fixed as 150 nm. The thermodynamic calculation showed that the transition from the ferroelectric-like state to the paraelectric-like state with increasing AO thickness occurs at ~3 nm thickness. This paraelectric-like state should have exhibited a NC behavior without permanent polarization switching if no other adverse effects are involved. However, experiments showed typical ferroelectric-like hysteresis loops without the NC effects, which could be explained by the carrier injection through the thin AO layer and trapping of the carriers at the AO/PZT interface.

Finally, therefore, short pulse measurements were adopted not to allow sufficient time for the charge injection for the direct proof of the NC effects in DE/FE structure. From these experiment set-up, it was demonstrated that capacitance (charge) boosting effects can be observed in the Al_2O_3/$BaTiO_3$(AO/BTO) bi-layer capacitors as expected from the theoretical model. This results also revealed that the hysteresis phenomenon in NC devices originated from the dielectric leakage of the dielectric layer. The suppression of charge injection via the dielectric leakage, which usually takes time, inhibits complete ferroelectric polarization switching during a short pulse time. It was also demonstrated that a non-hysteretic NC effect can be achieved only within certain limited time and voltage ranges. Although the static operation is severely hindered, the NC effect in a general DE/FE system is still favorable for modern electronic devices which have an extremely high operation speed.

Table of Contents

List of Tables

List of Figures

List of Abbreviations

FE	Ferroelectric
DE	Dielectric
PE	Paraelectric
NC	Negative Capacitance
P-V	Polarization-Voltage
C-V	Capacitance-Voltage
ALD	Atomic Layer Deposition
PLD	Pulsed Laser Deposition
MOSFET	Metal-Oxide-Semiconductor Field-Effect-Transistor
NCFET	Negative Capacitance Field-Effect-Transistor
FeFET	Ferroelectric gate Field-Effect-Transistor
SS	Subthreshold-Slope
LK	Landau-Khalatnikov
LD	Landau-Devonshire
T_c	Curie Temperature
TEM	Transmission Electron Microscope
XRD	X-Ray Diffraction
XRR	X-Ray Reflectivity
AFM	Atomic Force Microscopy
PZT	$Pb(Zr,Ti)O_3$, lead zirconate titanate
BTO	$BaTiO_3$, barium titanate
STO	$SrTiO_3$, strontium titanate
AO	Al_2O_3, alumina

1. Introduction

1.1. Overview and Issues on Negative capacitance

Voltage scaling in metal-oxide-semiconductor field-effect-transistor (MOSFET) is a most pressing issue at the integrated circuits application for low power consumption devices. However, the scalability of operation voltage in MOSFET is basically limited to the threshold voltage which corresponds the minimum gate voltage required to turn the transistor "ON". The intermediate region a bit below the ON state is called sub-threshold regions, and narrowing this region has been a strategy to reduce the operation voltage of MOSFET. Meanwhile, in the perspective of device physics, a term of subthreshold-slope (SS) were introduced for describing the transfer characteristic of the subthreshold region. And, the SS is defined as the change in Vg which is required for a tenfold increase in the drain current. At this point, the SS directly determine the width of subthreshold region, hence lower SS has been a prerequisite condition for low power MOSFET. However, the SS of MOSFET has its thermal lower limit which corresponds the Boltzmann limit, i.e. 60mV/dec at room temperature. Hence, the ultimate scaling of operation voltage is theoretically restricted in a traditional MOSFET structure. In order to overcome this Boltzmann limit, recent studies have focused on the

renovation of materials, structure and operation mechanism extended from the traditional MOSFET devices, such as negative capacitance FET (NCFET).[1] The NCFET, which structure is similar to the ferroelectric gate FET (Figure1.1) reported firstly in 1974,[2] has drawn a great attention over the last decade, especially due to the unveiled negative capacitance (NC) effects of ferroelectric (FE) materials and its potential applications to electronic devices.

Earlier research found the possibility that FE materials can have NC state according to their negative polarization-electric field (P-E) relation as shown in Figure 1.2. The S-shape P-E relations of FE materials are originated from the phenomenological free energy equation based on Landau-Devonshire (LD) theory. The free energy equation (U-P) of FE materials with uniform polarization and electric field is

$$U_s = \alpha P_s^2 + \beta P_s^4 + \gamma P_s^6 - E P_s \qquad (1.1)$$

,where, α,β and γ are Landau coefficient, P_S is spontaneous polarization and E is electric field. And the $\alpha<0$ and β, $\gamma>0$ below the Curie temperature (T_c) in condition for FE materials with second order transition. Figure 1.2 shows the free energy curve of FE under E=0, and double minima of energy curve describe the bi-stable P_S state. The roots of the first derivative of equation (1.1) with respect to polarization represents the steady state of FE system. Therefore, the P-E relation can be written as follows,

$$\frac{dU_s}{dP} = 2\alpha P_s + 4\beta P_s^3 + 6\gamma P_s^5 - E = 0 \qquad (1.2)$$

The black dot line in Figure 1.3 represents the NC state of FE materials.[3] As shown in Figure 1.3, the NC states locate at the local maxima point in the U-P diagram. Hence, the realization of NC state from single layer FE is hampered in general conditions. However, the stabilization of this NC state can be stabilized by stacking a dielectric (DE) layer when the total internal energy of the DE/FE bi-layer is minimized near the local maxima region. This could occur through the electrostatic coupling between the DE and FE layer, where the polarization of each layer has an identical value. Under this condition, an overall capacitance of bi-layer capacitor can be higher than that of single DE layer. The significant underlying properties of the NC effects, beside of capacitance enhancement, is voltage amplification effects which means that an internal voltage across the DE layer can be larger than the external voltage applied to the DE/FE bi-layer. In case of NCFET structure, the surface potential of Si channel can be amplified due to the NC operations of FE layer. In fact, there has been a large progress in NCFET with sub 60mV/dec in SS, [4,5] but reduction of actual voltage scaling limit is far behind due to the memory effects arose from the "hysteresis" in FE materials. For example, it has been reported that the SS value of ~18mV/dec in a commercial MOSFET device with an externally connected large FE capacitor as a gate stack, but the hysteresis voltage in transfer curve was extremely high as 3~4V. Considering that required gate voltage for an on/off ratio of 10^8 in

3

the ideal MOSFET structure (SS=60mV/dec) is approximately 480mV, it is obvious that this hysteric NCFET cannot have a beneficial effect on the transistor operation. As a matter of fact, there are several reports on non-hysterical NC effects in FE materials where a dielectric (DE) layer was directly stacked over the FE layer, but these can be realized under only limited structural conditions such as an epitaxial or superlattice structure composed of peroveskite materials.[6,7]
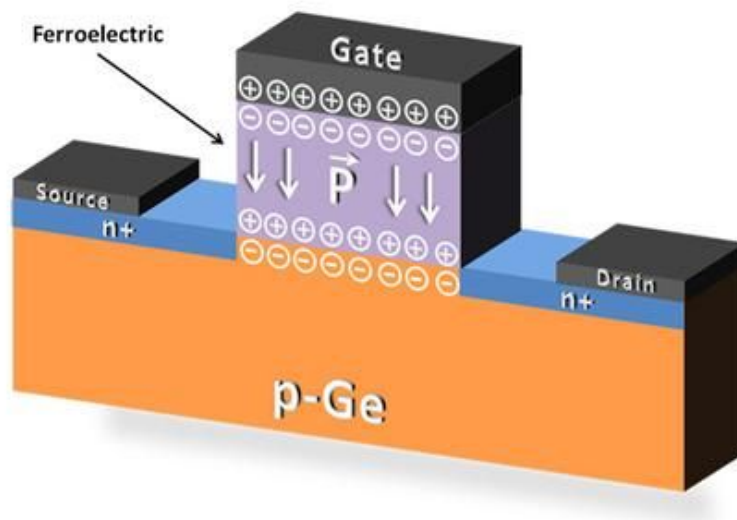
Figure 1.1 Schematic diagram of FeFET cell.[8]
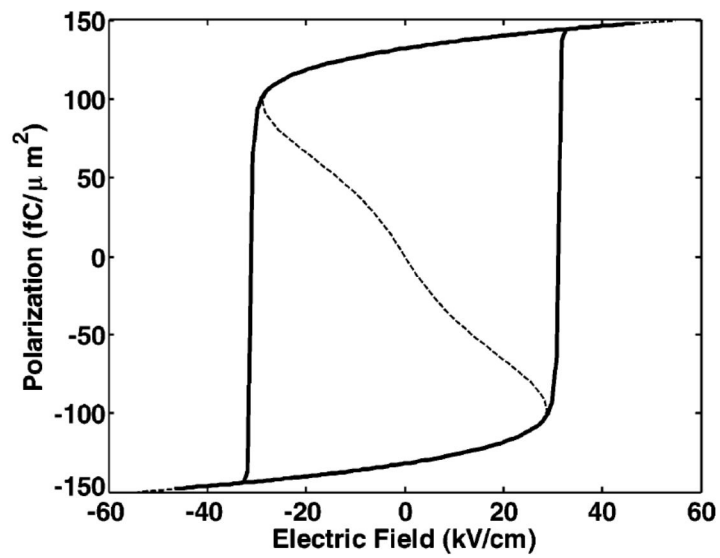
Figure 1.2 Polarization vs electric field for a typical ferroelectric

Material.[1]
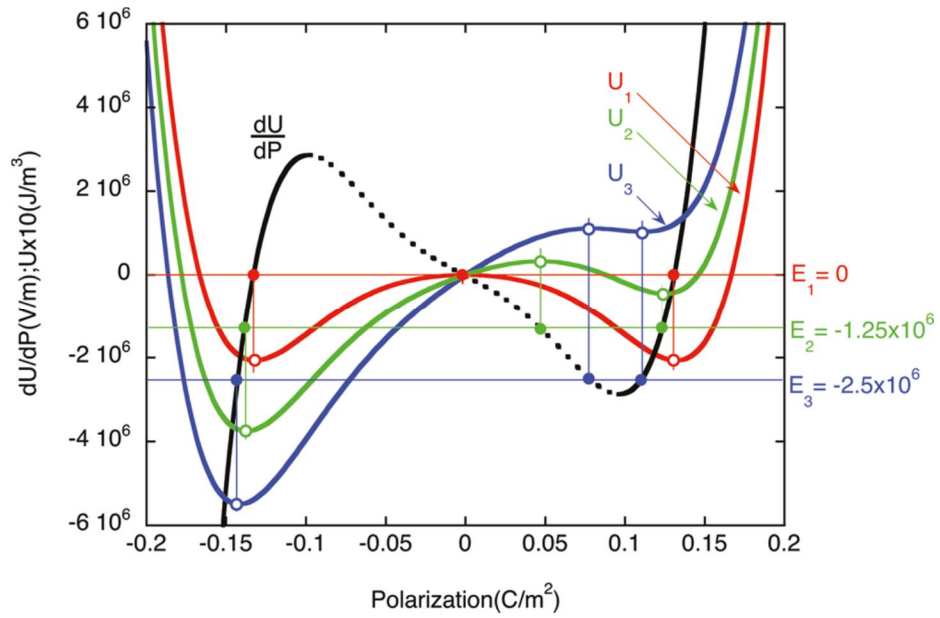
Figure 1.3 Calculated free energy curve for barium titanate as a function of polarization. dU/dP is also plotted, and the correlation between polarization values of the intersection points of dU/dP with the corresponding values of E and maxima and minima of free energy are noted.[3]

1.2. Objective and Chapter Overview

The objective of this dissertation is to study on the NC phenomena in DE/FE bi-layer structures through both theoretical and experimental approaches.

Chapter 3 present the theoretical study of NC phenomena in DE/FE bi-layer structure. Firstly, the previous theoretical NC model is criticized for a self-contradictive problem related with the voltage amplification effects of NC phenomena. And, an alternative theoretical model on NC effects is suggested based on the depolarization theory in FE thin films. The alternative model takes into account the charging effect at DE/FE interface, and elucidate that involvement of interfacial charging obscure the emergence of NC effect from DE/FE bi-layer during the voltage application.

Chapter 4 covers the investigation of the NC effects in Al_2O_3 (AO) /$Pb(Zr_{0.4},Ti_{0.6})O_3$ (PZT) capacitors with various AO film thicknesses. The thermodynamic calculation exams the possibility of NC state in AO/PZT structure, and qualitatively matches with the experimental data. This chapter also deals with the frustration of NC effects in AO/PZT capacitor and the connection between NC effects and tunnel switching behavior in AO/PZT structures, which could be explained by the interface charging through the thin AO layer.

Chapter 5 present the direct evidence of NC effects in AO/BTO structures where the interface charging was suppressed by adopting short time measurement method. This chapter reveals that the hysteresis phenomenon in NC devices originated from the dielectric leakage of the dielectric layer, and demonstrates that a non-hysteretic NC effect can be achieved only within certain limited time and voltage ranges.

Finally, in chapter 6, the conclusion of the dissertation is made.

1.3. Bibliography

1. S. Salahuddin and S. Datta, *Nano Lett.* **8**, 405-410 (2008).

2. W. Shu-Yau, *IEEE Trans. Elect. Dev.* **21**, 499-504 (1974).

3. C. M. Krowne, S. W. Kirchoefer, W. Chang, J. M. Pond, and L. M. B. Alldredge, *Nano Lett.* **11**, 988–992 (2011).

4. Jo, W. Y. Choi, J. -D. Park, J. W. Shim, H. -Y. Yu, and C. Shin, *Nano Lett.* **15**, 4553-4556 (2015).

5. A. I. Khan, K. Chatterjee, J. P. Duarte, Z. Lu, A. Sachid, S. Khandelwal, R. Ramesh, C. Hu, and S. Salahuddin, *IEEE Elect. Dev. Lett.* **37**, 111-114 (2016).

6. A. I. Khan, D. Bhowmik, P. Yu, S. J. Kim, X. Pan, R. Ramesh, and S. Salahuddin, *Appl. Phys. Lett.* **99**, 113501 (2011).

7. D. J. R. Appleby, N. K. Ponon, K. S. K. Kwa, B. Zou, P. K. Petrov, T. Wang, N. M. Alford, and A. O'Neill, *Nano Lett.* **14**, 3864-3868 (2014).

8. https://cns.utexas.edu/news/new-research-points-way-to-less-vulnerable-computer-memory

2. Literature

2.1. Theory of Negative Capacitance

According to the phenomenological theory of ferroelectric (FE) phase transition made by Landau-Devonshire (LD),[1] the free energy of FE materials can be written as

$$U_f = \alpha_f P_f{}^2 + \beta_f P_f{}^4 + \gamma_f P_f{}^6 - EP_f \tag{2.1}$$

,where, α_f, β_f and γ_f are LD coefficient of FE materials, P_f is order parameter and E is electric field. The order parameter corresponds the orientation dipole in FE system, such as the off-site B^{4+} ion in ABO perovskite system. And, α_f describes the temperature dependency in the free energy equation related with the Curie temperature (T_C) of FE materials, *i.e.* $\alpha_f = \alpha_0(T-T_C)$, $\alpha_0 > 0$. The emergence of nonzero P_f value below the T_C indicates the symmetry change from paraelectric (PE) phase to FE phase.

For the free energy relation of a serially stacked system of FE and PE material can be expressed as [2]

$$U_{tot} = l_f(\alpha_f P_f^2 + \beta_f P_f^4 + \gamma_f P_f^6 - E_f P_f) + l_d(\alpha_d P_d^2 + \beta_d P_d^4 + \gamma_d P_d^6 - E_d P_d)$$

$$(2.2)$$

,where, l_f and l_d are thickness of FE and PE layer respectively; α_d, β_d and γ_d are LD coefficient of the PE material ($\alpha_d > 0$); and P_d and E_d is polarization and electric field of PE layer respectively. To satisfy the displacement continuity theorem,

$$\varepsilon_0 E_f + P_f = \varepsilon_0 E_d + P_d \qquad (2.3)$$

,and Kirchhoff's voltage law,

$$V = E_f l_f + E_d l_d \qquad (2.4)$$

,the total free energy (U_{tot}) of FE/PE system can be rewritten as follows,

$$U_{tot} = l_f(\alpha_f P_f^2 + \beta_f P_f^4 + \gamma_f P_f^6) + l_d(\alpha_d P_d^2 + \beta_d P_d^4 + \gamma_d P_d^6)$$
$$- V\frac{P_f l_f + P_d l_d}{l_f + l_d} + \frac{l_f l_d (P_f - P_d)^2}{\varepsilon_0(l_f + l_d)} \qquad (2.5)$$

The electrostatic energy of polarization mismatch between two layer (last term in equation 2.5) is extremely large compared to other energy terms, hence total energy of FE/PE system should be stabilized at $P_d = P_f = P$. Terefore, U_{tot} can be simply modified into a linear combination of LD equation of each layer as follows,

$$U_{tot} = (l_f\alpha_f + l_d\alpha_d)P^2 + (l_f\beta_f + l_d\beta_d)P^4 + (l_f\gamma_f + l_d\gamma_d)P^6 - PE \qquad (2.6)$$

The simplified equation has identical mathematical structure of LD equation with synthesized coefficients. In this regards, the U_{tot} of bi-layer structure can have FE-PE transition by adjusting the relative thickness of FE and PE layer at fixed temperature. Figure 2.1 shows the energy landscape of FE/PE bi-layer system. Under the condition of $l_f\alpha_f + l_d\alpha_d > 0$, the PE-like energy state is developed in the bi-layer structure, and the polarization is stabilized at P=0 as shown in figure 2.1. This means the FE is stabilized in the NC state (see Chapter 1.1).

From the U-P relation, the capacitance relation can be derived using the equation 2.7

$$C = (d^2U \ / \ dP^2)^{-1} \qquad (2.7)$$

Therefore, the capacitance at the zero bias (C_0) (precisely zero polarization, nevertheless, PE-like energy state always satisfies the condition that P=V=0) corresponds to the inverse of the P^2 coefficient. From the equation 2.6, therefore, the C_0 of FE/PE bi-layer system can be denoted as $(l_f\alpha_f + l_d\alpha_d)^{-1}$. As shown in figure 2.2, the C_0 of FE/PE system is always higher than the capacitance of PE layer ($=(l_d\alpha_d)^{-1}$) below the critical thickness of FE layer which indicates the transition from FE-like ($C_0 < 0$) to PE-like ($C_0 > 0$) energy

state. (It is noteworthy that the C_0 of FE materials is negative due to the negative value of α_f below the T_c.)

This result show the capacitance enhancement effect induced by the NC phenomena in FE layer, and can be simplified as the serial capacitance formula as follows

$$C_{tot} = \left(\frac{1}{C_{FE}} + \frac{1}{C_{PE}} \right)^{-1} \tag{2.8}$$

From this relation, the FE/PE bi-layer can have an infinite capacitance at C_{FE}=-C_{PE}.[3] In addition, this is identical to the critical thickness condition in figure 2.2. The state of negative C_0, however, is unstable because the total energy of FE/PE system has local maxima at P=0. In this circumstance, the system changes into the spontaneously polarized state with positive capacitance i.e. FE state.
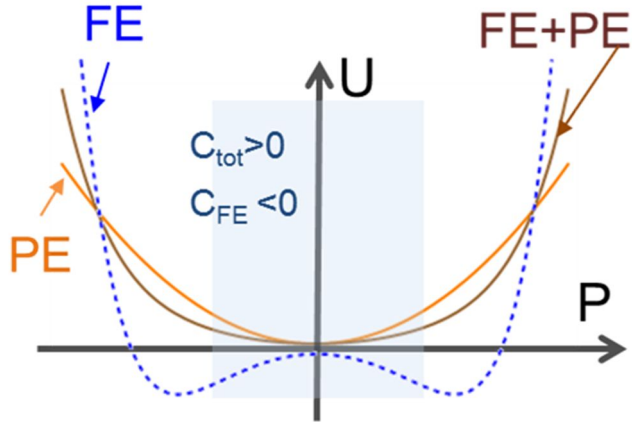
Figure 2.1 Energy landscapes of ferroelectric (FE), paraelectric (PE) and ferroelectric/paraelectric bi-layer (FE+PE) system.
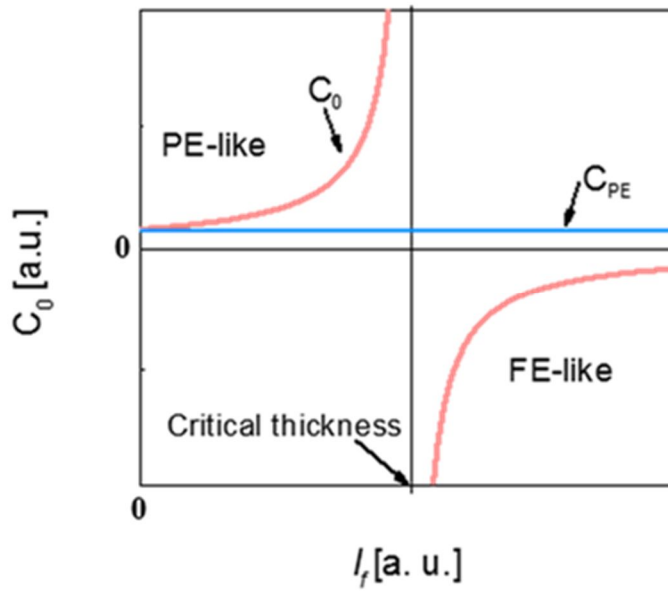
Figure 2.2 Schematic relation between total capacitance (C_0) and ferreoelctric layer thickness (l_f) in paraelectric/ferroelectric bi-layer capacitor.

2.2. Depolarization in Ferroelectric Thin Films

When the uniform dielectric medium is exposed by external electric field (E_0) (figure 2.3), the polarization become generated from dielectric medium. The polarization develops the charge sheet at the dielectric surfaces normal to polarization direction, and this charge sheet can build up the depolarization field (E_{dep}) inside of dielectric medium. By the definition of condensed matter physics, [4] the depolarization field and total macroscopic field inside dielectric medium are

$$E_{dep} = -\frac{P}{\varepsilon_0} \qquad (2.9)$$

$$E = E_0 + E_{dep} \qquad (2.10)$$

In case of normal dielectric materials, the polarization is also function of electric field ($P=\varepsilon_0\chi E$), the depolarization field can be expressed by E_0 and susceptibility (χ) as follows,

$$E_{dep} = \frac{\chi}{1+\chi} E_0 \qquad (2.11)$$

However, the charging capacitor in real system is in the difference situation. Charging of capacitor include the charge carrier accumulation at the metal electrode until the macroscopic field of dielectric layer reaches the applied source voltage. In case of ideal plate capacitor, as shown in figure

2.4, the total accumulated charge density (Q) at metal electrode directly reflects the displacement of dielectric materials. In this case, the polarization of dielectric (P) is perfectly compensated by free carrier of the electrode in this ideal capacitor structure. Therefore, depolarization field cannot be generated, and the macroscopic field in the dielectric layer is identical to the applied electric field.

If the charge carrier does not fully compensate the induced polarization of dielectric medium, a depolarization field can be built-up in a direction opposite to polarization. This depolarization phenomenon is a common in FE materials due to their spontaneous polarization component. Unlike the polarization of normal dielectric, the spontaneous polarization has non-linear electric response and has none zero value in an absent of external electric field. Theoretically, in an ideal capacitor structure with short circuit condition, the spontaneous polarization is also fully compensated by carrier of metal electrode. However, in actual system, the charge screening of the polarization is imperfect due to a dead layer at the metal/FE interface. The dead layer include both the extrinsic dead layer formed from thin film process and the intrinsic dead layer arising from spatial charge distribution of a realistic metal electrode (figure 2.5)[5]. Therefore, there is a finite depolarization field inside of the FE layer. As assuming effective screening length of metal electrode, which is called Thomas-Fermi screening length (λ_{TF}), [6] the depolarization field of real system can be expressed as

$$E_{dep} = \frac{P_s \lambda_{TF}}{\varepsilon_e d} \qquad\qquad (2.12)$$

where, d is the thickness of FE layer, and ε_e is the permittivity of metal. From equation 2.12, it can be noted that the depolarization effect is crucible to the very thin FE films. Therefore, it has been reported that the disappearance of spontaneous polarization in metal/FE/metal thin film capacitor due to the depolarization field effects. [7]
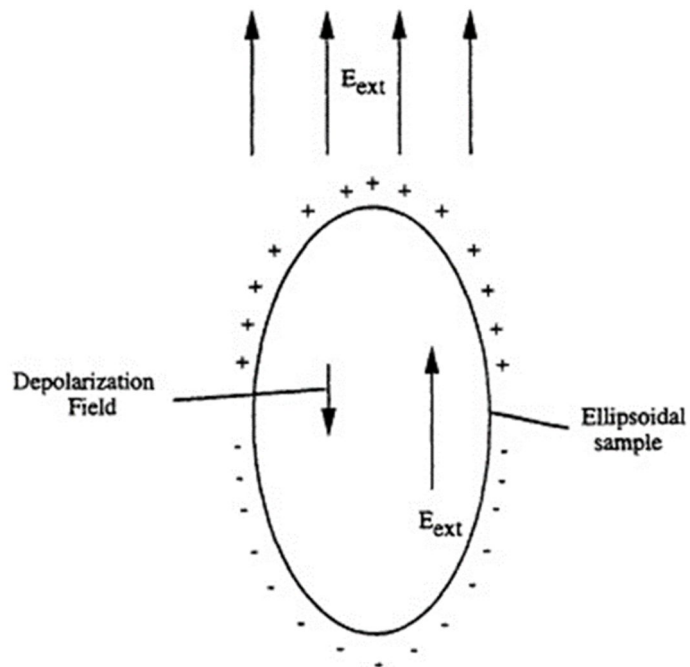
Figure 2.3 The field outside the sample E_{ext} and that inside is the sum of E_{ext}

and a depolarization field. [4]

$$E = \frac{Q - P}{\varepsilon_0}$$
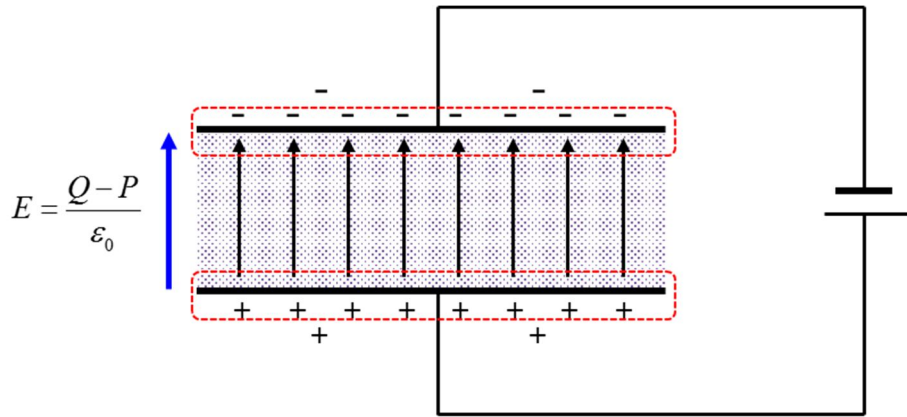
Figure 2.4 Schematic diagram of dielectric capacitor under a finite potential.
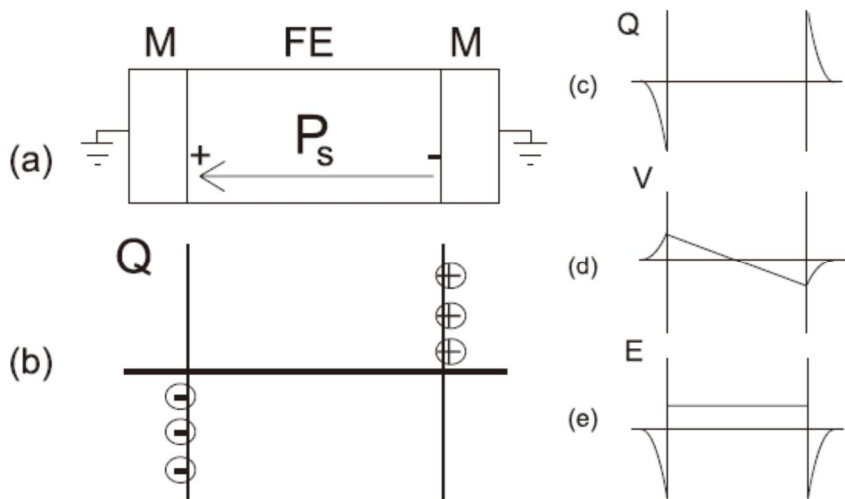
Figure 2.5 Schematic diagram of (a) a short-circuited electrode–ferroelectric structure (b) its charge distribution in the presence of perfect electrodes; its (c) charge distribution, (d) voltage and (e) field profiles in the presence of realistic electrodes. [6]

2.3. Tunnel Switching Behavior

Electronic properties and polarization switching behavior in dielectric/ferroelectric (DE/FE) bi-layer system have been excessively studied using various analysis methods. Because the inevitable and irreducible non-FE interfacial layer has become more important to understand operation mechanism of FE devices, as the physical dimension of the devices scale down to the nanometer. Therefore, the purpose of these studies was to elucidate the role of DE layer in DE/FE system. Earlier studies had treated this interfacial DE layer as a passive capacitor component serially connected to the active FE layer. According to the study by Tagantsev et al,[8] the polarization of the FE system can be severely affected by a interface DE layer. As shown in figure 2.6, the reductions of remanent polarization and saturated polarization are expected in DE/FE/DE sandwich structure as increase of the interfacial DE layer thickness. Furthermore, the coercive field of bi-layer system is expected to increase due to the large potential drop across the interfacial DE layer.[9] Therefore, the interfacial DE layer had been considered as an obstacle for utilizing FE thin films into nanoscale device with full functionalities.

On the other hand, it was reported that interfacial DE layer can be utilized constructively. Jiang et al.[10] suggested that an interposed thin DE layer can improve the reliability of a FE by the tunnel switching mechanism. Figure

2.7 shows the operation scheme of tunnel switch that acts as resistor (on state) only during FE switching but switch to capacitor (off state) immediately after complete FE domain switching. The off state effectively prevents charge injection from the adjacent electrode during the retention time, and the polarization switching in FE layer is not interfered due to fluent carrier injection trough quantum tunneling of thin DE layer. The tunnel switching behavior of DE/FE bi-layer system can be understood by a potential distribution effects of multilayer capacitor system; the voltage is distributed inversely proportional to the capacitance of each layers. The FE material has been known to have a large capacitance during polarization switching, [11] the potential drop of DE layer should be exceptionally high. In case of thin DE layer, the electric field induced to the DE layer easily exceeds the FN tunneling threshold. In a non-switching case, the capacitance of FE layer is relatively small compared with that from FE switching. Therefore, the electric field of the DE layer becomes much smaller than the tunneling threshold, hence the DE eventually block the charge flow of DE layer, including injected charge for compensating the switched polarization in FE layer. As a result, the back-switching effect of FE layer can be effectively suppressed in this tunnel switch device, because the back switched domain experience a large depolarization field which induced by that injected charge.
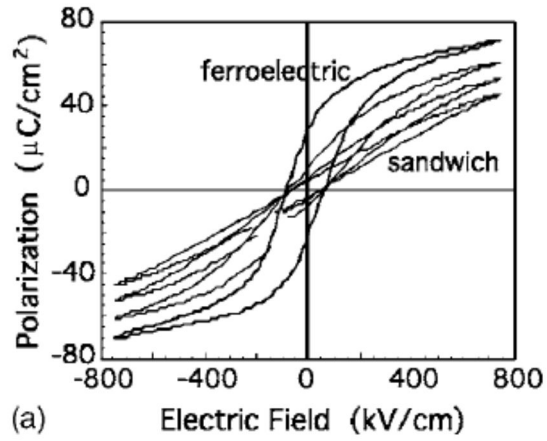
Figure 2.6 (a) Hysteresis loop of a ferroelectric, and the calculated loops of the sandwich for different values of $d/\kappa_d h$=0.003, 0.009, 0.018.
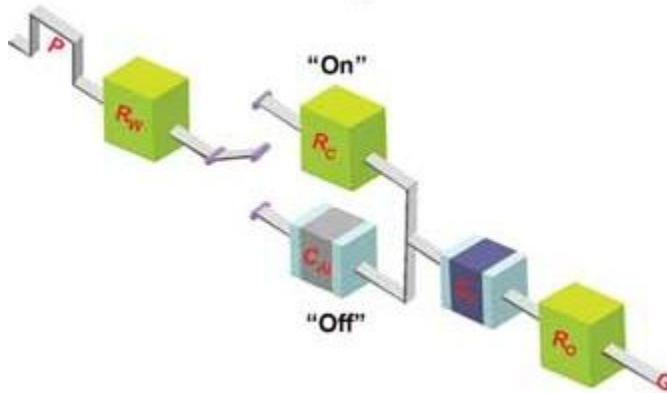
Figure 2.7 Equivalent-circuit description of the in-series resistors and capacitors for the domain switching performance with the tunnel switch in differenct states.[10]

2.4. Bibliography

1. A. F. Devonshire, *Phil. Mag.* **40**, 1040-1063 (1949).

2. A. I. Khan, D. Bhowmik, P Yu, S. J. Kim, X. Pan, R. Ramesh and S. Salahuddin, *Appl. Phys. Lett.* **99**, 113501 (2011).

3. C. S. Hwang, *Adv. Electron. Mater.* **1**, 1400056 (2015).

4. C. Kittel, in *Introduction to Solid State Physics* (John Wiley, New York, USA, 1996)

5. M. Dawber, P. Chandra, P. B. Littlewood and J. F. Scott, *J. Phys.: Condens. Matter.* **15**, L393–L398 (2003).

6. N. W. Ashcroft and N. D. Mermin, in *Solid State Physics* (Thomson Learning, Toronto, Canada, 1976)

7. J. Junquera and P. Ghosez, *Nature* **422**, 506-509 (2003)

8. A. K. Tagantseva and G. Gerra, *J. Appl. Phys.* **100**, 051607 (2006)

9. P. K. Larsen, G. J. M. Dormans, D.J. Taylor and P. J. van Veldhoven, *J. Appl. Phys.* **76**, 2405 (1994).

10. A. Q. Jiang, H. J. Lee, G. H. Kim and C. S. Hwang, *Adv. Mater.* **21**, 2870 (2009).

11. A. Q. Jiang, X. J. Meng, D. W. Zhang, M. H. Park, S. Yoo, Y. J. Kim, J. F. Scott and C. S. Hwang, *Sci. Rep.* **5**, 14618 (2015).

3. Alternative Approach on Negative Capacitance Effects

3.1. Introduction

The high capacitance capacitor is essential for many electronic devices, including computers, digital televisions, cell phones, and electric vehicles.[1,2] Formerly, the dielectric thickness was decreased and higher dielectric constant materials were used to achieve a larger capacitance.[3] These conventional strategies can be well acknowledged by the extremely thin, high dielectric constant layer in dynamic random access memory capacitors and high performance logic transistors.[4,5] However, this approach is no longer compatible with the extreme miniaturization and lower operation voltage trends found in futuristic electronic devices and, therefore, an alternative, yet fundamentally disparate, method is necessary. The negative capacitance (NC) effect found in ferroelectrics (FE) can be an intriguing contender to solve this problem since the serial connection of NC and positive capacitance (PC), in principle, can result in an unlimited capacitance density ($C_{total}^{-1} = C_{PC}^{-1} + C_{NC}^{-1}$, meaning that total capacitance is ∞ when absolute magnitude of the NC equals to PC).[6] This combined

capacitance is not determined by the thickness or relative dielectric constant of each dielectric layer, but by the combination of dielectric thickness and relative dielectric constants of the NC and PC layers for a given area.

The capacitance is proportional to the inverse of the second order differential of internal energy (U) vs. electric polarization (P) curve of a dielectric (DE) or FE material.[7] According to the Landau's model, the NC effect can be expected in the ferroelectrics only when the ferroelectric is unstable (polarization P ~ 0) with respect to the stable spontaneous polarization (Ps) state. Therefore, NC effect from the single FE layer cannot be realized under normal situation because FE stays at the P = Ps state. Salahuddin and Datta,[6] however, suggested the possibility that the NC effect of a FE layer in a DE/FE stacked system can be stabilized when the total internal energy of the DE/FE bi-layer is minimized near P = 0 (also voltage V = 0). This could occur through the DE and FE coupling, where the polarization of each layer has an identical value, without developing domain structure. Under this circumstance, the FE layer in the DE/FE structure then shows the NC effect. Khan et al.[8] recently reported that the NC effect can be observed in the hetero-epitaxial STO/Pb(Zr,Ti)O$_3$ (PZT) bi-layer system only when the sample was heated up to near the Curie temperature (T$_c$) of PZT. Pb-based ferroelectrics generally show stronger FE property compared with Ba-based ferroelectrics in a sense that T$_c$ of the Ba-based ferroelectrics is substantially lower than that of the Pb-based ferroelectrics. Based on this

27

idea, Appleby et al.[9] recently reported an experimental verification of the NC effect at room temperature from the STO/BaTiO$_3$ (BTO) hetero-epitaxial layer. Furthermore, Gao et al.[10] also reported a similar NC effect at room temperature from the LaAlO$_3$/(Ba,Sr)TiO$_3$ (LAO/BSTO) superlattice structure. The alloying of STO with BTO to make the BSTO would further lower the TC which facilitates the emergence of the NC effect. Up to now, the NC effect from the DE/FE bi-layer structure has been explained based on the linear combination of the free energies with respect to polarization of DE and FE layers, which were described by the phenomenological expression of Landau-Devonshire (LD).[11-13] However, there were conceptual difficulties in using the displacement equation within the bi-layer structure.[8,9] The detailed discussions on this aspect of the former energy description in the DE/FE structure could be found in chapter 3.2.. Another difficulty regarding the LD theory in DE/FE system is as follows. In principle, the DE layer does not necessarily have the perovskite structures, such as STO, but could be a normal dielectric material, such as amorphous Al$_2$O$_3$, of which the dielectric constants are generally much lower than that of the perovskites. The LGD parameters for these materials are not very well-known, making the application of LGD theory to these cases difficult. In the case of the low dielectric DE, such as Al$_2$O$_3$, and high dielectric FE, such as BTO, are stacked, the electric field must be applied very unevenly over the stacked structure. Under a given external bias voltage, the FE layer in the DE/FE

stack structure may play a role as the NC layer, which induces a voltage across the DE layer whose magnitude is even higher than the applied voltage (voltage boosting effect). This might induce unwanted problems, such as charge injection across the thin DE layer, which has not been considered in the previous NC effect model. When such charge injection occurs and the injected charges are trapped at the DE/FE interface, stable Ps can be developed within the FE layer which largely mitigates the NC effect of the FE layer.

In this work, therefore, the authors suggest an alternative approach to the possible NC effect in general DE/FE bi-layer structures adopting the depolarization theory.[14-18] In this model, the well-known LD theory is extended to encompass the case where the high depolarization field is present due to an imperfect polarization compensation by the interposed thin DE layer between the FE and the metal electrode. Based on this model, it was proved that the depolarization state corresponds to the aforementioned NC condition. When an external bias voltage is applied to the DE/FE system to polarize the FE layer, the FE bound charge of the FE layer at the interface between the FE layer and metal electrode can be fluently compensated by free carriers in the metal electrode. However, the FE bound charge at the DE/FE interface cannot be fully compensated by the presence of the DE layer between the FE layer and the opposite metal electrode. This induces depolarization field across the FE layer, and if the FE film is thin enough, the

direction of overall field across the FE layer can be opposite to the applied field direction. In order to make the total applied voltage over the DE/FE layer equal to the external voltage, a voltage which is even higher than the applied voltage must be applied to the DE layer. This corresponds to the NC effect, i.e. voltage boosting effect, leading to the capacitance boosting effect.

This work also discusses the conditions that have hindered the operation of the NC effect in general DE/FE systems and it is the charge injection across the thin DE layer during voltage sweep. As shown in the next section, the trapped charges can largely mitigate the depolarization effect, leading to decrease in the voltage and capacitance boosting. Even more complicated problem is that the sign of the trapped charges can be reversely changed according to the polarity of the applied bias of which the magnitude is large enough to induce tunneling of carriers through the thin DE layer. Under this circumstance, the Ps of the FE layer can be reversibly switched as it is the case for a single layer FE, which may correspond to the frustration of the NC effect in the DE/FE layer.

Cano and Jimenez have indicated that the formation of multidomain structure, which is assumed to correspond to the depolarized state of the FE layer, can drastically decrease the probability of involving the NC effect in the structure.[19] It might be probable that FE switching involving the multidomain structure in the DE/FE system occurs when the system has high

density of defect sites or embryos for the nucleation of reverse domains, where the minimization of the depolarization effect can be achieved through the closure domain pattern formation.20 Under these circumstances, the NC effect cannot be induced because the system always stays at the minimum energy state (two positive curvature regions of the U-P curve of the FE layer). However, it can be anticipated that such effect is minimized in a high quality epitaxial BTO thin film, which was adopted in this work. Therefore, such possibility, i.e. FE switching mediated by the reverse domain nucleation and growth, is not taken into consideration in this work.

3.2. Review on Previous Theoretical Model

According to the original publication of Khan et al.[8], the following two equations constitute the basic formalism in explaining the NC effect from the DE/FE structure.

$$\varepsilon_0 E_f + P_f = \varepsilon_0 E_d + P_d \tag{3.1}$$

$$U_{tot} = l_f(\alpha_f P_f^2 + \beta_f P_f^4 + \gamma_f P_f^6) + l_d(\alpha_d P_d^2 + \beta_d P_d^4 + \gamma_d P_d^6) - V\frac{P_f l_f + P_d l_d}{l_f + l_d} + \frac{l_f l_d (P_f - P_d)^2}{\varepsilon_0(l_f + l_d)}$$

$$(3.2)$$

ε_0 represents vacuum permittivity; α_f (α_d), β_f (β_d) and γ_f (γ_d) are the LD coefficients of the FE (DE) material; P_f (P_d) is the polarization value of the FE (DE) capacitor; E_f (E_d) is the electric field inside the FE (DE) capacitors.

In fact, they should have used fraction, i. e., $l_f/(l_f + l_d)$ and $l_d/(l_f + l_d)$, in place of the length l_f and l_d, in equation 3.2 to correctly represent the total energy per unit volume of the system. So, the correct equation must be;

$$\begin{aligned} U_{tot} &= \frac{l_f}{l_f + l_d}(\alpha_f P_f^2 + \beta_f P_f^4 + \gamma_f P_f^6) + \frac{l_d}{l_f + l_d}(\alpha_d P_d^2 + \beta_d P_d^4 + \gamma_d P_d^6) \\ &\quad - E\frac{P_f l_f + P_d l_d}{l_f + l_d} + \frac{l_f l_d (P_f - P_d)^2}{\varepsilon_0(l_f + l_d)^2} \end{aligned} \tag{3.3}$$

They also assumed that $P_f = P_d$, which corresponds to the strong electrostatic coupling between the DE and FE layers, which would eliminate the last term in equation 3.3. As a result, the external field must be applied equally to the two layers ($E_f = E_d$, equation 1.1). This result is counterposed against the fact that voltage amplification effects should be observed in DE/FE structure by NC phenomena.

Figure 3.1 shows the change in the U-P curves of the STO, BTO, and STO/BTO layers when an E_{ext} of 300 kV cm^{-1} was applied to the stacked layer, calculated from the previous model. The energy minimum of the each layer was achieved at P = 0.074 and 0.284 C m^{-2} for the STO and BTO layer, respectively, which is already self-contradictory to the assertion of $P = P_f = P_d$, while the overall energy minimum of the stacked layer was achieved at P = 0.169 C m^{-2}. This result shows that the equation 3.1 is obviously incorrect. Previous authors might have ignored the background dielectric constant of dielectric displacement of a FE layer, which caused the miscalculation. These inaccuracies resulted in errors in estimating theoretical capacitance values for the given DE/FE stack. Another conceptual difficulty related with equation 3.2 and 3.3 is that the U of several simpler DE layer, such as LaAlO$_3$ and Al$_2$O$_3$, of which relative dielectric constant is much lower than STO, can hardly be represented by the general LD formula.
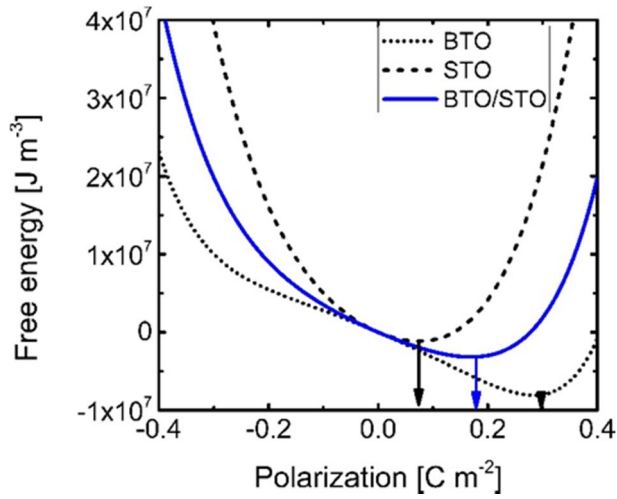
Figure 3.1 Landau free energy diagrams from previous model in 25nm STO/50nm BTO heterostructure under Eext=300kV cm^{-1}. The dash and dot line show Landau free energy of STO and BTO single layer.The minimum positions of each energy curves represent stable polarization of each layer or structure

3.3. Alternative Theoretical Model on Negative Capacitance

In a typical metal/ferroelectric/metal (MFM) system, the net polarization charge on the FE layer surfaces generally can easily be compensated by the free carriers in the nearby metal electrodes, although it cannot be fully compensated due to the finite screening length of normal metals.[14] Almost no involvement of such adverse effect has been theoretically expected from the Pt/BTO interface,[21,22] which is very different from normal occasions. For the case of metal-insulator-ferroelectric-metal (MIFM) system, which corresponds to the DE/FE stack system in this work, charge compensation at the insulator side of the ferroelectric interface is hindered due to the presence of an insulator layer (DE layer). Hence, a large depolarization field across the FE layer is developed which destabilizes spontaneous polarization.[14] Figure 3.2a shows the schematic diagram of a general DE/FE structure. When depolarization field (E_{dep}) is developed within the FE layer, it influences not only the spontaneous polarization (order parameter of Landau equation, which is sometimes called orientation polarization) but also the rest part of the FE materials, which can be considered as background polarization (P_b). In other words, the displacement of the FE layer could be divided into two different components: spontaneous and background

displacement. In contrast, there is no Ps in the DE layer, and thus, the equation of the displacement continuity at the DE/FE interface under the short circuit condition with or without external bias voltage should be written as equation 3.4,

$$\varepsilon_0 E_f + P_b + P_s = \varepsilon_0 \varepsilon_b E_f + P_s = \varepsilon_0 \varepsilon_d E_d \quad\quad (3.4)$$

, where ε_0 represents the vacuum permittivity; E_f (E_d) is the electric field inside the FE (DE) layer; ε_b is the background dielectric constant of the FE layer; and ε_d is the dielectric constant of the DE layer. While the presence of ε_b is widely accepted in electrostatic calculations of critical phenomenon,[23,24] depolarization,[14-18] and dielectric response of the DE/FE superlattice structures,[23-25] the precise definition and its value are controversial. From literatures, various ε_b values, such as optical dielectric constant ($\sim$5),[14,15,25,28] $\sim$10,[18,29] $\sim$50[22,30] and >100,[17,31] could be found for various perovskite FE materials. In this work, 50 were taken for the ε_b of the c-axis oriented BTO epi-layer to calculate the thermodynamic states and the dielectric response of the FE single layer as well as the DE/FE stacked layer. Actually, ε_b of BTO varies according to the electric field because it could vary with variation of Ps along the applied field direction. However, this is generally the case for randomly oriented material, where its Ps state is heavily dependent on the applied field. In this work, where the epitaxial BTO film is c-axis oriented and its c-axis lattice parameter is even elongated

along the surface-normal direction, the Ps is always aligned along the out-of-plane direction. This makes the ε_b quite invariant throughout the most part of voltage application. There could be bias conditions where the permittivity increases when the material is depolarized near the coercive voltage region. In fact, the depolarized state variation is quite small in one case but could be as three times high as the polarized state.[32] However, such voltage region is very narrow compared with the entire tested voltage region. Hence, a constant permittivity assumption in the calculation induced minimum error. In many theoretical cases, [14, 15, 17, 18, 20, 22, 25, 28-31] this value has been taken as constant.

As can be understood from the equation 3.4, the displacement in the DE layer could be induced by only the $\varepsilon_0\varepsilon_d E_d$ term. Therefore, if $\varepsilon_0\varepsilon_d$ of the DE layer is much smaller than the capacitive contribution from $\varepsilon_0\varepsilon_b$ and Ps, E_d becomes very high. When the DE layer is very thin, interface charge (σ_i) can be formed at the DE/FE interface by carrier injection across the DE layer. Under this circumstance E_{dep} in the FE layer decreases, which can stabilize Ps. The electric field generated by the presence of Ps and σ_i at the FE and DE layer under the short circuit condition can be represented as follows,

$$E_{dep} = \frac{\sigma_i - P_s}{\varepsilon_0 \cdot l_f} \cdot \left(\frac{\varepsilon_b}{l_f} + \frac{\varepsilon_d}{l_d} \right)^{-1} \tag{3.5}$$

$$E_{\text{int}}{}^{d} = -\frac{\sigma_i - P_s}{\varepsilon_0 \cdot l_d} \cdot \left(\frac{\varepsilon_b}{l_f} + \frac{\varepsilon_d}{l_d} \right)^{-1} \tag{3.6}$$

, where $E_{\text{int}}{}^{d}$ is the internal electric field across the DE layer, and l_f (l_d) is the thickness of the FE (DE) layer. Figure 3.2 shows the distribution of E_{dep} and $E_{\text{int}}{}^{d}$ within the Al_2O_3 (AO)/BTO stacked layer, where the BTO layer possesses Ps and the AO/BTO interface contains σ_i.

The free energy (or thermodynamic potential) of an order parameter (Ps) in a FE layer can be described by LD equation as shown in equation 3.7.

$$U_s = \alpha P_s^{2} + \beta P_s^{4} + \gamma P_s^{6} \tag{3.7}$$

Then, the electrostatic field acting on Ps, can be expressed as

$$E_{pol} = \left. \frac{\partial U_s}{\partial P_s} \right|_{E_{ext}} = 2\alpha P_s + 4\beta P_s^{3} + 6\gamma P_s^{5} \tag{3.8}$$

, where α, β and γ are LD coefficients of a FE material. Figures 3a and b show the electric force-polarization diagrams for the cases of $\sigma_i=0$ and $\sigma_i < 0$, respectively. Here, the electric force can be easily calculated by multiplying the electric field with charge. The reason why an electric force is invoked can be easily understood from figures 3c and d; when the two forces acting on the central cation in the oxygen octahedron balance each other, the cation remains at the center position making the material paraelectric (FE polarization is completely frustrated), whereas if polarization force

38

overcomes the depolarization force, by the presence of σ_i, the material can show the FE polarization. This depolarization behavior is well established by a number of studies, especially dead layer effects in MFM thin film capacitor. When the FE film is thinner than the critical thickness, it becomes paraelectric which corresponds to the circumstance represented by figures 3a and c. On the other hand, even when the film is thinner than the critical thickness, the presence of σ_i at the interface could shift the force equilibrium point from the origin and Ps can be stabilized depending on the different values of σ_i.
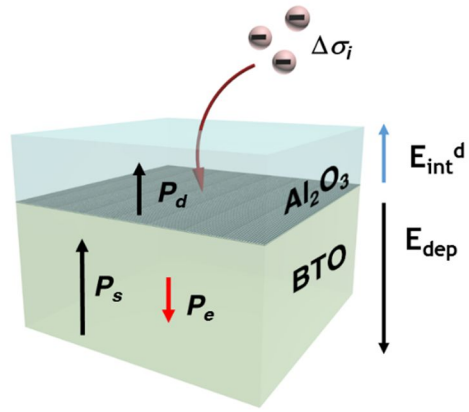
Figure 3.2 Schematic diagram of NC model in Al2O3/BTO bi-layer structure
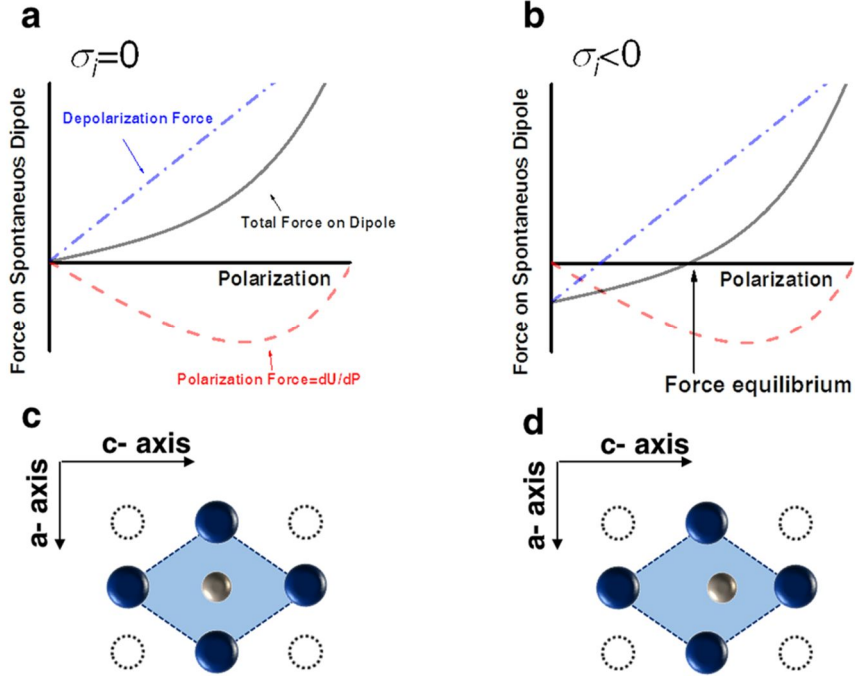
Figure 3.3 (a,b) force landscapes of DE/FE where $\sigma_i=0$ and $\sigma_i<0$, (c,d) stable Ps configurations where the system is in (a) and (b) states, respectively.

The LD free energy equation of a FE layer under the presence of Edep can be obtained by integrating the equations 3.5 and 3.8 with respect to Ps. For the sake of simplicity, the uniform polarization in ferroelectric materials is assumed. Then, the LD equation of FE materials with a homogeneous polarization (Ps) and a constant σ_i under an external electric field (E_{ext}^f) can be expressed as

$$U_f = \alpha P_s^2 + \beta P_s^4 + \gamma P_s^6 - \left[E_{ext}^f \cdot P_s + \frac{\sigma_i \cdot P_s - \frac{1}{2}P_s^2}{\varepsilon_0 \cdot l_f} \cdot \left(\frac{\varepsilon_b}{l_f} + \frac{\varepsilon_d}{l_d} \right)^{-1} \right] \quad (3.9)$$

Here, the E_{ext}^f is the portion of E_{ext} applied over the FE layer. The coefficient of Ps^2 term ($\alpha' = \alpha + [2(\varepsilon_0\varepsilon_b + \varepsilon_0\varepsilon_d l_f /l_d)]^{-1}$) is determined by the relative magnitude of E_{dep} and E_{pol}. If $E_{pol} > E_{dep}$, α' has a negative value and the FE layer is in the FE state. If $E_{pol} < E_{dep}$, α' becomes positive, and the FE layer becomes paraelectric-like. This state is critical for the emergence of the NC effect from the DE/FE structure. Detailed material parameters in equation 3.9 for the AO/BTO system are summarized in table I. It should be noted that the equation 3.9 represents the thermodynamic energy function for a given σ_i. If σ_i varies, the function needs to be rewritten for new σ_i, and the transition states between different values of σ_i cannot be thermodynamically described by this method. Therefore, only the thermodynamic states before and after the σ_i change are described analytically in this work, and the transition between them is only empirically described.

Then the capacitance of the paraelectric-like DE/FE system could be achieved from the general definition of capacitance. In fact, for DE/FE system, there are two distinctive layers, so the capacitance can be calculated from either layers. The derivation processes are described in detail in appendix section based on displacement-continuity at the interface between DE and FE layers and minimization of electrostatic energy. Capacitance of the DE/FE system can be represented by equation 3.10.

$$C = \varepsilon_0 \left(\frac{l_f}{\varepsilon_b} + \frac{l_d}{\varepsilon_d} \right)^{-1} (1 + \frac{dE_{int}{}^d}{dE_{ext}{}^d}) = \varepsilon_0 \left(\frac{l_f}{\varepsilon_b} + \frac{l_d}{\varepsilon_d} \right)^{-1} \cdot \left[1 + \left(\frac{\varepsilon_b}{l_f} + \frac{\varepsilon_d}{l_d} \right)^{-1} \frac{\varepsilon_d}{\varepsilon_0 \varepsilon_b l_d} \cdot \frac{dP_s}{dE_{ext}{}^f} \right] \quad (3.10)$$

Based on these formalisms, the electrical behavior of the AO/BTO bi-layer structure was examined. First, the case with σ_i=0 is considered in figure 3.4. Figure 3.4a shows the free energy diagram (U – P diagram) of a 5nm-thick AO/150nm-thick BTO bi-layer structure calculated using the equation 3.9 at room temperature. For reference, the U - P curves of a single layer AO and BTO were also plotted. With this geometry, the U - P curve shows a single minimum at P = 0, suggesting that the ferroelectricity of the FE layer is totally destabilized due to the influence by the large depolarization field. This behavior is influenced by the relative thicknesses of the DE and FE layers. Figure 3.4b shows the graph of $(d^2U/dP^2)^{-1}$ at P = 0, which corresponds to α', as a function of AO thickness for the given BTO thickness of 150 nm calculated by the equation 3.9. The capacitance showed critical variations at 3.5 nm, which is called the critical thickness (l_{cr}). When the AO film is thinner than the l_{cr}, C has a negative value and diverges to -∞ as l_{cr} is approached. This corresponds to the unstable state of the DE/FE system near P = 0, so such overall negative capacitance cannot be experimentally achieved. By contrast, when the AO film is thicker than the l_{cr}, C has a positive value and diverges to ∞ as l_{cr} is approached. This is a very useful stable state of the DE/FE for the capacitance boost near l_{cr}, which is due to the involvement of the NC state of a FE layer. Nevertheless, there

are two limitations on the use of such increased capacitance, which can be found from figures 3.4c and d. Figure 3.4c shows the capacitance – voltage (C-V) curve of the 5nm-thick AO/150nm-thick BTO bi-layer. Here, V was calculated by multiplying the field and thickness of each layer and summing them. The C-V curve of single layer AO is also plotted within the same graph and shows a constant value which corresponds to a dielectric constant of 8.9. Within the voltage range from ~-5 V to ~5 V, the C value of the bi-layer is higher than that of the AO single layer, suggesting the emergence of the NC state within the FE layer. However, at voltages outside this range, the C value decreases to lower values than the value of a single AO layer, which is due to the fact that the capacitance of the BTO layer changes from negative to positive at certain high voltages. Figure 2d shows the calculated P-V curves of the bi-layer. For reference, P-V curves of single layer AO and BTO are also plotted. The P-V curve of the bi-layer does not contain any negative slope region, suggesting that AO/BTO is overall in the PC state, whereas BTO layer shows the NC state. Usefulness (and limitation too) of the AO/BTO bi-layer as the charge storage capacitor can be understood from these figures. For example, when the bi-layer capacitor was biased from -6V to +6V, ~ 0.4C m^{-2} is stored within the capacitor. In contrast, the single layer AO capacitor can store only ~ 0.2C m^{-2}. For the single BTO layer capacitor, it can store a much higher value of ~ 0.7 C m^{-2}. However, when the capacitor voltage was released to 0V, only ~ 0.05 C m^{-2} could be extracted from the

single BTO layer capacitor because it is now with FE state, so ~ 0.65 C m^{-2} remains within the capacitor as a Pr. For the single layer AO and bi-layer capacitor, half of the stored charges is released by the same operation. As the applied voltage range increases, the stored (so released) charge density increases linearly for the AO capacitor and non-linearly for the bi-layer capacitor, and finally the charge density values become almost identical for - 20 – 20 V range. This can be understood from the decrease of capacitance at higher voltages for the case of bi-layer capacitor while that of AO capacitor is constant over a whole range of voltage in figure 3.4c. The maximum storable charge density in the bi-layer cannot be higher than the 2Ps of the BTO layer, which is the ultimate limitation of DE/FE systems as high capacitance capacitors. One may be curious about what would happen when the thickness of the AO layer is near l_{cr}? According to figure 3.4b, the capacitance can be infinite, whereas figure 3.4c shows that the voltage range for such enhanced capacitance becomes infinitesimal. Therefore, there is an upper bound for the drivable charge density, which is ~2Ps. Meanwhile, there is another critical side effect that mitigates the emergence of the capacitance boosting effect.
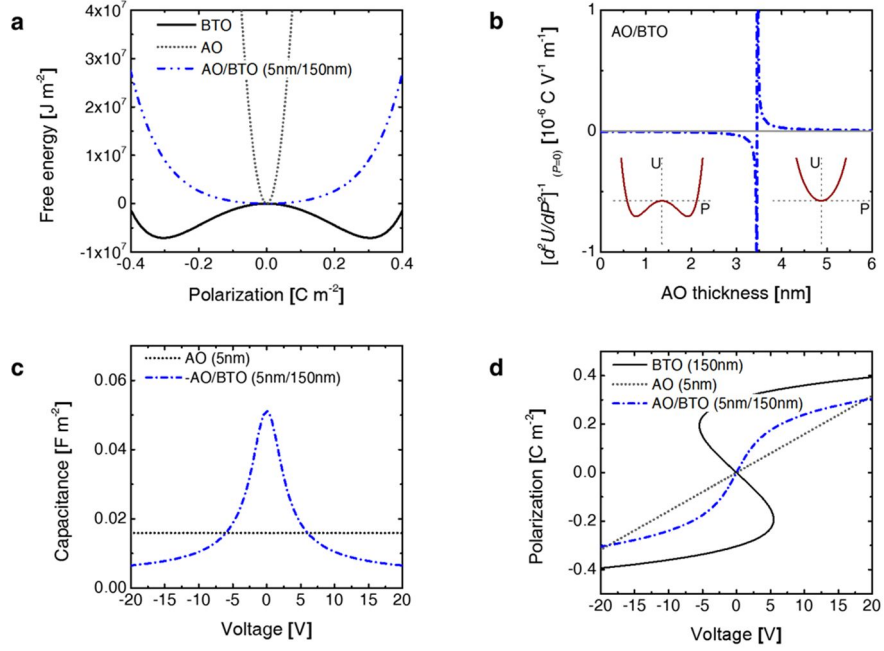
Figure 3.4 (a) Landau free energy diagrams of BTO layer in 5nm-AO/150nm BTO heterostructure. (b) AO thickness dependency of the curvature of U-P diagram, the inset figure represent energy landscape where curvature is negative (left) and positive (right) (c) capacitance-voltage curves, and (d) the spontaneous polarization–voltage curves of BTO layer in 5nm-AO/150nm BTO heterostructure.

Figure 3.5 shows the variations in the electric field over the AO and BTO layers as a function of E_{ext} when the field was applied over the 5nm-thick AO/150nm-thick BTO structure with $\sigma_i = 0$. In this graph, E_{ext} was simply calculated by dividing the applied voltage (V_{app}) by a total film thickness (155 nm). For the actual field calculation in each layer, the Eext was divided into two parts: $E_{ext}{}^f$ and $E_{ext}{}^d$, which are inversely proportional to the dielectric constant of each layer (50 for BTO and 8.9 for AO), and E_{dep}, calculated from the equation 3.5, was added to estimate the net electric field over the BTO layer. Similarly, $E_{int}{}^d$ was calculated from the equation 3.6, which is determined by the field exerted by the spontaneous polarization from the FE layer and interface charge density. $E_{int}{}^d$ was added to the component of E_{ext} over the AO layer. It is quite notable that the internal field across the BTO layer decreases when E_{ext} increases within -2.5MV cm^{-1} < E_{ext} < +2.5 MV cm^{-1}, meaning that the BTO layer works as a NC layer under this circumstance. Such decrease in the internal field of the BTO layer is compensated by the increase of the internal field across the AO layer, meaning that the capacitance boosting might be acquired. This outcome is obvious from the NC operation of the BTO layers. It is also notable that the field over the AO layer is extremely high even for the quite small E_{ext}, which significantly influences the charge distribution as will be discussed below.

Figure 3.6a shows a schematic energy band diagram of the Pt/5nm-thick AO/150nm-thick BTO/Pt capacitor when E_{ext}=100kV cm^{-1} was applied to total structure (V_{app} = 1.55 V). Due to the NC effect of BTO under this bias condition, the BTO band is tilted in the opposite way to the applied bias direction which is compensated by the very high tilting of the AO band in accordance with the applied bias direction. The opposite tilting of the BTO band within the NC region occurs because E_{ext}^{f} is overcompensated by E_{dep}. Under this circumstance, a deep potential well is formed at the AO/BTO interface of which the depth is deeper than the conduction band offset at the Pt/AO interface. Due to a very high band tilting of the AO layer, in addition to its small thickness (5 nm), there must be a very high chance of carrier injection (by most probably tunneling) as represented by the lateral arrows in Figure 3.6a. When such carrier injection occurs, the σ_i can compensate for the polarization charge within the BTO layer totally or partially at the interface, and E_{dep} will be diminished. This means that the NC effect could be also diminished under this circumstance. Nevertheless, it has to be noted that the influence of σ_i on the NC operation of the BTO layer is dependent on the bias application and carrier transport across the AO layer as discussed below. An approximate time estimation of the charge transport across the 5nm-thick AO layer by the Fowler-Nordheim tunneling to compensate about 0.2 C m^{-2} varies from several μs to several tens μs depending on the bias

48

voltage magnitude and other interface conditions. The influence of such carrier injection effect will be discussed in detail.

By contrast, it could be quite different for the case of the STO/BTO as shown in Figures 3.6b. The band diagram was calculated for $SrRuO_3$ (SRO)/25nm-thick STO/50nm-thick BTO/SRO structure. Due to a non-linear dielectric response of the paraelectric STO, the calculation was performed using a self-consistence method based on the LGD equation of STO. When E_{ext}=100kV cm^{-1}, the calculated E_{int}^d of the STO layer was 364 kV cm^{-1} and relative dielectric constants of STO layer were calculated as 215. Due to the relatively high dielectric constant of the STO, the internal band tilting of the STO layer (~0.9eV) was much lower than that of the AO layer under the identical E_{ext} condition. The BTO band also tilts in the opposite direction to the bias voltage suggesting that the BTO layer is in NC mode. Under this band configuration, the electron tunneling from the SRO into the DE/FE interface is not expected to be active, and thus, the chance for observing the NC effect from this structure would be high.[9]

This carrier injection does not necessarily correspond to the total elimination of the NC effect as long as the value of σ_i is invariant during the subsequent bias application. Here, the U-P and P-V curves of the previously mentioned AO/BTO structure were formulated again based on the equation 3.9 assuming σ_i, present at the AO/BTO interface, to be -0.2, -0.1, 0, 0.1, and

0.2 C m^{-2}, which stayed invariant throughout the entire voltage application. The results are shown in figures 3.7a and b. As can be understood from figure 3.7a, the structure shows certain monostable polarization values corresponding to a minimum energy, with different σ_i values. Figure 3.7b shows that the P-V curves are non-hysteretic due to the monostable configuration of polarization under these circumstances, and the capacitance enhancement could be achieved for all cases. However, the voltage region to observe the NC operation (region with steep slope in the P-V curve) varies according to the σ_i values. The presence of σ_i induced an invariant internal field inside the structure and shifted the P-V response along the voltage direction. Therefore, the NC effect is achieved at a shifted V (or E_{ext}) without a hysteretic P-V switching behavior according to this internal field effect. This can be qualitatively understood as that the invariant σ_i stabilizes only one of the two possible Ps's of the BTO layer, and this stabilized Ps decreases uniformly making the BTO layer be within the NC region when a bias, whose polarity is opposite to this stabilized Ps, is applied to the AO/BTO structure. Nonetheless, as discussed previously, the change of σ_i along with the change in the bias polarity largely decreases the amount of retrievable charge at the discharging step, hindering the NC effect. Experimental proof of such NC frustration is demonstrated in the next chapter.

Table I The material parameter for thermodynamic calculation

Material	T_c(K)	$\varepsilon_b / \varepsilon_d$	$\alpha(10^5\,C^{-2}\cdot m^2\cdot N)$	$\beta(10^8\,C^{-4}\cdot m^6\cdot N)$	$\gamma(10^9\,C^{-6}\cdot m^{10}\cdot N)$
$BaTiO_3$	368.5	50	$3.3\cdot(T\text{-}368.5)$	1.37	2.76
Al_2O_3	-	8.9	-	-	-
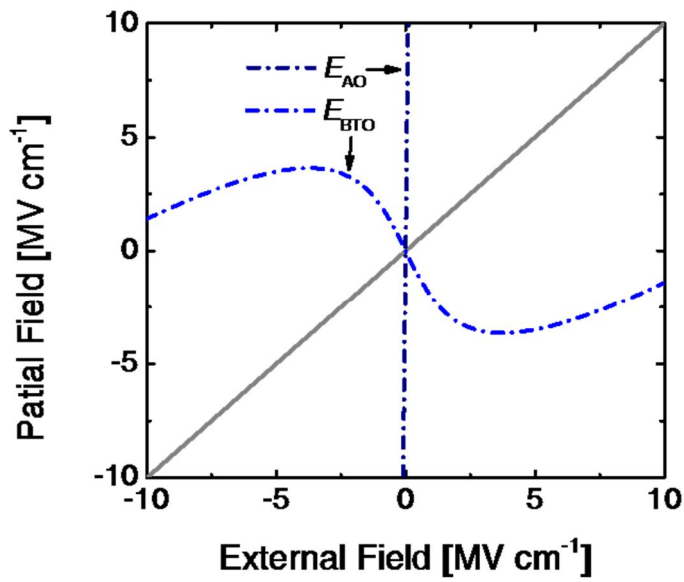
Figure 3.5 External field dependence of total field ($E_{ext}+E_{int}$) of each layer in 5nm-AO/150nm BTO stack structure.
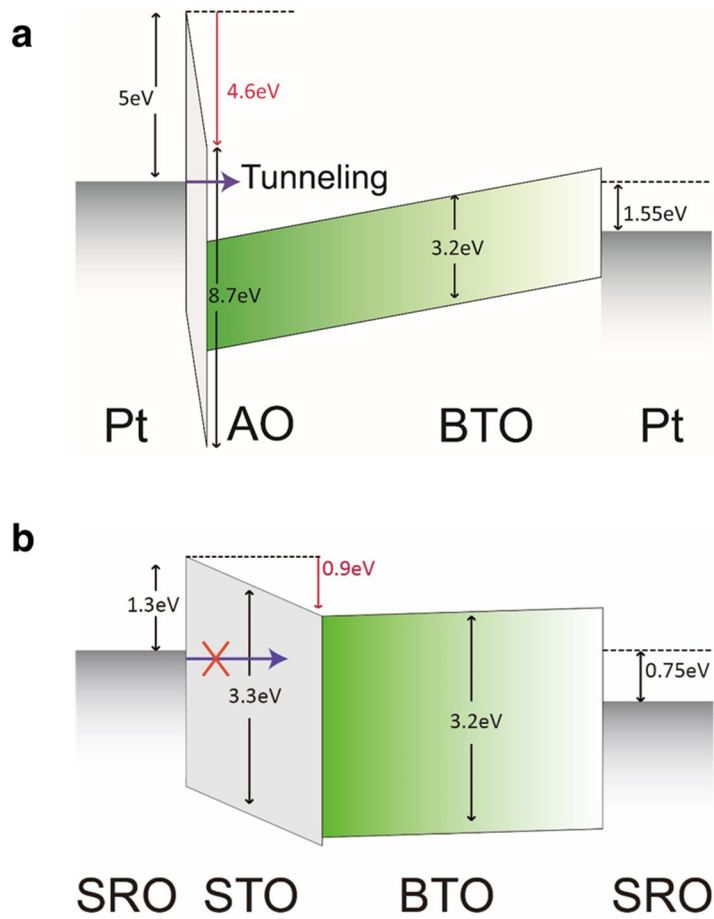
Figure 3.6 (a) Band diagrams of bi-layer capacitor of Pt/5nm-AO/150nm-BTO/Pt bi-layer capacitor when applying 1.55V potential, and (b) SRO/25nm-STO/50nm-BTO/SRO bi-layer capacitor when applying 0.75V potential.
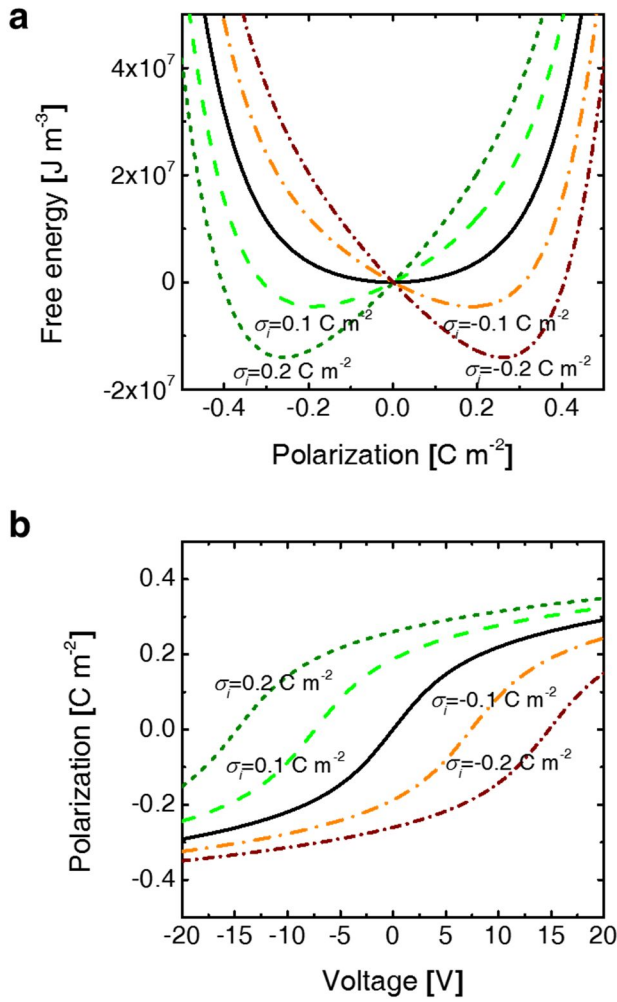
Figure 3.7 (a) Landau free energy diagrams and (b) polarization-voltage functions of 5nm-AO/150nm BTO stack structure with various σ_i values at the DE/FE interface.

3.4. Summary

In summary, the capacitance boost effect in a DE/FE system by the NC effect of a FE layer, which was originally suggested by Khan,[8] could be realized under certain limited conditions, such as no FE poly-domain formation and well-balance between the thickness and material parameters of the DE and FE layers as long as the total capacitance is in the positive regime. However, the original studies had taken some problematic assumptions, which induced a self-contradictory outcome from the calculation of the DE/FE system. In addition, when a low dielectric DE layer is adopted, its LD formula is not generally well known making the application of the previous formalism (Landau-Khalatnikov model)[8] to calculate the total free energy to such cases improbable. Therefore, an alternative model was suggested in this work that could calculate the capacitance at the DE/FE system based on the general theory on the depolarization effect[14-18] of the FE layer when the FE bound charge is not compensated well. This approach explains the experimental results more accurately. The model was also adopted to the case where the DE/FE interface had trapped charges which could (partly) compensate for the Ps of the FE layer. The charge trapping could be induced by tunneling through the thin DE layer during the NC operation of the FE layer, which augmented the potential applied over the DE layer. The interfacial charging appeared to be almost inevitable when a low permittivity DE layer, such as AO, was

adopted of which the thickness must be very thin to match the absolute capacitance values of the DE and FE layers. The trapped charges stabilize one of the two Ps's of the FE layer, which could have induced the emergence of the NC effect from the BTO layer in the AO/BTO bi-layer during the subsequent voltage application with opposite bias polarity. However, when the FE layer falls within the NC region, a significant change in the trapped charge occurs making the opposite Ps stabilized. Therefore, a FE-like hysteretic P-V loop is achieved, major portion of the accumulated charges during a voltage application is retained as the remanent polarization and injected charges in the capacitor during the subsequent voltage are released. This is detrimental to use the AO/BTO capacitor as an extremely high capacitance capacitor. It was also elucidated that even when the positively infinite capacitance is realized by the perfect match between the PC of DE and the NC of FE, the overall driven charge density cannot be higher than 2Ps of the FE layer. This is because as the capacitance increases, the voltage range for the enhanced capacitance decreases inversely proportional to the capacitance.

3.5. Appendix

Appendix I. Internal field calculations

The static one-dimension Maxwell equation of each layer must satisfy the following relationship;

$$D_d = \varepsilon_0 \varepsilon_d E_d \text{ (for dielectric layer), } D_f = \varepsilon_0 \varepsilon_b E_f + P_s \text{ (for ferroelectric layer)} \quad (3.11)$$

It is assumed that the polarization (Ps) of the FE layer is homogeneous and that the trapped charges existing at the interface between the DE and FE layers fully or partly compensate the Ps. It is further assumed that the displacements in the dielectric and ferroelectric layers D_d, D_f and Ps are constants inside each layer. Then, the Maxwell equation for each layer can be rewritten as follows from the Poisson's equation;

$$\varepsilon_d \frac{\partial^2 \varphi_d}{\partial z^2} = 0 \text{ (for dielectric layer), } \varepsilon_b \frac{\partial^2 \varphi_f}{\partial z^2} = 0, \text{ (for ferroelectric layer)} \quad (3.12)$$

Here, the ε_b is the background dielectric constant of the FE layer. The boundary condition of equation 3.12 with a sheet interface charge density (σ_i) at the DE/FE interface can be expressed as

$$\varphi_d(z = l_d) = 0, \quad \varphi_f(z = -l_f) = 0, \quad \varphi_d(z = 0) = \varphi_f(z = 0) \quad (3.13)$$

, where z = 0 corresponds to the location of the interface between the DE and FE layers. By the continuity theorem at the interface, the electrical

57

displacement and interface charge density should follow the following relationship;[33]

$$D_f - D_d = -\varepsilon_0 \varepsilon_b \frac{\partial \varphi_f}{\partial z} + P_s + \varepsilon_0 \varepsilon_d \frac{\partial \varphi_d}{\partial z} = \sigma_i \qquad (3.14)$$

$$-\varepsilon_0 \varepsilon_b \left. \frac{\partial \varphi_f}{\partial z} \right|_{z=0} + \varepsilon_0 \varepsilon_d \left. \frac{\partial \varphi_d}{\partial z} \right|_{z=0} = \sigma_i - P_s \qquad (3.15)$$

Using the geometric relationship between electric potential and static electric field,

$$E_{int}{}^d = -\nabla \varphi_d = -\frac{\varphi_d}{l_d}, \quad E_{int}{}^f = E_{dep} = -\nabla \varphi_f = \frac{\varphi_f}{l_f} \qquad (3.16)$$

Thus, the equation 3.15 leads to

$$-\varepsilon_0 \varepsilon_b \frac{\varphi_f(z=0)}{l_f} - \varepsilon_0 \varepsilon_d \frac{\varphi_d(z=0)}{l_d} = \sigma_i - P_s \qquad (3.17)$$

Finally, the polarization dependent internal electric field across the DE layer ($E_{int}{}^d$) and FE layer ($E_{int}{}^f$) which coincides with the depolarization field across the FE layer (E_{dep}) can be obtained as follows;

$$E_{int}{}^d = -\frac{\varphi_d(z=0)}{l_d} = -\frac{\sigma_i - P_s}{\varepsilon_0 l_d} \left(\frac{\varepsilon_d}{l_d} + \frac{\varepsilon_b}{l_f} \right)^{-1} \qquad (3.18)$$

$$E_{dep} = \frac{\varphi_f(z=0)}{l_f} = \frac{\sigma_i - P_s}{\varepsilon_0 l_f} \left(\frac{\varepsilon_d}{l_d} + \frac{\varepsilon_b}{l_f} \right)^{-1} \qquad (3.19)$$

Appendix II. Capacitance of a DE/FE bi-layer

In MDFM (metal/dielectric/ferroelectric/metal) structure, the accumulated charge density at M/D and F/M interfaces must be identical under any arbitrary condition. Furthermore, under the absence of any interfacial trapped charges, continuity of displacement at the DE/FE interface must be maintained. Under this circumstance, the accumulated charge, Q, can be described either at M/D or F/M interface as follows;

$$Q = D = \varepsilon_0 \varepsilon_b E_{tot}{}^f + P_s \, (\text{F/M interface}) = \varepsilon_0 \varepsilon_d E_{tot}{}^d \, (\text{M/I interface}) \quad (3.20)$$

Where $E_{tot}{}^f$ and $E_{tot}{}^d$ are total electric field in ferroelectric and dielectric respectively, and ε_d is a permittivity of an insulator. Here, the $E_{tot}{}^f$ and $E_{tot}{}^d$ encompass both electric field components from the externally applied voltage and internal charge mismatch. The capacitance of the MIFM capacitor, therefore, is

$$C = \frac{dQ}{dV} = \frac{d(\varepsilon_0 \varepsilon_b E_{tot}{}^f + P_s)}{dV} = \frac{d(\varepsilon_0 \varepsilon_d E_{tot}{}^d)}{dV} \quad (3.21)$$

According to equation 3.21, capacitance of MDFM structure could be described conveniently by the charge variation at either interface. The right-hand term of equation 3.21 was taken to describe the capacitance here because it is more straightforward. The capacitance equation is, then, given as follows,

$$C = \frac{dQ}{dV} = \varepsilon_0 \left(\frac{l_f}{\varepsilon_b} + \frac{l_d}{\varepsilon_d} \right)^{-1} \cdot (1 + \frac{dE_{int}^d}{dE_{ext}^d}) = \varepsilon_0 \lambda (1 + \frac{dE_{int}^d}{dE_{ext}^d}) \qquad (3.22)$$

, where l_f and l_d are thickness of the ferroelectric and insulator respectively. According to Kirchhoff's law,

$$V = E_{ext} l_{tot} = E_{ext} \cdot (l_f + l_d) = E_{tot}^f l_f + E_{tot}^d l_d \qquad (3.23)$$

, and the total electric field in each layer could be constituted by the two element as aforementioned

$$E_{tot}^j = E_{ext}^j + E_{int}^j \qquad (j = f \text{ or } d) \qquad (3.24)$$

, where the subscript $_{ext}$ and $_{int}$ represents the external and internal, respectively. Therefore,

$$\frac{dQ}{dV} = \frac{\varepsilon_0 \varepsilon_d}{l_{tot}} \cdot \frac{dE_{tot}^d}{dE_{ext}^d} \frac{dE_{ext}^d}{dE_{ext}} = \frac{\varepsilon_0 \varepsilon_d}{l_{tot}} \cdot (1 + \frac{dE_{int}^d}{dE_{ext}^d}) \frac{dE_{ext}^d}{dE_{ext}}$$

$$= \frac{\varepsilon_0 \varepsilon_d}{l_{tot}} \left[\frac{l_f + l_d}{\varepsilon_d \left(\frac{l_f}{\varepsilon_b} + \frac{l_d}{\varepsilon_d} \right)} \right] \cdot (1 + \frac{dE_{int}^d}{dE_{ext}^d}) \qquad (3.25)$$

The internal field of DE layer is

$$E_{int}^d = -\frac{\sigma_i - P_f}{\varepsilon_0 \cdot l_d} \cdot \left(\frac{\varepsilon_b}{l_f} + \frac{\varepsilon_d}{l_d} \right)^{-1} \qquad (3.26)$$

, which takes into account the possible presence of an interfacial trapped

charge, σ_i. From the continuity of displacement at the DE/FE interface,

$$\varepsilon_f E_{ext}{}^f = \varepsilon_d E_{ext}{}^d \qquad (3.27)$$

Thus, finally, equation 3.28 can be obtained.

$$
\begin{aligned}
C &= \varepsilon_0 \lambda \left(1 + \frac{dE_{int}{}^d}{dE_{ext}{}^d} \right) = \varepsilon_0 \lambda \left(1 + \left(\frac{\varepsilon_f}{l_f} + \frac{\varepsilon_d}{l_d} \right)^{-1} \frac{\varepsilon_d}{\varepsilon_0 \varepsilon_f l_d} \cdot \frac{dP_f}{dE_{ext}{}^f} \right) \\
&= \varepsilon_0 \left(\frac{l_f}{\varepsilon_f} + \frac{l_d}{\varepsilon_d} \right)^{-1} \cdot \left[1 + \left(\frac{\varepsilon_f}{l_f} + \frac{\varepsilon_d}{l_d} \right)^{-1} \frac{\varepsilon_d}{\varepsilon_0 \varepsilon_f l_d} \cdot \frac{dP_f}{dE_{ext}{}^f} \right]
\end{aligned}
\qquad (3.28)
$$

It is noteworthy that the capacitance of the MDFM structure can be simply calculated from the external field dependency of spontaneous polarization in a ferroelectric layer.

3.6. Bibliography

1. P. Banerjee, I. Perez, L. Henn-Lecordier, S. B. Lee, & G. W. Rubloff, *Nat. Nano.* **4**, 292-296 (2009).

2. A. S. Arico, P. Bruce, B. Scrosati, J. M.   Tarascon & W. Van Schalkwijk, *Nat. Mater.* **4**, 366-377 (2005).

3. S. K. Kim, G.-J. Choi, S. Y. Lee, M. Seo, S. W. Lee, J. H. Han, H.-S. Ahn, S. Han & C. S. Hwang, *Adv. Mater.* **20**, 1429 (2008).

4. S. K. Kim, S. W. Lee, J. H. Han, B. Lee, S. Han & C. S. Hwang, *Adv. Funct. Mater.* **20**, 2989-3003 (2010).

5. A. I. Kingon, J. –P. Maria & S. K. Streiffer, *Nature* **406**, 1032-1038 (2000).

6. S. Salahuddin & S. Datta, *Nano Lett.* **8**, 405-410 (2007).

7. C. M. Krowne, S. W. Kirchoefer, W. Chang, J. M. Pond & L. M. B. Alldredge, *Nano Lett.* **11**, 988-992 (2011).

8. A. I. Khan, D. Bhowmik, P. Yu, S. J. Kim, X. Pan, R. Ramesh & S. Salahuddin, *Appl. Phys. Lett.* **99**, 113501 (2011).

9. D. J. R. Appleby, N. K. Ponon, K. S. K. Kwa, B. Zou, P. K. Petrov, T. Wang, N. M. Alford & A. O'Neill, *Nano Lett.* **14**, 3864-3868 (2014).

10. W. Gao, A. Khan, X. Marti, C. Nelson, C. Serrao, J. Ravichandran, R. Ramesh & S. Salahuddin, *Nano Lett.* **14**, 5814-5819 (2014).

11. V. Ginzburg, *Nuovo Cimento Series 10* **2**, 1234-1250 (1955).

12. A. F. Devonshire, *Phil. Mag.* **40**, 1040-1063 (1949).

13. W. Cao & L. Cross, *Phys. Rev. B* **44**, 5 (1991).

14. J. Junquera & P. Ghosez, *Nature* **422**, 506-509 (2003).

15. I. Kornev, H. Fu & L. Bellaiche, *Phys. Rev. Lett.* **93**, 196104 (2004).

16. C. H. Woo & Y. Zheng *Appl. Phys. A* **91**, 59-63 (2008).

17. D. J. Kim, J. Y. Jo, Y. S. Kim, Y. J. Chang, J. S. Lee, Jong-Gul Yoon, T. K. Song & T. W. Noh, *Phys. Rev. Lett.* **95**, 237602 (2005).

18. A. K. Tagantsev, G. Gerra & N. Setter, *Phys. Rev. B* **77**, 174111 (2008).

19. A. Cano & D. Jimenez, *Appl. Phys. Lett.* **97**, 133509 (2010).

20. S. Kasamtsu, S. Watanabe, C. S. Hwang & S. Han, A*dv. Mater.* **28**. 335–340 (2015).

21. M. Stengel & N. A. Spaldin, *Nature* **443**, 679-682 (2006).

22. M. Stengel, D. Vanderbilt & N. A. Spaldin, *Nat. Mater.* **8**, 392-397 (2009).

23. Y. Wang, X. Liu, J. D. Burton, S. S. Jaswal, & E. Y. Tsymbal, *Phys. Rev. Lett.* **109**, 247601 (2012).

24. J. Wang, X. Ma, Q. Li, J. Britson & L. -Q. Chen, *Acta Mater.* **61**, 7591-7603 (2013).

25. M. Stengel, C. J. Fennie & P. Ghosez, *Phys. Rev. B* **86**, 094112 (2012).

26. A. P. Levanyuk & I. B. Misirlioglu, *Appl. Phys. Lett.* **103**, 192906 (2013).

27. J. B. Neaton & K. M. Rabe, *Appl. Phys. Lett.* **82**, 1586-1588 (2003).

28. T. Sluka, A. K. Tagantsev, D. Damjanovic, M. Gureev & N. Setter, *Nat. Commun.* **3**, 748 (2012).

29. V. O. Sherman, A. K. Tagantsev, N. Setter, D. Iddles & T. Price, *J. Appl. Phys.* **99**, 074104 (2006).

30. Y. Liu, X. Lou, M. Bibes & B. Dkhil, *Phys. Rev. B* **88**, 024106 (2013).

31. Y. A. Genenko & D. C. Lupascu, *Phys. Rev. B* **75**, 184107 (2007).

33. K. Abe, S. Komatsu, N. Yanase, K. Sano & T. Kawakubo, *Jpn. J. Appl. Phys.* **36**, 5846 (1997)

35. E. A. Eliseev, A. N. Morozovska, G. S. Svechnikov, E. L. Rumyantsev, E. I. Shishkin, V. Y. Shur, & S. V. Kalinin, *Phys. Rev. B* **78**, 245409 (2008).

4. Competitive Relation between Negative Capacitance Effect and Tunnel Switch Behavior in Al$_2$O$_3$/PZT Bi-layer Capacitor

4.1. Introduction

Although ferroelectric (FE) switching is one of the most significantly researched topics in solid state physics, it is still an intriguing research area for modern electronic devices. Ferroelectric random access memory is perhaps the most well developed solid state device, which utilizes the two stable remanent polarizations (±Pr) to represent the two digital memory states.[1] Recent research interests on the FE thin films are shifting toward the multi-layer structures, where the FE films are combined with other functional layers, such as ferromagnetic,[2-4] semiconductor[5-7] or dielectric (DE) materials.[8, 9] In particular, DE/FE bi-layer structure has drawn a great deal of attention due to its novel electronic properties.[8-12] Among them, the recent arguments on its negative capacitance (NC) effects[13-15] are especially appealing to the semiconductor community because it can boost capacitance of capacitors in dynamic random access memory[16] and semiconductor surface voltage to a value higher than the applied gate voltage[17] in metal-insulator (ferroelectric)-semiconductor field effect transistor. The NC region corresponds to the negative slope of the S-shaped polarization-electric field

curves which are derived from the Landau-type thermodynamic relation of FE materials. Nonetheless, the NC region of single layer FE materials is unstable due to its local maximum energy state,[18] which makes the observation of the NC effects in a single FE layer challenging.[15] However, stacking the DE layer onto a FE layer can stabilize the NC region by an electrostatic coupling between the two layers. According to the phenomenological model for the internal energy of ferroelectrics, the NC behavior can be observed only when ferroelectric polarization is highly suppressed.[10] Since theoretical expectation for this effect in a DE/FE structure has been first proposed by Salahuddin and Datta,[17] several experiments have confirmed the increased capacitance of the DE/FE layer compared with the capacitance of a single DE or FE layer.[10-12] In those experimental results, non-hysterical paraelectric-like electrical response could be observed as expected from theoretical studies. Nevertheless, emergence of stable NC effects can be hindered by the involvement of reverse domain nucleation and growth, of which states always correspond to the stable minimum energy state, and, thus, so far, the evidence of NC effects could be found only under certain limited experimental conditions, i.e. hetero-epitaxial bi-layer or superlattice systems. It appears that the nucleation and growth of reverse domain are suppressed in these systems, where the density of sites for nucleation and subsequent growth of reverse domains is quite limited.

While the reports on the emergence of the NC effect are intriguing in terms of exploring new physics in FE thin film, the practical applicability of these hetero-epitaxial system is limited in the main stream semiconductor industry due to their incompatibility with Si substrate. Therefore, evaluating the polarization property and confirming the possible NC effect from the polycrystalline FE film combined with a polycrystalline or amorphous DE layer fabricated on a Si substrate are impending task in this field. Generally, the dielectric constant of a FE film is much higher than that of a usual DE layer. This requires the DE film thickness to be much thinner than FE film to achieve the capacitance match (one is positive (DE) and the other is negative (FE)) between the two layers in a DE/FE structure. In addition, when the FE plays a role as a NC layer, the voltage applied to the DE layer, under the given applied voltage (Va), becomes higher than Va, thus, in conjunction with its thin thickness, the charge transport across that layer can be significant. The authors recently revealed that such charge transport, and subsequent trapping at the DE/FE interface, could be detrimental to the emergence of the NC effect from $Al_2O_3/BaTiO_3$ (AO/BTO) system, where AO and BTO films have amorphous and single crystalline structures, respectively.[19]

In this regard, the work reported by Jiang et al.[20] on the FE performance of $Al_2O_3/Pb(Zr,Ti)O_3$ (AO/PZT) system, where the AO and PZT layers show the amorphous and polycrystalline nature, respectively, is worth being recognized again. They reported a great enhancement of FE properties in terms of the

polarization hysteresis behavior (Pr and retention increase), owing to the AO layer as a "tunnel switch", which was clearly distinctive from the NC effect. In the tunnel switch model, the AO layer becomes conductive when the FE layer shows polarization switching while it remained insulating when the FE layer retains its original polarization state. The discrepancy between the NC effect and the tunnel switch behavior was investigated with a phenomenological method in author's previous report.[19] Actually, these two phenomena share similar aspects of the FE physics, which is related with internal electric field originated by a mismatch between spontaneous polarization charge and compensating charge at the DE/FE interface. When Va is applied to the DE/FE system, and if the FE layer shows the NC state a very high internal field must be induced across the DE layer due to a voltage amplification effect by the NC operation in the FE layer. If the DE layer is thin enough to allow the current pass through that layer, the NC effect can no longer exist in this system, because the FE layer switches to the stable reverse Pr state. In this case, the NC effect and tunnel switching behavior may occur in sequence, suggesting that the system response to the external bias would be time-dependent. The alternation between two phenomena is crucial for actual applications in electronic devices. Hence, understanding electrical behaviors of the DE/FE structures, especially when they are not of the hetero-epitaxial structure, is essential, but has not been fully established. Therefore, in this work, the authors reported electrical analysis of AO/PZT system in detail,

where the various thicknesses (2 – 10 nm) of the amorphous AO layer were grown by atomic layer deposition (ALD) on a 150nm-thick polycrystalline PZT (Zr:Ti = 0.4:0.6) film, which was grown by a metal-organic chemical vapor deposition (MOCVD) at an wafer temperature of 600 $^{\circ}$C on Ir bottom electrode/SiO$_2$/Si substrate. Among the various electrical tests, the polarization – voltage (P-V) loop represents the most critical aspects of these samples. Therefore, P-V loops of the various film stacks were obtained, and were theoretically fitted using the phenomenological model based on the general Maxwell equation for dielectric displacement, assuming the presence of interfacial charge at the DE/FE interface (σ_i). The key conceptual development in this work is the systematic change in σ_i according to the polarization switching (or change in the polarization according to the change in σ_i), and its correlation with the energy band structure.

Up to now, the NC effect from the DE/FE bi-layer structure has been explained based on the phenomenological expression of Landau -Devonshire (LD) which used linear combination of the free energies with respect to polarization of DE and FE layers.[10-12, 17] In principle, the DE layer could be a normal dielectric material, such as amorphous Al$_2$O$_3$, of which LD parameters are not very well-known, making the application of LD theory to these cases difficult. In this work, therefore, the authors used an alternative approach to the possible NC effect in general DE/FE bi-layer structures adopting the depolarization theory.[19] In this model, the well-known LD theory is applied

to the PZT layer while the influence of high depolarization field due to the presence of AO layer could be taken into account from the fundamental theory on electrostatic energy. Based on this model, it was proved that the depolarization state corresponds to the aforementioned NC condition.

4.2. Experimentals

The polycrystalline 150-nm-thick PZT films were grown by a metal-organic chemical vapor deposition on $Ir/IrO_2/SiO_2/Si$ substrate. The AO layer was deposited by atomic layer deposition process using trimethylaluminum and O_3 (with a concentration of $250 gm^{-3}$) as the Al-precursor and oxygen source, respectively, at a substrate temperature of 250 ^{o}C with thicknesses ranging from 2 to 10 nm on the PZT layer. Top electrode with an area of 1 x 10^5 μm^2 was fabricated by DC-magnetron sputtering with an 80nm thickness at room temperature using a photolithography and lift-off process. The fabricated capacitors were post-annealed at 300 ^{o}C for 30 min in air to cure the possible sputtering damage of Pt top electrode.

The P-V loops of the Pt/AO/PZT/Ir capacitors were tested using an axiACCT TF-2000 analyzer at a frequency of 1kHz in virtual ground mode. Capacitance – voltage (C-V) and current – voltage (I-V) characteristics were also checked using Hewlett Packard 4194 impedance analyzer and Hewlett Packard 4145B semiconductor parameter analyzer, respectively, to confirm the feasible dielectric performance of all the capacitors. Although the data are not shown, well behaved butterfly shaped C-V curve and low enough leakage current ($< 10^{-6}$ Acm^{-2}) in the tested voltage range for P-V were achieved. All bias was applied to top Pt electrode while bottom electrode was grounded.

4.3. Results and Discussions

According to the previous chapter,[19] the free energy of a ferroelectric layer (U_f) in a DE/FE structure taking the depolarization effect into consideration is given by,

$$U_f = \alpha P_f^{\,2} + \beta P_f^{\,4} + \gamma P_f^{\,6} - \left[E_{ext}^{\,f} \cdot P_f + \frac{\sigma_i \cdot P_f - \frac{1}{2} P_f^{\,2}}{\varepsilon_0 \cdot l_f} \cdot \left(\frac{\varepsilon_b}{l_f} + \frac{\varepsilon_d}{l_d} \right)^{-1} \right] \quad (4.1)$$

, where ε_0 represents vacuum permittivity; α, β and γ are the LD coefficients of the FE material; P_f and $E_{ext}^{\,f}$ are the spontaneous polarization and effective external field across the FE layer, which are assumed as constant over the FE layer; l_d and ε_d are the thickness and relative dielectric constant of the DE layer; lf and ε_b are the thickness and background dielectric constant of the FE layer, respectively. Details for the derivation of energy equation based on the depolarization model are given Appendix at the end of this report. The concept of ε_b is widely used in electrostatic calculations for polar materials.[21, 22] Marcus[23] reported that the polarization of polar materials should be divided into the equilibrium and non-equilibrium components. The non-equilibrium polarization corresponds to the P_f of FE materials, and the equilibrium polarization is relevant to the ε_b. The equilibrium polarization consists of electronic and the lattice polarizations, which means that the ε_b is identical to the infrared dielectric constant of FE materials. More recently,

Bernardini et al.[24] calculated the dielectric tensor of a polar crystal based on a geometric quantum phase polarization theory. They presented that the lattice polarization includes the contribution of piezoelectricity-related lattice distortion. Therefore, the perovskite ferroelectric materials could have high ε_b value due to their large piezoelectric coefficient and Born effective charge. In particular, the experimentally reported infrared dielectric constant of $Pb(Zr_{0.3}Ti_{0.7})O_3$ is as high as 120 to 250.[25, 26]

In this study, the U_f-P_f characteristic of an AO/PZT bi-layer structure were calculated using equation (1). ε_b of the PZT layer was taken to be 250, in order to calculate the electrostatic potential of the AO/PZT stacked layer. In fact, ε_b of the PZT layer varies according to the applied bias voltage but was taken as a constant, otherwise the description of energy function becomes too complicated to be dealt with analytically. Due to this difficulty, many reports took the same simplification,[21 ,22] while the error induced by such simplification was not significant.

Cano and Jimenez have indicated that the formation of multidomain structure, which is assumed to correspond to the depolarized state of the FE layer, can drastically decrease the probability of involving the NC effect in the DE/FE structure.[27] It might be probable that FE switching involving the multidomain structure in the DE/FE system occurs when the system has a high chance of fluent change compensation for the FE bound charge as in the

case of metal/FE/metal structure. Under these circumstances, the NC effect cannot be induced because the system always stays at the minimum energy state (two positive curvature regions of the U-P curve of the FE layer). However, it can be anticipated that the change for such effect is not high in a DE/FE structure because the intervened DE layer interferes the rapid charge compensation. Therefore, such possibility, i.e. FE switching mediated by the multidomain formation via the reverse domain nucleation and growth, is not taken into consideration in this work.

Figure 4.1a shows the free energy curves of the 5nm-thick AO/PZT bi-layer structures at E_{ext}^f=0 with two distinctive σ_i (= ±0.1C m^{-2}, blue and red curves). For comparison, U_f-P_f curve for AO/PZT layer with no involvement of σ_i is also appended (black line). In this case, the curve shows a single minimum when P = 0 due to the electrostatic coupling between the AO and PZT layer, which corresponds to the NC state. The overall trends in U_f-P_f curves in this structure are in agreement with that of AO/BTO bi-layer structure from the previous study.[19] The single minimum in U_f-P_f curves at non-zero P_f values for the cases of σ_i = ±0.1C m^{-2} indicates that the bistable ferroelectric polarization of PZT layer became mono-stable by addition of AO layer and σ_i. The schematic diagrams for polarization state of each free energy curves are described in figure 4.1b. As shown in figure 4.1b, the stable polarization state varied with the σ_i, which means that multi-state P_f could be stabilized by changing the σ_i even at a given bias condition. In this perspective, the

74

polarization hysteresis could be observable in a DE/FE structure by charge exchange between a metal electrode and DE/FE interface. If the charge exchange occurs with the fully developed P_f being retained, the system cannot be in the NC state.
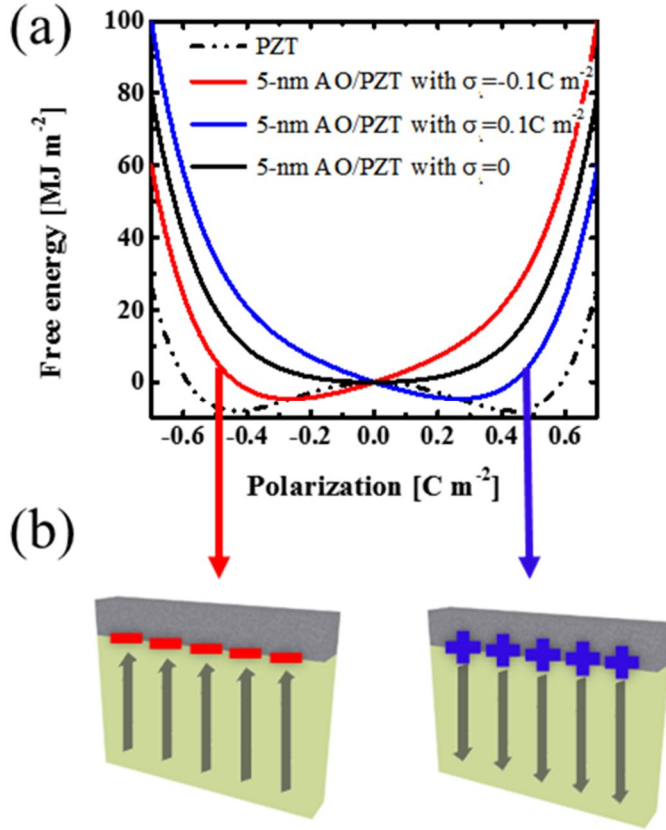
Figure 4.1. (a) Free energy diagrams of a 5nm-thick AO/PZT bi-layer structure with $\sigma_i = \pm 0.1$ Cm^{-2} and 0 Cm^{-2}. The dash line represents the free energy diagram of the PZT single layer. (b) Schematic diagrams illustrating the polarization state of AO/PZT structure with $-\sigma_i$ (left panel) and $-\sigma_i$ (right panel).

From the given energy equation 4.1 and Kirchhoff's law, the P-V relation can be written as follows,

$$V = \varepsilon_b \left(\frac{l_f}{\varepsilon_b} + \frac{l_d}{\varepsilon_d} \right) \left[2\alpha P_f + 4\beta P_f^{\;3} + 6\gamma P_f^{\;5} - \frac{\sigma_i - P_f}{\varepsilon_0 \cdot l_f} \cdot \left(\frac{\varepsilon_b}{l_f} + \frac{\varepsilon_d}{l_d} \right)^{-1} \right] \quad (4.2)$$

Figure 4.2 shows the calculated P-V curves of 5nm-thick AO/150nm-thick PZT with $\sigma_i = 0$ and ± 0.1 C m^{-2}. For the case of $\sigma_i = 0$, the P-V curve passes through the origin (P=0 at V=0) of the graph, where the slope of the curve is much higher than that of the single AO layer, suggesting that the NC effect operates. The curve does not show the characteristic S-shape of a FE film, due to the dominance of the 5nm-thick AO layer. The critical thickness of the emergence of an S-shape in AO/PZT system was calculated to be 3nm.

The P-V curves are laterally shifted from the original position (P=0 at V=0) when the σ_i is involved. As long as the σ_i remained invariant, the non-hysteretic paraelectric-like P-V curves are maintained suggesting that FE polarization does not vary in the whole voltage range. This means that the (experimental) hysteresis loop of this AO/PZT system could not be constructed from two P-V curves (equi-σ_i lines). Therefore, if an experiment shows hysteretic P-V loops, there should be a change in σ_i most probably through the charge transport across the DE layer. This may correspond to the vertical lines connecting (A), (B) and (C), (D) in figure 4.2.
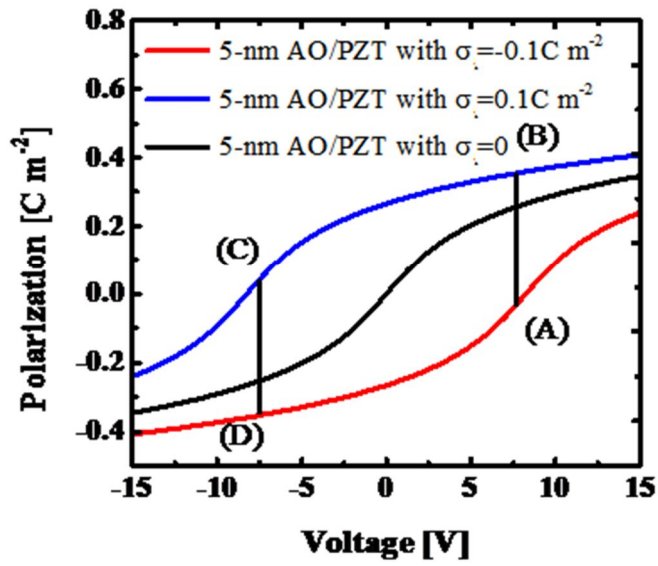
Figure 4.2 Polarization-voltage curves (equi-σ_i lines) of the 5nm-thick AO/PZT bi-layer structure with $\sigma_i = \pm 0.10$ Cm^{-2} and 0 Cm^{-2}. The equi-voltage lines are indicated by the vertical black lines.

Figure 4.3. shows experimentally measured P-V hysteresis loops of Pt/AO/PZT/Ir capacitor with various AO film thicknesses using an aixACCT TF 2000 Analyzer with a virtual ground mode, where the triangular voltage pulses with 1 kHz frequency was applied on the Pt top electrode, of which area was $10^5 \mu m^2$ and was electron-beam evaporated. All capacitors clearly showed saturated P-V hysteresis loops except for the 2nm-thick AO/PZT capacitor. From the P-V hysteresis loops, 2Pr and coercive voltage (V_c) were extracted and plotted as a function of AO thickness in figures 4.4a and b, respectively. The absolute values of positive and negative V_c increased with the AO thickness in an AO/PZT capacitor, which is consistent with the voltage distribution in a series capacitor model (AO layer takes up a certain portion of Va, so higher Va is necessary to induce change in the FE polarization state). In contrast, the 2Pr was inversely proportional to the AO thickness. While the magnitude of 2Pr in the AO/PZT bi-layer was enhanced compared to the value for the PZT single layer capacitor when the AO thickness is 2 and 3nm, which is consistent with the report by Jiang et al.[20] based on tunnel switch model of an AO layer, it becomes smaller when the AO thickness becomes > ~4nm. This critical change in P-V behavior according to the AO thickness could be understood from the total energy calculation as a function of AO thickness as shown in figure 4.5. Figure 4.5 shows a two-dimensional plot of total energy for P_f (y-axis) and AO thickness (x-axis) for $\sigma_i = 0$. The plot shows that there

are two energy minima when the AO thickness is lower than ~3nm, which corresponds to the overall FE behavior of the DE/FE stack. When the AO film becomes thicker than ~3nm, the system shows a single minimum energy, meaning that the DE/FE stack is paraelectric-like. The transition between ferroelectric-like and paraelectric-like state is closely related to the depolarization phenomenon in ferroelectric thin films with a finite non-ferroelectric layer. The depolarization field is inversely proportional to the capacitance of a non-ferroelectric layer. Therefore, the paraelectric-like state could emerge by high depolarization field at the thicker dielectric layer in DE/FE bi-layer system. In AO/PZT system, due to relatively low dielectric constant of AO layer, such thin AO layer (~3nm) could effectively destabilize the spontaneous polarization. Hence, the energy landscape of the DE/FE stack with AO thicknesses > 3 nm shows a single minimum at P = 0 meaning that the stacked layers should not show hysteretic P-V curves if no σ_i effect is involved. In contrast, the P-V curve of the 2 and 3nm thick AO/PZT samples corresponds to the genuine hysteretic FE switching, mediated by the reverse domain nucleation and growth. Thus, samples with 2 and 3nm are excluded for further discussion in this work. The hysteretic P-V loops of the samples with thicker AO layer, therefore, must be induced by the change of σ_i, probably from the charge transport across the AO layer. It needs to be noted that this type of calculation is not possible when the Landau-type energy equations, i. e. $U = \alpha P^2 + \beta P^4\ldots$, are attempted to be used for both AO and

PZT layers, because the AO layer does not follow the Landau-type energy equation. Therefore, equation 4.1, which describes the additional electrostatic energy due to the depolarization field effect, in addition to the Landau-type energy function of PZT layer, is useful for such cases.
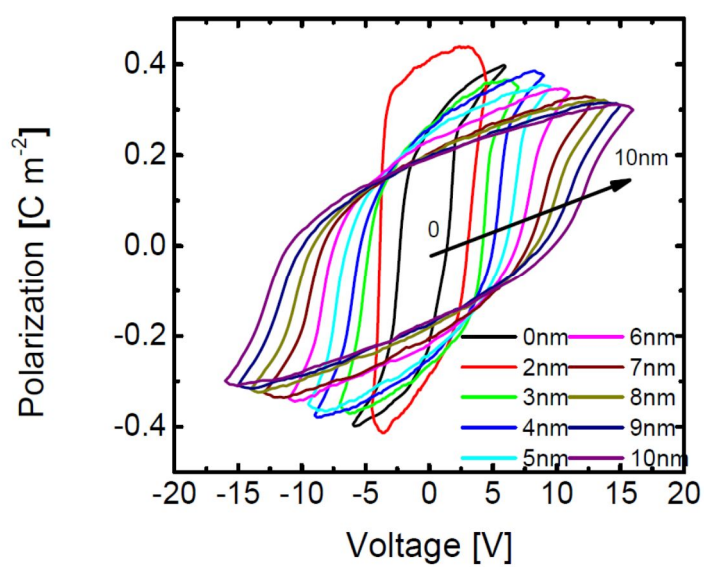
Figure 4.3 Polarization-voltage hysteresis loops of Pt/AO/PZT/Ir capacitor with various AO thickness
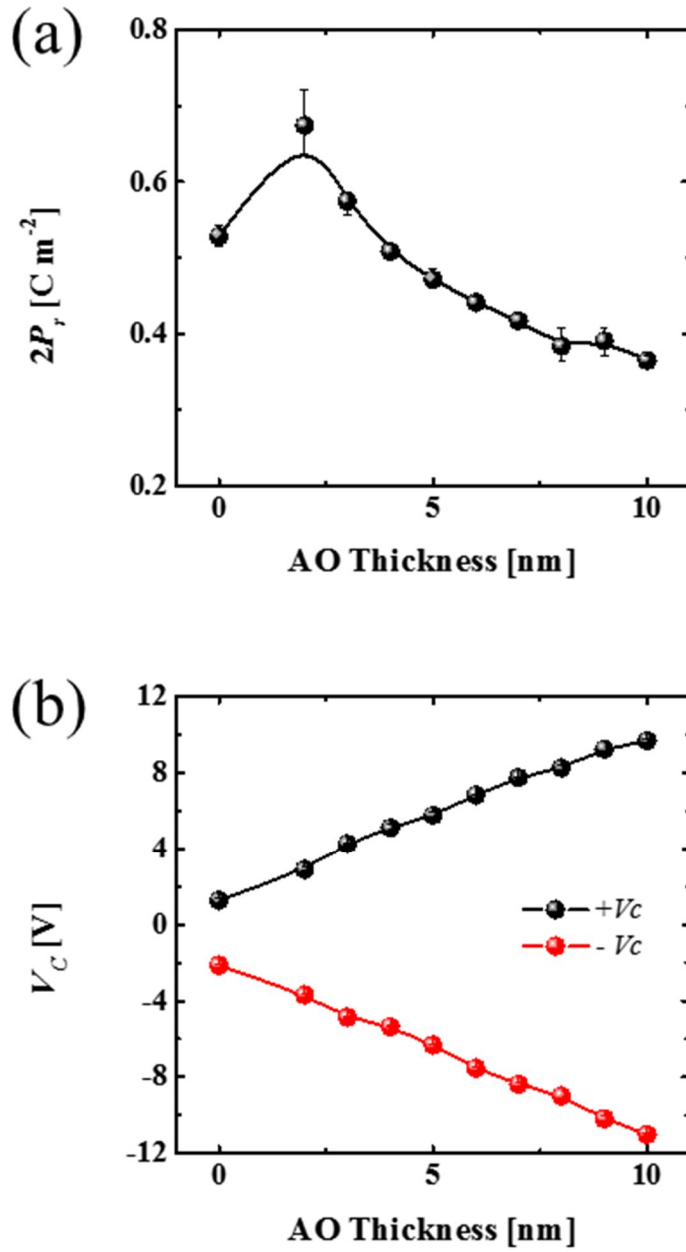
Figure 4.4 (a) Remanent polarizations values and (b) coercive voltages of Pt/AO/PZT/Ir capacitor with various AO thickness.
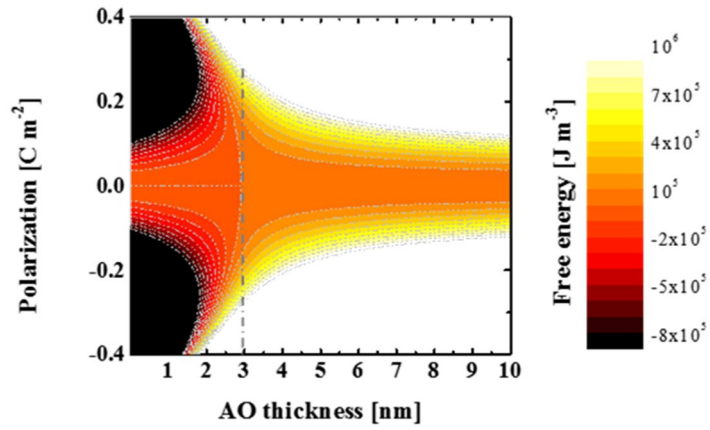
Figure 4.5 The free energy diagram of AO/PZT structures as functions of AO thickness. The dash line indicates the transition points between ferroelectric-like state (with double well potential) and paraelectric-like state (with single well potential).

The P-V curves of AO/PZT capacitors with different AO thickness (4~10nm) are shown separately in figure 4.6-4.7 (dotted data points). The upper and lower branches of the experimental P-V loops are fitted with positive and negative values of σ_i, which are assumed to be constant across the whole voltage region, using equation 4.2 and the best fit results were displayed as red lines in figure 4.6-4.7. The material parameters of equation 4.2 used for fitting can be found in Table II. For all AO/PZT capacitors, the simulated results agreed very well at the upper and lower portions (P saturated region) of P-V curves. This indicates that the capacitor charging process well followed a thermodynamically equilibrium pathway without any σ_i change in the voltage regions where the theory fits the experimental results. However, there are certain voltage regions where the theory does not fit the experiment, which are believed to be due to the σ_i change. From these fitting results, σ_i values can be estimated as a function of AO thickness, which are depicted in figure 4.8.

It is noteworthy that the estimated σ_i values were invariant ($\sim\pm0.1$ C m^{-2}) under all AO layer thickness range. On the other hand, the P-V loops started deviating from these equi-σ_i lines when the V_a reaches the threshold (V_t). The values of V_t were also plotted as a function of AO thickness in figure 4.9a. At these $V_a = V_t$ values, the threshold field ($E_{AO}*$) for charge exchange can be estimated from the equation 4.3 below, and the results are plotted in figure 4.9b.

$$E_d = \frac{V}{\varepsilon_d}\left(\frac{l_f}{\varepsilon_d}+\frac{l_d}{\varepsilon_d}\right)^{-1} - \frac{\sigma_i - P_f}{\varepsilon_0 \cdot l_d}\cdot\left(\frac{\varepsilon_b}{l_f}+\frac{\varepsilon_d}{l_d}\right)^{-1} \qquad (4.3)$$

, where in this case V is V_t shown in figure 4.9a. When the V_a exceeds the V_t, the change of σ_i occurred and the ferroelectric polarization switching proceeded until reaching another thermodynamically stable state. The values surprisingly came out to be almost constant without large deviation (~±10MV/cm) for all the AO thickness examined. Therefore, it can be inferred that when the field across the AO layer reaches $E_{AO}*$, a common phenomenon occurs for all samples as described below. However, the transition trajectories between two stable states in figure 4.6-4.7 did not directly coincide with the equi-voltage lines (vertical lines) as expected in figure 4.2. This might arise from the time dependent change in σ_i. Considering the fact that the leakage current through the AO layer could govern the change of σ_i in an AO/PZT system, the speed of transition could be comparable to that of the P-V measurement. It is estimated that a high current density over 0.01 A cm^{-2} is needed to complete the transition within a single voltage cycle, and this current density corresponds to a typical Fowler-Nordheim tunneling (FN tunneling) in a thin oxide film.[28] The current density of FN tunneling (J_{FN}) is given by[29]

$$J_{FN} = \frac{q^3}{16\pi h\phi_b}E_d^2 \exp\left[-\frac{4}{3}\frac{\sqrt{2m_d^*}\phi_b^{3/2}}{\hbar q}\frac{1}{E_d}\right] \qquad (4.4)$$

, where m_d^* is the effective mass of carrier in DE, and ϕ_b is the barrier height of metal/DE interface. For Pt/AO interface, the ϕ_b of electron tunneling (5.0 eV) is larger than that of hole tunneling (3.7eV), assuming fully developed band gap of the AO layer (8.7 eV) and no Fermi-level pinning.[30] For this case, the J_{FN} via hole transport can be calculated to be ~0.041A cm^{-2} for the Pt/AO interface with $E_d=10MV$ cm^{-1} and $m_d^*=0.17m_0$,[31] which quantitatively matches the estimated current density from P-V measurement. However, the actual current flow could be influenced by many other factors, such as traps (which induces trap assisted tunneling,) interface states that may change the ϕ_b for electrons and holes, and even smaller the band gap of an AO layer than the theoretical value due to its amorphous nature. Therefore, precise current fitting cannot be sought for in this work, but an approximate estimation is made that sufficient current flows to change σ_i during the standard P-V test. The almost identical change in σ_i during the given P-V test condition suggests that the identical current flows irrespective of the AO thickness, which goes along with almost identical E_{AO}^* for all AO thickness range at V_t.

From the usual anti-clockwise rotation direction of the hysteretic P-V loops and involvement of negative (-0.1Cm^{-2}) and positive σ_i (+0.1Cm^{-2}) for the lower and upper branches, respectively, of the P-V loops in figure 4.6-4.7, the change in σ_i is understood as follows. When the AO/PZT capacitor is negatively biased first with sufficient voltage (on Pt top electrode) the

interfacial σ_i becomes $-0.1 Cm^{-2}$, due to the electron injection from the Pt top electrode into the AO/PZT interface. During the subsequent V_a sweeping to maximum value, σ_i starts changing to positive value at $+V_t$, and is completed at a slightly higher voltage, but lower than the maximum V_a, as discussed in detail below. When a highly positive V_a is applied, two possible carrier injections can be considered; hole injection from the top Pt electrode to AO/PZT interface via tunneling through thin AO layer, and electron injection from the bottom Ir electrode through PZT layer probably via thermionic emission. The former induces positive charge accumulation and the latter induces negative charge accumulation at the AO/PZT interface, and, thus, hole injection via AO layer must be the mechanism for charge injection in this case. Much higher thickness of PZT layer compared with the AO layer also makes it less likely that the carrier injection from bottom electrode onto the AO/PZT interface to occur. Similar consideration can be made for the change in the σ_i from positive to negative under the highly negative V_a condition; in this case, the electron injection from the top Pt electrode to the AO/PZT interface is responsible for the change.

Table II Landau-Devonshire coefficient of Pb $(Zr_{1-x}Ti_x)$ O_3 (SI units).[36]

α (C^{-2} m^2 N)	$(T-T_0)$ / $2\varepsilon_0 C_0$
β (C^{-4} m^6 N)	$(10.612 - 22.655x + 10.955x^2) \times 10^{13}$ / C_0
γ (C^{-6} m^{10} N)	$(12.026 - 17.296x + 9.179x^2) \times 10^{13}$ /C_0
T_0 (K)	$462.63 + 846.4x - 2105.5x^2 + 4041.8x^3 - 3828.3x^4 + 1337.8x^5$
C (10^5)	2.1716 / $[1 + 500.05(x - 0.5)^2] + 0.131x + 2.01$, when $0.0 \leq x \leq 0.5$
	2.8339 / $[1 + 126.56(x - 0.5)^2] + 1.4132$, when $0.5 \leq x \leq 1.0$

89
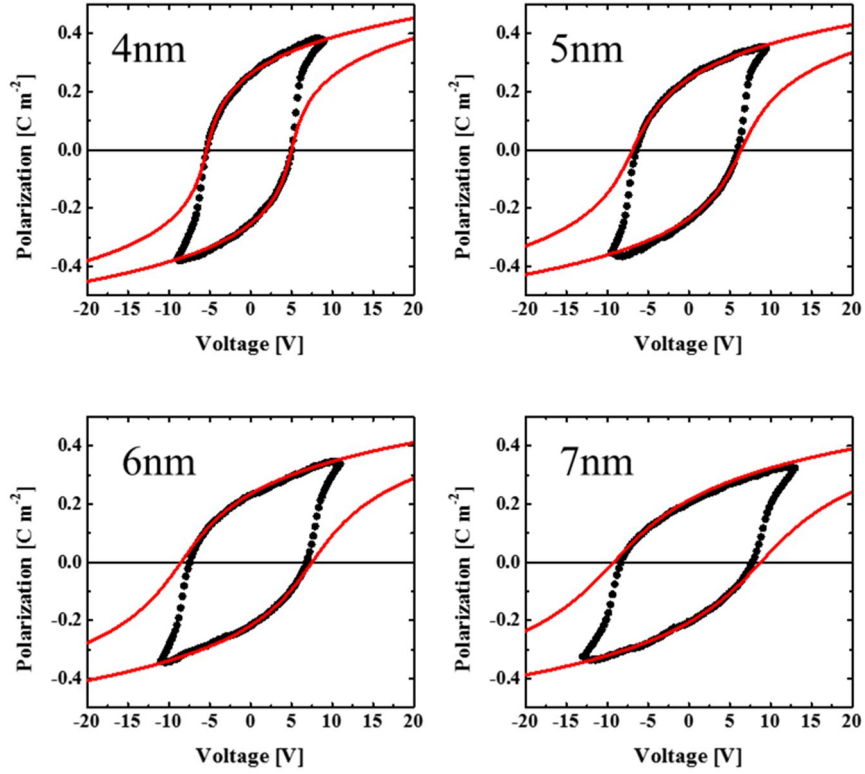
Figure 4.6 Separated polarization-voltage hysteresis loops of Pt /4nm~7nm-thick AO / PZT/ Ir capacitor. The red lines represent simulated equi-σ_i lines using equation 3.2.
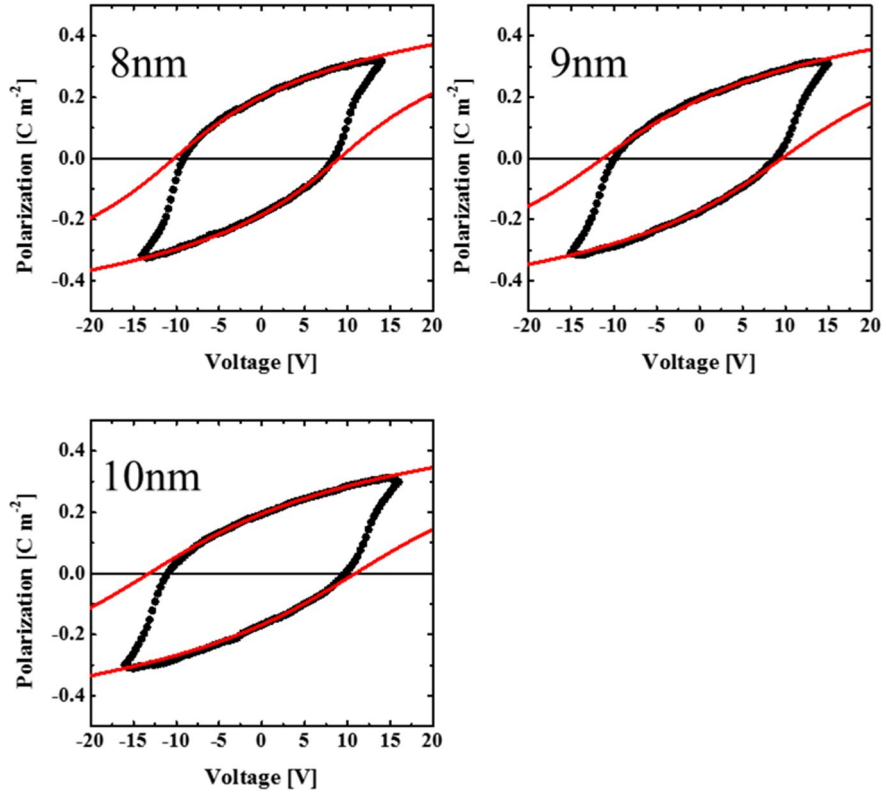
Figure 4.7 Separated polarization-voltage hysteresis loops of Pt /8nm~10nm-thick AO / PZT/ Ir capacitor. The red lines represent simulated equi-σ_i lines using equation 3.2.
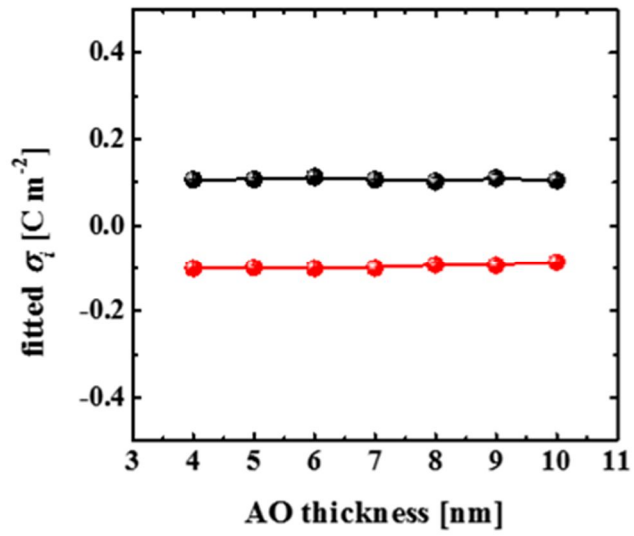
Figure 4.8 Fitted σ_i values from Pt/4~10nm thick-AO/PZT/Ir capacitor.
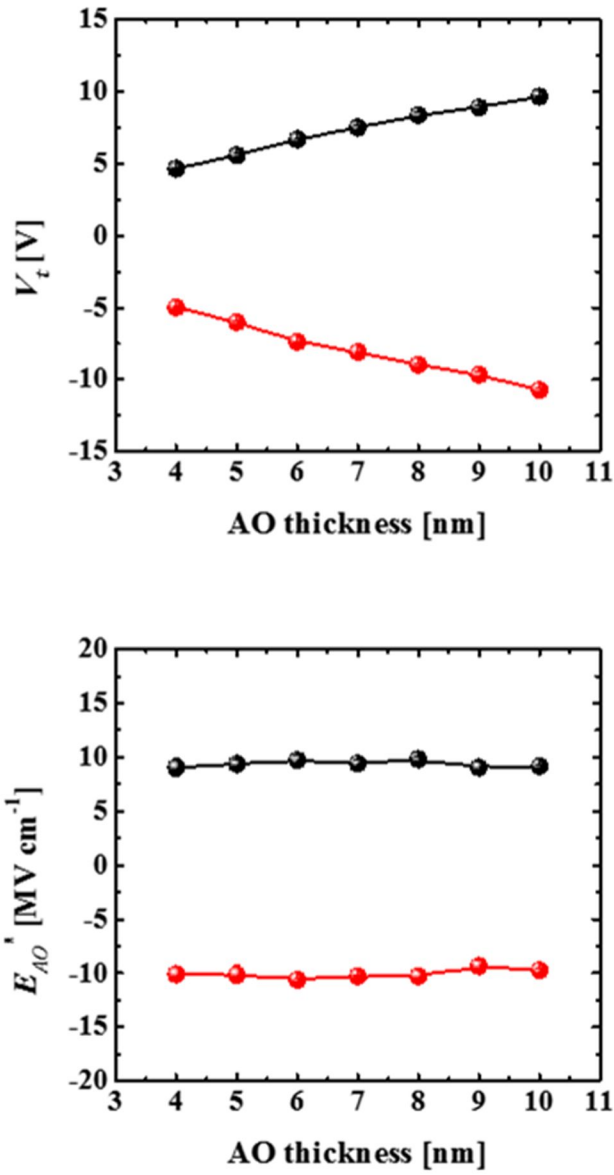
Figure 4.9 (a) Extracted V_t from Pt/4~10nm thick-AO/PZT/Ir capacitor. (b) The calculated electric fields of AO layer at V_t using equation 4.3.

The remaining questions are why the transition started at such a certain (high) $E_{AO}*$ and a single specific value of σ_i is achieved irrespective of the different AO thicknesses for all the AO/PZT capacitors. In order to answer these questions, the followings are investigated. Lower portions of figures 4.10a and b show the calculated voltage applied to the AO layer (V_{AO}) as a function of V_a with various σ_i values in 4 and 8nm-thick AO layers, respectively. The calculations were performed using equation 4.3 with extracted P_f -V_a data from figure 4.6-4.7. The black lines in figures 4.10a and b refer to the condition for $V_{AO}=V_a$, and at this condition, the potential drop only occurs across the AO layer. And the energy band of the PZT layer remains at a "flat" configuration under this condition, which can be induced by the balance between the depolarization field and the external field.[19] Therefore, at each σ_i value, when the calculated V_{AO} is higher than $V_{AO}=V_a$, i. e. $V_{AO} > V_a$, the voltage on PZT layer (V_{PZT}) must be negative to always maintain $V_a = V_{AO} + V_{PZT}$. This means that this condition may correspond to the NC operation of the FE PZT layer in these structures, which is actually not the case by the charge exchange as previously discussed.

For the V_a region where V_{AO} is lower than $V_{AO}=V_a$ condition, there must be certain positive VPZT across the PZT layer, which actually coincides with a quantum-well-like structure of electron confinement (negative σ_i) at the AO/PZT interface. The schematic diagram showing the energy band structures, where V_{AO} and V_{PZT} are calculated based on equation 4.3, at each state along

94

the P-V loop is included in figure 4. 12. The upper portions of figures 4.10a and b show the portions of the respective whole P-V loops in positive V_a region. It is highly interesting to note that V_t, at which the experimental P-V curves start deviating from theoretical curves (red lines), precisely coincides with the V_a at which the calculated V_{AO}, represented by the red dotted line crosses the $V_{AO} = V_a$ line in the lower portions of the figures. Therefore, when $V_a < V_t$, the quantum-well-like band structure of the AO/PZT stably retains the negative σ_i of -0.1Cm^{-2}. However, when V_a becomes equal to V_t, the PZT band becomes flat and V_{AO} increases to a very high value (see lower right corner band structure of figure 4.12, making the E_{AO}* high enough to change σ_i (+10 MVcm^{-1}) via tunneling through the AO layer. Another critical point can be found from the shape of the P-V curve during the further increase in V_a, indicated by the voltage V_{ip} in figures 4.10a and b, at which the P-V curve shape again changes abruptly. It was found that this V_{ip} value coincides with the V_a at which the $V_{AO} = V_a$ line crosses the V_{AO} calculation line with σ_i = +0.1Cm^{-2} (blue dotted line in lower portions of the figures). It was also noted that upper branches of the P-V curves can be well fitted with the calculated curves assuming the σ_i to be +0.1Cm^{-2}. Therefore, it can be understood that in the V_a region between from V_t to V_{ip}, the σ_i changes continuously from -0.1Cm^{-2} to +0.1Cm^{-2}, while the PZT band remains flat. The band tilting of AO layer increases with increasing V_a (in this V_a region, $V_{AO} = V_a$, see figure 4.12). Since there is no further increase in σ_i even when V_a further increases

to maximum voltage over V_{ip}, the V_{AO} should follow the line represented by blue triangles, meaning that PZT band tilts in an opposite direction to that of the AO layer. Therefore, this structure can form another quantum-well-like structure for hole as shown in upper right corner of figure 4.12. Such configuration of band (i. e. opposite tilting of the AO and PZT layer bands) can be maintained along the upper branches of the P-V loops down to $V_a = 0$. This opposite tilting of PZT band to that of AO band might be an indication that the PZT layer works as the NC layer. However, this may not be the case because Pf of the PZT layer in this voltage region coincides with almost its fully developed value, so the PZT cannot be remained at the NC state. Rather, the opposite band tilting can occur by the trapped holes at the AO/PZT interface. Similar model but with the opposite bias and charge polarities can be considered for the negative portion of V_a.

Figure 4.11 shows the comparison between the V_t and V_{ip} values estimated from the P-V loops (upper portions of figure 4.10a and b) and from the independent calculation of V_{AO} and its cross points with the $V_{AO} = V_a$ line (lower portions of figure 4.10a and b) for the AO thicknesses ranging from 4 to 10 nm. These V_{AO} values are denoted as V_{fb} and $V_{fb}*$, respectively, in figure 4.11. It can be understood that these values coincide very well with each other suggesting the accuracy of above mentioned P-V hysteresis model accompanied with the change in σ_i.

This FE switching model induced by interfacial charge trapping requires a presence of a quite high interfacial trap density (D_{it}) at the AO/PZT interface. In this regard, the estimation of D_{it} at the AO/PZT interface by Thanh et al. [32] is notable, where D_{it} of PZT as high as $\sim 1.2 \times 10^{14}$ eV^{-1} cm^{-2} was estimated. This approximately corresponds to ~ 0.2 C m^{-2} of interfacial charge when all traps are filled with carriers, meaning that the traps across ~ 0.5 eV are filled with either electrons (upper portion of band gap) or holes (lower portion of band gap) during the P-V sweep.

It is also noted that these values of σ_i only partly compensate for the polarization charge of the FE PZT layer since the maximum P_f was as high as ~ 0.4Cm^{-2}. Another critical finding from the comparison between the experiment and simulation of the P-V loops is that the V_t is similar to V_c (figure 4.6-4.7). In the single layer FE film, where FE switching is mediated by reverse domain nucleation and growth, V_c corresponds to a FE film state containing equal portions of two oppositely polarized FE domains. However, this is not the case as shown in figure 4.12. For sufficiently negative V_a, the FE polarization is pointing left (lower left corner of figure 4.12), where the negative FE bound charge of PZT layer at the bottom electrode interface is well compensated by the positive screening charge in Ir bottom electrode. However, the positive FE bound charges of the PZT layer at the DE/FE interface are partly compensated by the negative σ_i and the remaining portion of it are compensated by the negative dielectric displacement of the AO layer

at the interface. As the V_a increases to a positive value, the dielectric displacement of the AO changes from the negative value to a positive value, while the pointing left P_f of PZT layer also decreases slightly. However, σ_i is maintained invariably up to $V_a = V_t$. As the voltage increases further over V_t, σ_i starts changing from negative to positive values, which also induces polarization switching of the FE layer by the reverse domain nucleation and growth (center right corner in figure 4.12). It is believed that that the $P_f = 0$ state (i. e. identical portions of left and right FE domains in the PZT layer) occurs during the V_a sweep from V_t to V_{ip}. When V_a becomes equal to V_{ip}, the charge transfer is completed and the accompanying P_f switching also completes, as shown in figure 4.12 (upper right corner of figure 4.12). During this entire course, the FE film always maintains well developed P_f via domain structure, and, thus, this process does not involve the $P_f = V_a = 0$ state, i. e. NC state.
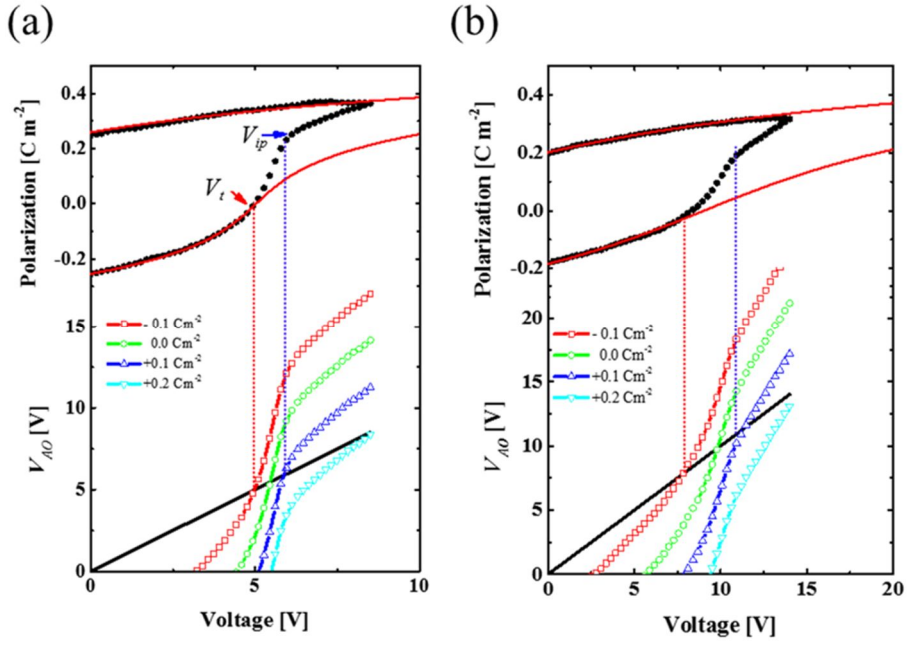
Figure 4.10 Calculated V_{AO} of (a) Pt/4nm-thick AO/PZT/Ir capacitor and (b) Pt/8nm-thick AO/PZT/Ir capacitor as function of external voltage. The calculations were performed assuming σ_i=-0.1, 0, 0.1 and 0.2 C m^{-2}.
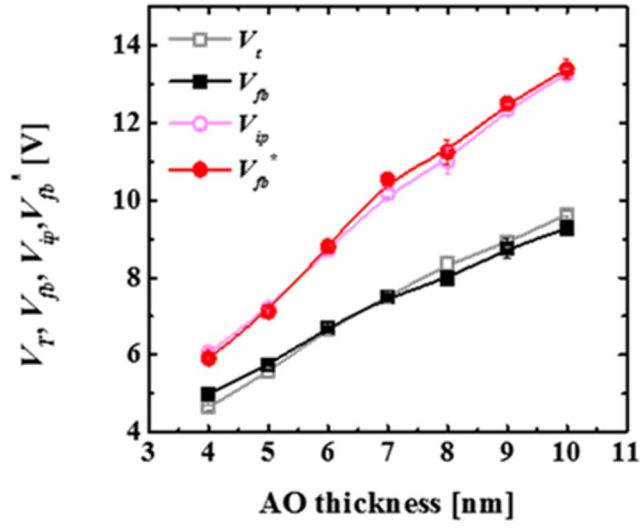
Figure 4.11 The extracted V_t (V_{ip}) value from P-V loops and calculated V_{fb}

(V_{fb}') value using equation 4.3 with fitted σ_i value from figure 4.8.
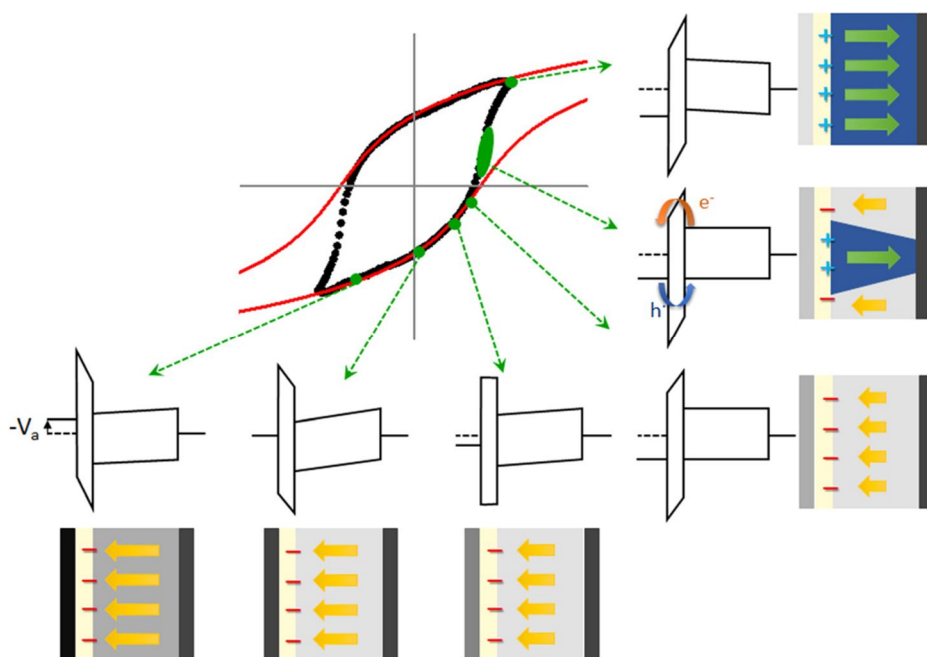
Figure 4.12 The schematic diagrams of band structure and spontaneous polarization of AO/PZT structure of each specific data points from P-V loop.

4.4. Summary

In summary, polarization switching behavior of an AO/PZT structure is examined by comparing the phenomenological thermodynamic model to the experimental P-V results. The calculation showed that the phase transition from the ferroelectric-like state to the paraelectric-like state with increasing AO thickness occurs at ~3nm thickness in the AO/PZT system. This paraelectric-like state should have known to exhibit a NC effect without permanent polarization switching if no other adverse effects are involved. However, this state can be only observable if the AO/PZT system retains the charge neutrality condition, which means that the charge exchange between outer systems (electrodes in most cases) can disrupt the operation of NC. In case of the AO/PZT system, the charge exchange mainly occurred between the electrode and AO/PZT interface trap sites by tunneling through a thin AO layer, and this interface trapping is relevant for hysteretic polarization switching behavior. The quantitative comparison between the expected voltage across AO and PZT layer during the voltage sweep with the observed P-V loop indicated that the charge exchange between the AO/PZT interface and Pt top electrode starts when $V_a \sim V_c$ for the overall AO/PZT layer, at which almost all V_a is applied to the AO layer while PZT layer is free from the voltage application. This charge exchange stops when the opposite charges with the identical density are trapped at $V_a \sim V_{ip}$. Between these two voltages,

i. e. $V_t < V_a < V_{ip}$, PZT experiences the domain switching accompanying with change of σ_i. In this region, the band configuration should vary with the areal position and time. Outside this voltage region, the AO/PZT band structure forms a quantum-well-like structure for electron (negative interface charge) or hole (positive interface charge). This work is also useful for understanding switching behavior of a nano-scale ferroelectric capacitor,[33] ferroresistive memory,[34] and ferroelectric gate field effect transistor,[35] of which ferroelectric layer experiences the imperfect polarization compensation due to the presence of an intrinsic or extrinsic DE layer (including depletion layer of semiconductor).

4.5. Bibliography

1. J. F. Scott, *in Ferroelectric Memories* (Springer-Verlag, Berlin, Germany 2000).

2. J. Ye, S. T. Lim, M. Bosman, S. Gu, Y. Zheng, H. H. Tan, C. Jagadish, X. Sun and K. L. Teo, *Sci. Rep.* **2**, 533 (2012).

3. Y. W. Yin, J. D. Burton, Y. M. Kim, A. Y. Borisevich, S. J. Pennycook, S. M. Yang, T. W. Noh, A. Gruverman, X. G. Li, E. Y. Tsymbal and Q. Li, *Nat. Mater.* **12**, 397 (2013).

4. T. D. Onuta, Y. Wang, S. E. Lofland and I. Takeuchi, *Adv. Mater.* **27**, 202 (2015).

5. Z. Wen, C. Li, D. Wu, A. Li and N. Ming, *Nat. Mater.* **12**, 617 (2013).

6. E. Y. Tsymbal and A. Gruverman, *Nat. Mater.* **12**, 602 (2013).

7. M. H. Park, H. J. Lee, G. H. Kim, Y. J. Kim, J. H. Kim, J. H. Lee and C. S. Hwang, *Adv. Funct. Mater.* **21**, 4305 (2011).

8. H. M. Christen, E. D. Specht, S. S. Silliman and K. S. Harshavardhan, *Phys. Rev. B* **68**, 020101 (2003).

9. H. N. Lee, H. M. Christen, M. F. Chisholm, C. M. Rouleau and D. H. Lowndes, *Nature* **433**, 395. (2005).

10. A. I. Khan, D. Bhowmik, P. Yu, S. J. Kim, X. Pan, R. Ramesh and S. Salahuddin, *Appl. Phys. Lett.* **99**, 113501 (2011).

11. D. J. R. Appleby, N. K. Ponon, K. S. K. Kwa, B. Zou, P. K. Petrov, T. Wang, N. M. Alford and A. O'Neill, *Nano Lett.* **14**, 3864 (2014).

12. W. Gao, A. Khan, X. Marti, C. Nelson, C. Serrao, J. Ravichandran, R. Ramesh and S. Salahuddin, *Nano Lett.* **14**, 5814 (2014).

13. V. V. Zhirnov and R. K. Cavin, *Nat. Nanotechnol.* **3**, 77 (2008).

14. G. Catalan, D. Jimenez and A. Gruverman, *Nat. Mater.* **14**, 137 (2015).

15. A. I. Khan, K. Chatterjee, B. Wang, S. Drapcho, L. You, C. Serrao, S. R. Bakaul, R. Ramesh and S. Salahuddin, *Nat. Mater.* **14**, 182 (2015).

16. C. S. Hwang, *Adv. Electron. Mater.* **1**, 1400056 (2015).

17. S. Salahuddin and S. Datta, *Nano Lett.* **8**, 405 (2007).

18. C. M. Krowne, S. W. Kirchoefer, W. Chang, J. M. Pond and L. M. B. Alldredge, *Nano Lett.* **11**, 988 (2011).

19. Y. J. Kim, M. H. Park, Y. H. Lee, H. J. Kim, W. Jeon, T. Moon, K. D. Kim, D. S. Jeong, H. Yamada and C. S. Hwang, *Sci. Rep.* **6**, 19039 (2016)

20. A. Q. Jiang, H. J. Lee, G. H. Kim and C. S. Hwang, *Adv. Mater.* **21**, 2870 (2009).

21. D. J. Kim, J. Y. Jo, Y. S. Kim, Y. J. Chang, J. S. Lee, J.-G. Yoon, T. K. Song and T. W. Noh, *Phys. Rev. Lett.* **95**, 237602 (2005).

22. Y. A. Genenko and D. C. Lupascu, *Phys. Rev. B* **75**, 184107 (2007).

23. R. A. Marcus, *J. Chem. Phys.* **24**, 979 (1956).

24. F. Bernardini and V. Fiorentini, D. Vanderbilt, *Phys. Rev. Lett.* **79**, 3958 (1997).

25. M. Nakada, K. Ohashi, H. Tsuda, E. Kawate and J. Akedo, *in Proc. IEEE Int. Symp. on Applications of Ferroelectrics*, Nara, Japan, 27-31 May 2007, edited by (IEEE, USA, 2007), pp. 528 - 530.

26. M. Li, J. Fortin, J. Y. Kim, G. Fox, F. Chu, T. Davenport, T.-M. Lu and X.-C. Zhang, *IEEE J. Sel. Top. Quantum Electron.* **7**, 624 (2001).

27. A. Cano and D. Jimenez, *Appl. Phys. Lett.* **97**, 133509 (2010).

28. M. Specht, M. Städele, S. Jakschik and U. Schröder, *Appl. Phys. Lett.* **84**, 3076 (2004).

29. J. C. Ranuárez, M. J. Deen and C.-H. Chen, *Microelectron. Reliab.* **46**, 1939 (2006).

30. Y.-C. Yeo, T.-J. King and C. Hu, *J. Appl. Phys.* **92**, 7266 (2002).

31. R. H. French, *J. Am. Ceram. Soc.* **73**, 477 (1990).

32. P. V. Thanh, B. N. Q. Trinh, T. Miyasako, P. T. Tue, E. Tokumitsu and T. Shimoda, *Ferroelectrics Lett.* **40**, 17 (2013).

33. J. Junquera and P. Ghosez, *Nature* **422**, 506 (2003).

34. R. Meyer, J. R. Contreras, A. Petraru and H. Kohlstedt, *Integr. Ferroelectr.* **64**, 77 (2004).

35. J. Hoffman, X. Pan, J. W. Reiner, F. J. Walker, J. Han, C. H. Ahn and T. Ma, *Adv. Mater.* **22**, 2957 (2010).

36. K. M. Rabe, C. H. Ahn and J. M. Triscone, *in Physics of Ferroelectrics: A Modern Perspective* (Springer, Berlin, Germany 2007)

5. Time Dependence Negative Capacitance Effects in Al$_2$O$_3$/BTO Bi-layer Capacitor.

5.1. Introduction

Achieving an extremely high charge density mostly through a high-capacitance-density device in modern electronic and energy storage devices is an impending task.[1] While the conventional approach generally includes adopting high-dielectric-constant materials, increasing the electrode area, and decreasing the dielectric thickness, these approaches faces significant challenges at a very small scale of integrated devices.[2] The negative capacitance (NC) effect, [3,4] which can be induced from a ferroelectric (FE) thin film near the P=V=0 state (P and V refer to polarization and voltage, respectively), is a highly intriguing topic recently invoked in this research field, especially when it is combined with a positive-capacitance (PC) dielectric (DE) layer.[1,5] Some of the earlier reports on this topic focused on proving the capacitance enhancement at the static mode, such as zero voltage static capacitance from impedance-type measurements,[6-8] and the current research focus is being shifted to its actual application to electronic devices. An example is to integrate the FE layer into the gate region of the metal oxide semiconductor field effect transistor (MOSFET), which in principle can decrease the subthreshold swing (SS) below its Boltzmann limit (60 mV/decade at room temperature).[3] For a given gate voltage (V$_g$), if the FE

layer in the gate stack is in the NC state, meaning that the polarity of the voltage over the FE layer is opposite that of V_g, the voltage across the rest of the gate dielectric and Si surface must be higher than Vg to make the overall gate stack voltage identical to V_g. As such, SS can be smaller than the theoretical limit. Achieving a small ¬SS is critically important to decrease the off-state leakage current of most advanced MOSFETs, which is directly related with the overall power consumption of various types of handheld devices.[9] This device type, called "ferroelectric gate field effect transistor (FEFET)," actually has a long history, dating back to its first report in 1974, and has mainly been explored as a non-volatile random access memory.[10,11] While the commercialization of FEFET has been minimally successful due mainly to the difficulty of integrating the chemically complicated FE layer, such as $(Pb,Zr)TiO_3$ (PZT), into the tiny gate area with a minimal adverse impact on the Si surface, [12,13] the physics and operation principle of memory have been very well understood. In these devices, the presence of a hysteretic drain current-gate voltage (i_d-V_g) curve according to the polarization direction of the FE layer provides the FEFET with two threshold voltages (V_{th}), which can be utilized as the two binary data states. Therefore, hysteresis, which is a characteristic of a general FE material, is the indispensable ingredient of such devices. Nevertheless, it is a very detrimental factor if the transistor is used as a switch device in a logic circuit, which requires a very well-defined and invariant single V_{th}. There have been

several reports of late on achieving SS<60 mV/decade from both a directly integrated MOSFET (i.e., an FE layer is deposited on the gate dielectric layer of the MOSFET) and an indirectly integrated MOSFET (i.e., a metal/ferroelectric/metal (MFM) FE capacitor is connected to the gate of the MOSFET through a wire),[14,15] but all the reported results clearly showed a significant hysteresis in the i_d-V_g curves, which severely limits the usefulness. According to the original model of the NC effect from the DE/FE-stacked layer suggested by Salahuddin and Datta in 2009, the hysteresis should not be involved.[3] In the ferroelectric community, the emergence of P-V hysteresis, which is believed to be the reason for the emergence of the hysteretic id-Vg curve of a FEFET, is known to be due to the involvement of reverse FE domain nucleation and growth. Such mechanism emerged to alleviate the FE system passing through the maximum energy state during the FE switching, which coincides with the P=V=0 state.[4] Therefore, the emergence of the hysteretic id-Vg curve of a FEFET can be a strong indication that some effects other than the NC effect may be involved, and the authors recently released detailed reports on the critical aspects of this subtle subject.16 Cano and Jimenez[17] reported the seriously limited NC performance of a FE layer when it forms a multi-domain structure. The earlier works by Bratkovsky and Levanyuk[18] are also very insightful in this regard as they first reported a voltage across the FE layer opposite the applied voltage due to the (temporal) mismatch between

the FE-bound charge and the compensating charge during polarization switching.

Besides, the authors elucidated the origin of such hysteretic P-V curve from a DE/FE system, which is not supposed to show such behavior due to the dominance of the DE energy over that of the FE energy, in their Landau-Devonshire (LD)-type energy formalism.[19,20] The suppression of FE polarization by the involvement of the DE layer is mainly due to the setting up of a depolarization field across the FE layer. The electrodes in the MFM structure generally provide the compensating charges (for the FE bound charges), but in an M/DE/FE/M system, the DE layer strongly interferes with such charge compensation, causing the FE polarization to become unstable. The theory and experiments on the thin-DE/thick-FE system, such as the 4- to 10-nm-thick amorphous Al_2O_3/150-nm-thick PZT (AO/PZT) as in this work, strongly suggested that the carrier transport across the thin DE layer (or the compensating charge injection in the DF/FE interface) stabilizes the FE polarization even in the stacked structure, and can show the FE hysteresis.[19] This in turn suggests that the hysteretic P-V can be suppressed if the charge injection can be inhibited. The suppression of the charge injection, however, is generally difficult because the field across the DE layer becomes extremely high when the FE layer remains in the NC state. Nonetheless, the carrier transport across the thin DE layer usually occurs through tunneling, thus taking time.[19,21] For a general P-V, using a virtual-

ground-type circuit and impedance measurements, the measurement time are in the order of ms~s, which are long enough to induce sufficient charge transport. Besides, FE switching can occur mostly through the reverse-domain nucleation and growth when the bound charges related with the reverse-domain are well compensated, and the hysteresis loops are observed. This in turn implies that if the measurements can be performed within a time regime much shorter than the integrated tunneling time for sufficient charge injection, the genuine NC effect without being interfered with by the reverse-domain formation and the accompanying hysteresis loop effect may be observed. This was indeed the case as shown in this work, where short-pulse-type measurements were systematically performed for the AO/ BaTiO$_3$ (BTO) samples with different AO layer thicknesses (5-10 nm).

5.2. Experimentals

The inset illustration in Figure 5.1 shows a schematic diagram of a Pt/AO/BTO/SuRuO$_3$ (SRO) bi-layer capacitor structure. AO thin films with 5, 8, and 10 nm thicknesses were deposited via atomic layer deposition (ALD) on epitaxially grown 150-nm-thick BTO layers with epitaxial-SRO/DyScO$_3$ (DSO) single-crystal substrates. The highly epitaxial BTO/SRO bi-layer was grown along (001) orientation on (110) DSO substrate by pulsed laser deposition. Figure 5.2 shows the X-ray diffraction spectra of 150nm-BTO/100nm-SRO/DSO structure. It is observed that out-of-plane (c-axis) lattice parameter of BTO films was elongated due to in-plane compressive strain resulting from differences in crystal lattice parameter. Therefore, BTO film is c-axis orientated, epitaxial, and coherent with the DSO substrate, under biaxial compressive strain. The amorphous dielectric layer, Al$_2$O$_3$, was deposited by atomic layer deposition (ALD). The thickness analysis of BTO/SRO/DSO and AO/BTO/STO/DSO layered structure was performed by X-ray reflectivity (XRR). Figure 5.3a and b shows the measured and the simulated XRR data for BTO/SRO/DSO and 5nm-AO/BTO/SRO/DSO structures, respectively. The measured film thicknesses are 5nm and 150nm for AO and BTO, respectively.

Figures 5.3a, b, and c show the bright field (BF) cross-section transmission electron microscopy (TEM) images of the cross section of the

sample, where b and c correspond to the images taken after the sample was illuminated by a 200 kV electron beam for ~ 10 sec, and ~20 sec, respectively. The BF images show highly uniform and smooth interfaces between the DSO substrate and epitaxial oxide films (SRO and BTO) as well as the clean and abrupt interface between the epitaxial oxide films and amorphous AO film, which was highly uniform and 5.0 ± 0.3nm-thick. The SRO and BTO film thicknesses were 100 and 150 nm, respectively. An interesting observation is that the electron beam illumination induced the crystallization of the amorphous AO film, which can be understood from the emergence of the dark-contrast in the BF images (figures 5.3b and c), while the epitaxial oxide films remained intact. This is more evidently shown in Figures 5.3d, e, and f, which are the magnified images of figures 5.3a, b, and c, respectively, near the Al_2O_3 film region. Figure 5.3g shows the high-resolution TEM (HRTEM) image of the crystallized AO film by the electron beam illumination, and the inset figure shows the fast-Fourier transformation image of the crystallized AO film portion indicated by the box. Due to the quite rapid crystallization of the amorphous AO upon the electron beam irradiation, HRTEM image of the amorphous state film could not be recorded, although the amorphous structure was initially confirmed by the naked eye. The identification of the diffraction pattern revealed that the crystallized AO film has a γ-Al2O3 spinel structure, which has an in-plane epitaxial relationship with the underlying BTO layer. Atomic layer deposited

AO films generally have an amorphous structure, due to its low deposition temperature (250 – 300 $^{\circ}$C) on a non-epitaxial substrate, such as Si/SiO$_2$, of which amorphousness could be retained after post-annealing at high temperature (up to ~ 1000 $^{\circ}$C). It appears that the epitaxial nature of the bottom layer and lattice match between the bottom oxide layer and spinel-structured AO induced such an unexpected solid state epitaxial phase transformation in the AO layer. While this is an interesting topic for further investigation, it is certainly over the scope of the present work. More importantly, however, the application of bias voltage for the electrical test will certainly not induce such solid state phase transition since the carrier transport across the AO must be much lower in the electrical test. Figures 5.3h, and i show the HRTEM images of the interface regions of DSO/SRO, and SRO/BTO, respectively. It could be understood that both interfaces are atomically flat and clear with little indication of any chemical intermixing.

Figure 5.4a and b show the topographic atomic force microscopy image of the BTO/SRO/DSO and AO/BTO/SRO/DSO structures, respectively. They show almost no difference suggesting that the growth of AO film by the ALD process on the BTO/SRO/DSO structure induced no structural damages. The root-mean-squared roughness values of the two samples estimated from an area of 1 x 1 μm^2 were 0.29 and 0.31 nm, respectively, suggesting highly smooth morphology and high quality of the films. Circular Pt top electrodes with 70 nm thicknesses and 50-100 μm diameters were

fabricated using photolithography followed by electron beam evaporation and lift-off.

The P-V measurements were performed using Aixacct TF-2000 ferroelectric tester with an AC frequency of 1 kHz in a virtual ground mode. The small-signal AC capacitance of the BTO and AO/BTO capacitors was measured using an impedance analyzer (HP4194A, Hewlett-Packard, USA) at an AC frequency of 100 kHz, and the hold time at each voltage step and the oscillation voltage were 1 sec and 0.1 V, respectively The top electrode was biased while the SRO bottom electrode was grounded during all the electrical tests.
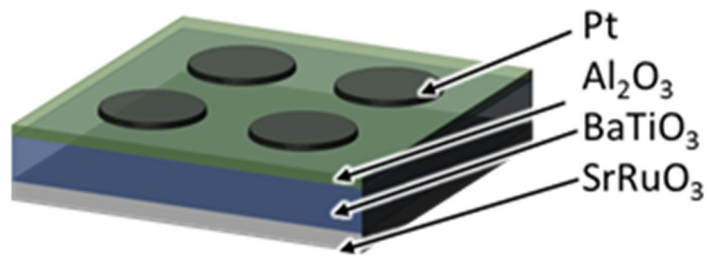
Figure 5.1 Schematic diagram of the AO/BTO capacitor.
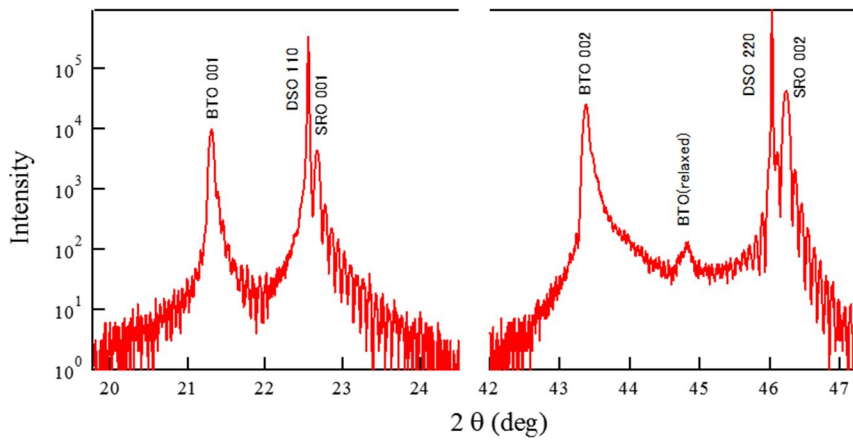
Figure 5.2 XRD spectrum of 150nm-BTO/100nm-SRO/DSO epitaxial

structure. Identical diffraction planes of each peak are marked in figure.
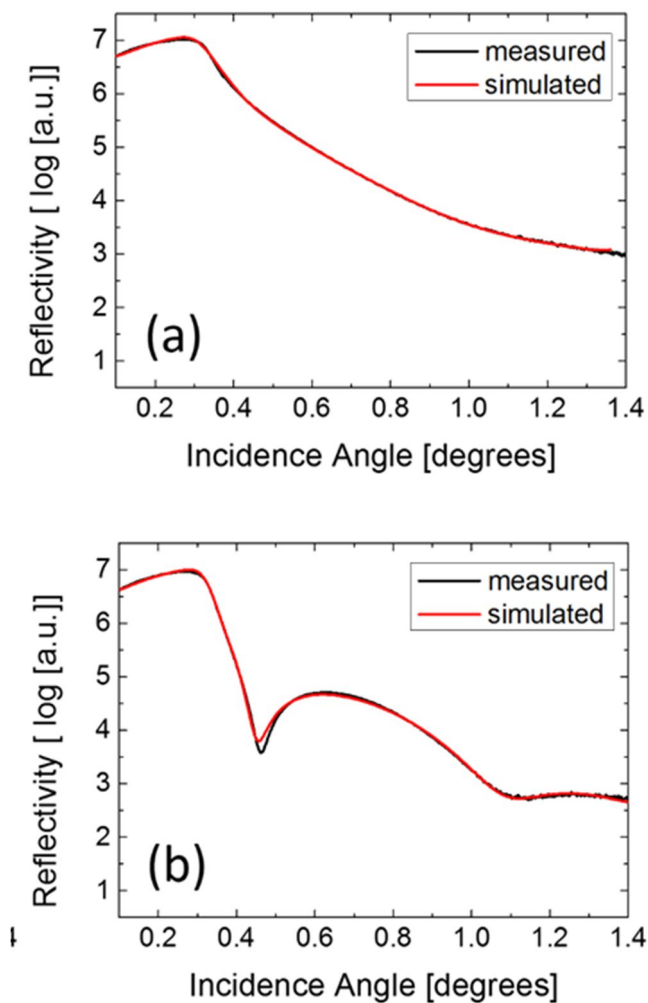
Figure 5.3 XRR spectra of (a) 150nm BTO/100nm SRO/DSO and (b) 5nm

AO/150nm BTO/100nm SRO/DSO.
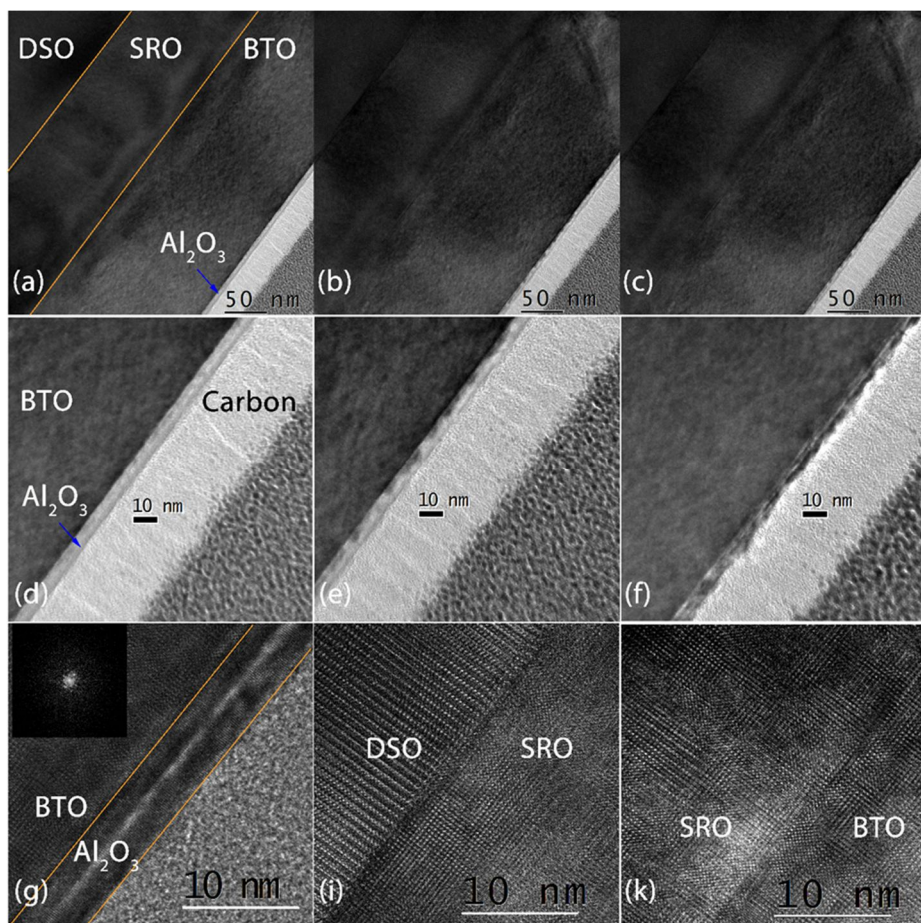
Figure 5.4 The bright field TEM images of the cross section of the AO/BTO/SRO/DSO under illumination of a 200 kV electron beam for (a) 0sec (b)~ 10 sec, and(c) ~20 sec. and the (d), (e), and (f) are the magnified images of (a), (b), and (c), respectively. The High resolution TEM image of interface of (g) AO/BTO, (i)DSO/SRO and (k)SRO/BTO. The inset figure in (g) is FFT image of AO layer.
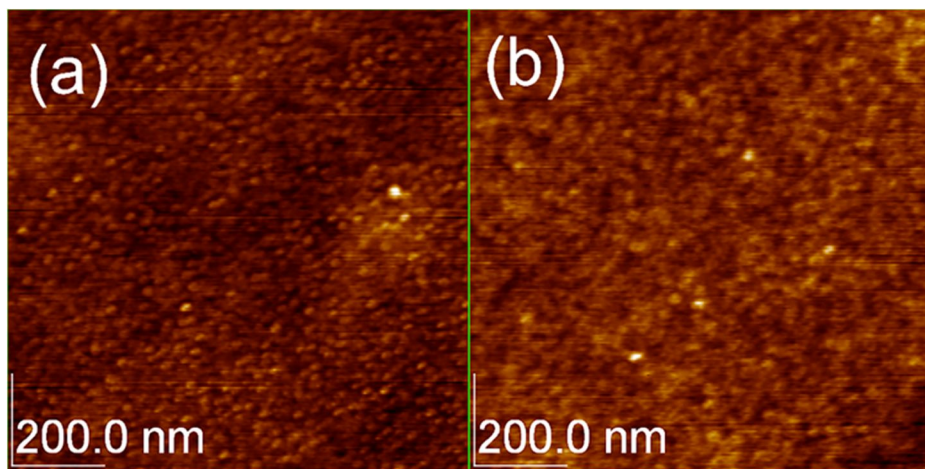
Figure 5.5 Topographic atomic force microscopy images of (a) the BTO/SRO/DSO and (b) AO/BTO/SRO/DSO structures.

5.3. Results and Discussions

Figure 5.6 shows the P-V characteristics of the BTO single-layer and AO/BTO bi-layer capacitors measured using the virtual ground mode of a FE tester (TF-2000, Aixacct, Germany) with 1 kHz triangular pulses. The P-V characteristic of the BTO single layer shows a laterally shifted hysteresis loop into the positive voltage direction, which indicates the occurrence of a polarization imprint phenomenon in the BTO film. The imprint phenomenon is common in thick epitaxial ferroelectric films due to the gradual stress relaxation along the interface's normal direction,[22] the asymmetric surface chemical state,[23] or the charge defect alignment.[24] The positive-shifted P-V curve signifies that the entire spontaneous polarization (Ps) was arranged in the positive direction at the pristine state (Ps is pointing towards the film surface direction). While such a severely imprinted behavior of a FE layer has been generally regarded as a demerit for memory applications, this property of this specific film provides this work with a highly useful methodology for examining the NC behavior. As the Ps is already uniformly pointing upward, there is no reason for the Ps to respond to a negative bias, whereas the Ps will sensitively react to the positive-bias application. Meanwhile, the P-V curves of the AO/BTO capacitor show broad deformations compared to the BTO capacitor. As the AO layer thickness increases, the positive (negative) remanant polarization changes from 0.203 (-0.295) C m^{-2} to 0.172 (-0.202), 0.203 (-0.240), and 0.204 (-0.229) C m^{-2},

and the positive (negative) coercive voltage increases from 3.6 (-0.6) V to 6.6 (-4.8), 9.5 (-7.3), and 12.2 (-10.2) V for the 5-, 8-, and 10-nm-thick AO/BTO capacitors, respectively. The shape change phenomenon in the P-V curve of the AO/BTO capacitor is consistent with the previous results of the AO/PZT capacitors.[19]

Being different from calculation results shown in chapter 3, the P-V curve of the AO/BTO bi-layer shows clear emergence of (distorted) hysteresis curve for the AO thicknesses. This phenomenon can be understood from the following calculation. From equation 3.9, P-V curve of this system can be simulated. Because of epitaxial strain, modified LD equation was adopted to correctly describe the U-P relationship as equation 5.1, which takes into account the ferroelastic energy terms,[25]

$$U_s^{epi} = (\alpha + \eta_3)P_s^2 + (\beta + \eta_{33})P_s^4 + \gamma P_s^6 + \frac{\delta_s^2}{s_{11} + s_{12}} \qquad (5.1)$$

where α, β, and γ are the Landau coefficients of the FE material; and the ferroelastic coefficients (η_3 and η_{33}) can be expressed as $\eta_3 = -(2\zeta_{12}\delta_s)/(s_{11}+s_{12})$ and $\eta_{33} = \zeta_{12}^2/(s_{11}+s_{12})$, where ζ_{12} and δ_s are the electrostrictive coefficient and biaxial strain, respectively, and s_{11} and s_{12} are elastic compliances. In addition, ε_0 represents the vacuum permittivity; l_d and ε_d are the thickness and relative dielectric constant of the DE layer, respectively; l_f and ε_b are the thickness and background dielectric constant of the FE layer[20]; and σ_i is the charge density at the AO/BTO interface. The

specific values of material parameters in equation 5.1 are shown in below;

$$\alpha = 3.3(T = -368.5) \times 10^5 \quad C^{-2}m^2N; \quad \beta = 1.37 \times 10^8 \quad C^{-4}m^6N; \quad \gamma = 2.76 \times 10^9 \quad C^{-6}m^{10}N^{[26]}; \quad \zeta_{12} = -0.034 \quad C^{-2}m^4; \quad s_{11} = -0.012 \times 10^{-12} \quad m^2 \ N^{-1}; \quad s_{12} = 6.4 \times 10^{-12} \quad m^2N^{-1} \ [25,27]; \quad \delta_s = -0.01; \text{ and } \varepsilon_b = 50 \text{ for the epitaxial BTO films.}$$

The upper and lower branches of the P-V hysteresis loop was fitted using the aforementioned formalisms under the assumption that the AO/BTO interface contains σ_i values of 0.080 (0.128) C m^{-2} and -0.120 (-0.155) C m^{-2} for 5nm (10nm) AO thickness, and the results are represented by the dash-dot lines in the figure 5.6b. The simulation fits the experimental P-V curve quite well in the voltage region of ~-1V – 10V for upper branch, and of -10V – 1V for lower branch, which means that the σ_i barely changed within each voltage region. The significant mismatch outside these voltage regions and transition between the two branches can be understood from the variations in σ_i according to the bias voltage application. For example, the P-V curve of the lower branch corresponds to the case where the negative σ_i (-0.120 C m^{-2}) is stabilized mostly in the negative bias region. However, as the voltage increased into the positive bias region, σ_i changes to positive value most probably by tunneling through the thin AO layer (indicated by an upward green arrow in the figure). As a result, when the bias voltage reaches to +10V it becomes 0.080 C m^{-2}. With decreasing bias voltage, this positive interface charge appears to be retained down to ~-1V but changes back to the

negative value also by another tunneling process (indicated by downward green arrows in the figure). Being compared with the P-V curve of a single layer AO (indicated by a black line in the figure), the P-V curves of the 5nm-AO/BTO bi-layer showed a higher slope especially in the P region with yellow background, suggesting that the capacitance of the double layer is higher than that of the single layer AO. This corresponds to the NC operation of a BTO layer.

Nevertheless, the consecutive change in σ_i occurring in this region makes it impossible to observe the desired NC effect in the AO/BTO structure. The capacitance enhancement could have been achieved if charging-discharging process follows the trajectory of (non-hysteretic) P-V curve within NC region. However, the change of σ_i during the high voltage application shifts the P-V curve from one position to another making the overall P-V curve shape to be ferroelectric-like hysteretic one. This means that an integral part of the stored charges during the charging step remained in the bi-layer capacitor as remanent polarization as well as the interfacial charge with the opposite sign during the discharging step. It has to be noted that the largely stored charge must be discharged spontaneously with voltage decrease when the capacitance was enhanced by the NC effect of the FE layer within the DE/FE bi-layer, which was not the case in this AO/BTO sample. The tunneling through the AO layer can be easily anticipated from the very high field when BTO layer operates in NC mode. The time range for the P

estimation at each V value during achieving the P-V loop was 100μs. This time constant is long enough to induce the sufficient charge transport across the AO layer which partly compensates for the polarization switching. It could be further noted that the trapped charge density was still lower than the Ps value of the BTO single layer, suggesting that induced charges on the metal electrodes were partly responsible for the stabilization of the ferroelectric bound charges.
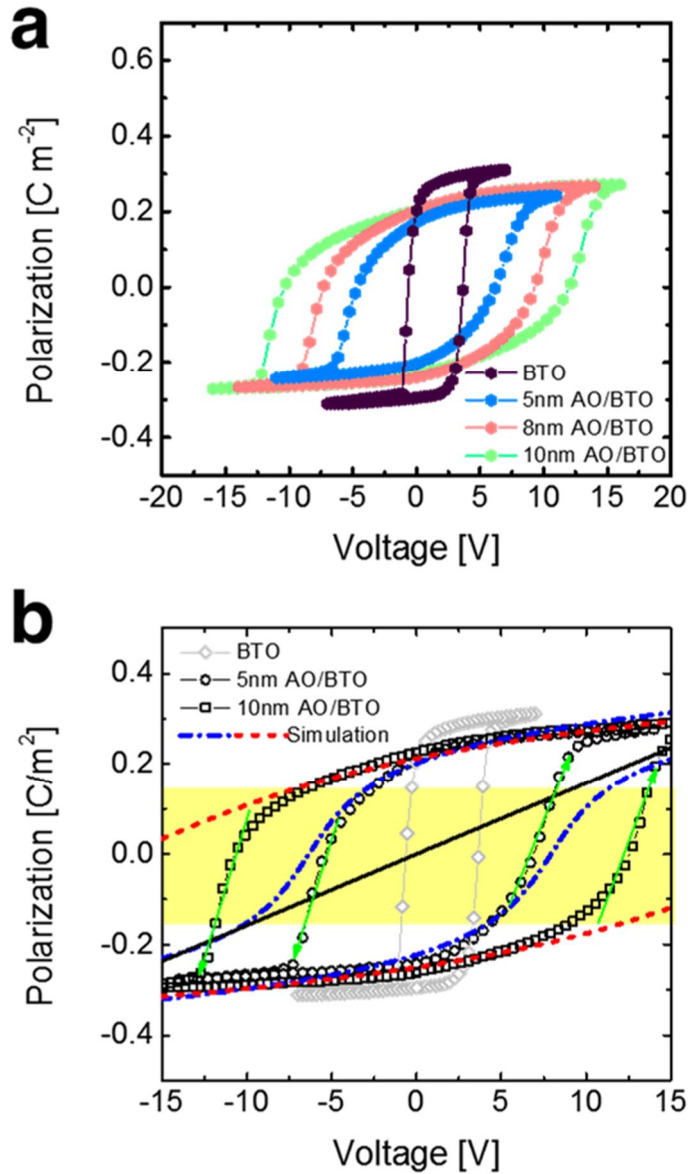
Figure 5.6 (a)-(b) Polarization-voltage characteristic of the BTO and AO/BTO capacitors. (b) The dash-dot blue and red dash lines represent the simulated P-V curves for 5nm and 10nm AO/BTO bi-layer, respectively. The black line represents a P-V response of 5nm-AO single layer. Yellow background area corresponds to the capacitance augmented region.

The small-signal AC capacitance of the BTO and AO/BTO capacitors was measured using an impedance analyzer (HP4194A, Hewlett-Packard, USA) at an AC frequency of 100 kHz, and the hold time at each voltage step and the oscillation voltage were 1 sec and 0.1 V, respectively. Figures 5.7a and b show the capacitance of the BTO and AO/BTO capacitors measured within a negative DC bias from their pristine state, and the arrows in Figure 5.7a show the DC voltage sweep sequence. There is almost no hysteresis in these negative-DC-bias regions, suggesting that no polarization switching occurs. This is consistent with the observation that the Ps of the pristine film is already aligned toward the film surface direction. With increasing AO layer thickness, a decrease in the capacitance of the AO/BTO capacitors was observed, which is an obvious result of the serial capacitance effect in the dielectric multilayer structure ($C_{tot}^{-1}=\sum C_n^{-1}$; n=layer index). The voltage dependence of the capacitance is mainly due to that of the BTO layer. The effective thickness ($l/\varepsilon_r=\varepsilon_0/C$) of each capacitor was statistically estimated from the capacitance at a DC bias of 0 V. Figure 5.8 shows the effective thickness of each capacitor, and the equivalent AO thickness ($l_{AO}*$) of each AO/BTO capacitor was calculated using the theoretical AO dielectric constant (8.9) from the relation of $l_{AO}*=8.9\times[(l/\varepsilon_r)-(l/\varepsilon_r)^B]$, where $(l/\varepsilon_r)^B$ is the effective thickness of the BTO single layer (3.25 ± 0.02 nm, which was estimated from the single layer BTO capacitor). The calculated $l_{AO}*$ was slightly different from the physical AO layer thickness, which was confirmed by HRTEM and

XRR. The estimated equivalent AO thicknesses were 4.18±0.50, 7.74±0.65, and 10.24±0.71 nm for the actual AO thicknesses of 5 (5±0.3), 8 (7.7±0.5), and 10 (9.8±0.5) nm, respectively. Figures 5.9a and b show the capacitances of the AO/BTO capacitor under positive DC bias. The typical butterfly-shape capacitance curves indicate that polarization switching occurred in all the capacitors, and the peak voltages are almost identical to the positive coercive voltages. The theoretical capacitances of the AO single layers were also calculated by assuming the relative permittivity of the AO layer as 8.9. The obtained values are shown in Figures 5.7b and 5.9b, and the data in Figures 5.7a and 5.9b are appended for comparison. None of the AO/BTO capacitors showed a sign of capacitance enhancement compared to the AO single layer. This is due to the sufficiently long (almost static) time scale of the AC capacitance measurements, which allowed sufficient time to change the interface charge state according to each DC bias condition. Therefore, the pulse charging system was adopted not to allow sufficient time for the charge injection but to acquire a direct evidence of the NC effect in the AO/BTO structure.

Figure 5.7 (a)-(b) Small-signal AC capacitance of the BTO and AO/BTO capacitors swept by negative DC bias voltages; and the horizontal dotted lines in (b) indicate the theoretical values of the AO single-layer capacitance for each AO layer thickness.
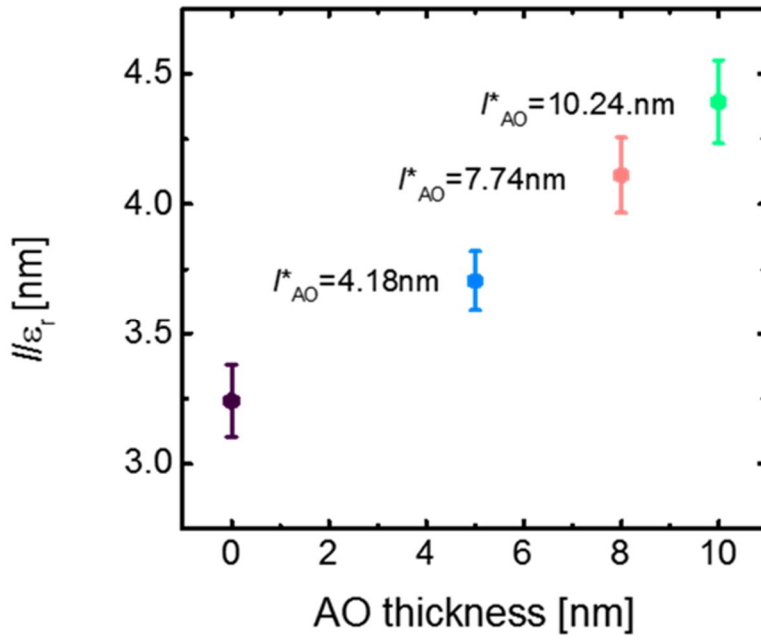
Figure 5.8 Effective thickness of the BTO and AO/BTO capacitors calculated from the capacitance value at zero DC bias in figure 5.7
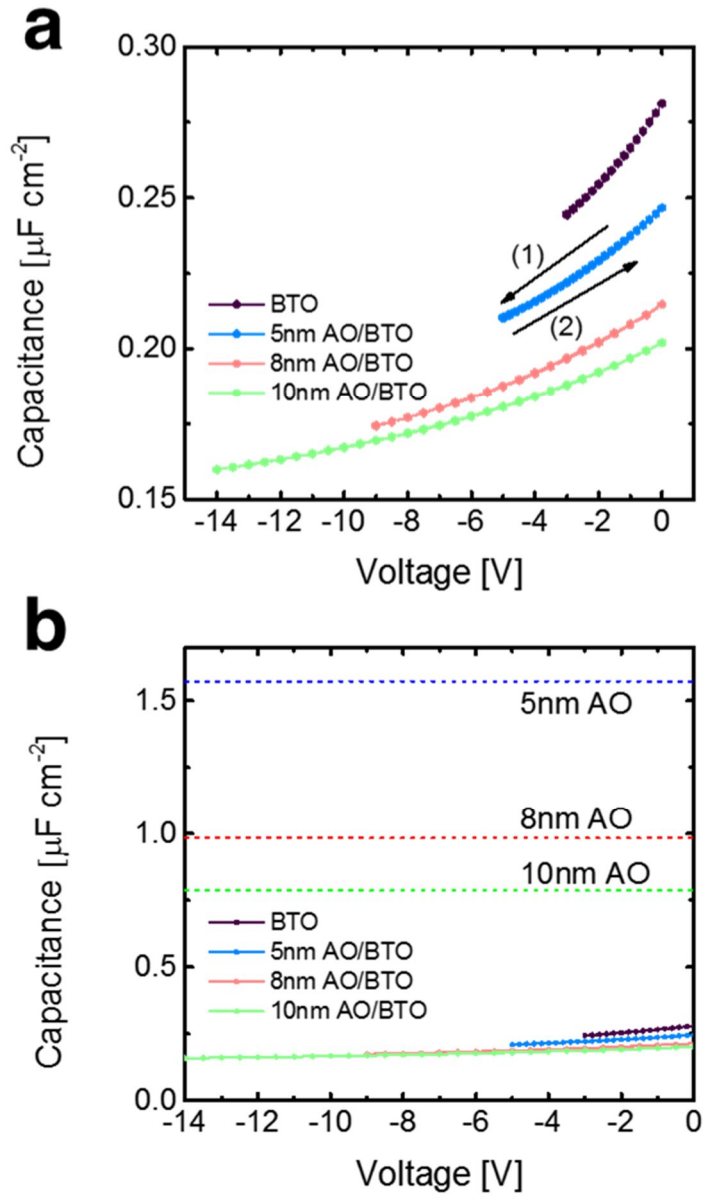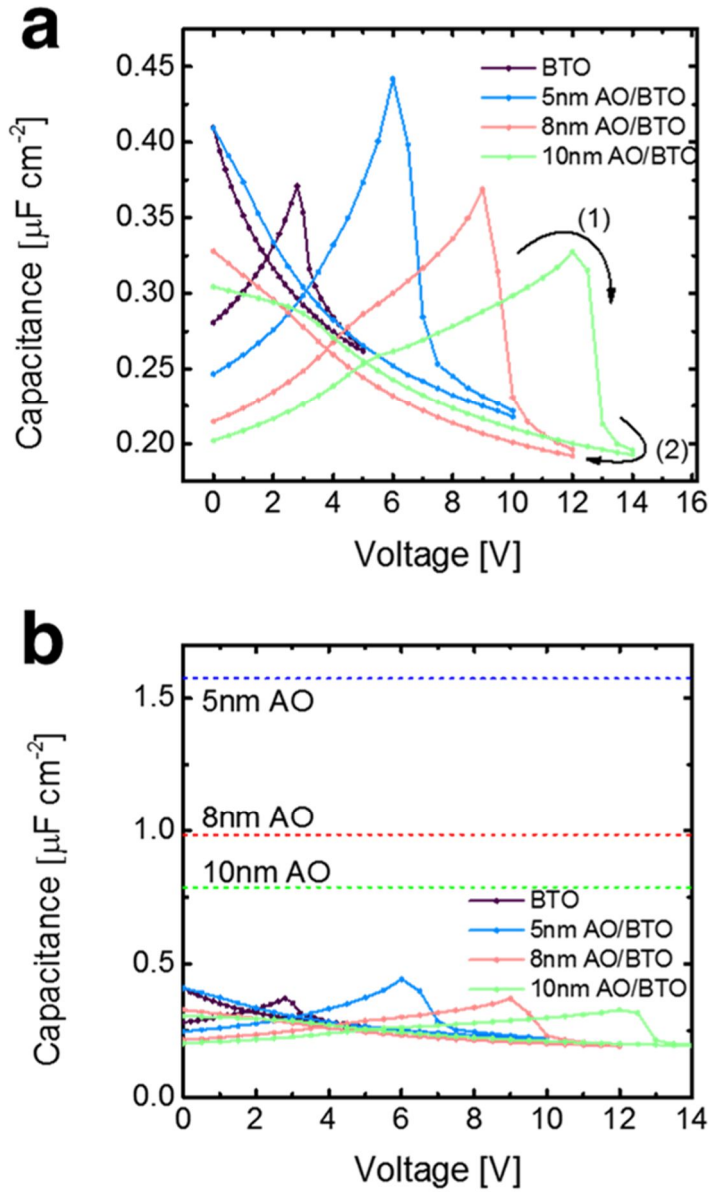
Figure 5.9 (a)-(b) Small-signal AC capacitance of the BTO and AO/BTO capacitors swept by positive DC bias voltages; and the horizontal dotted lines in (b) indicate the theoretical values of the AO single-layer capacitance for each AO layer thickness.

Figure 5.10 shows a circuit diagram equivalent to the pulse measurement system, where the pulse generator (Agilent 81110A/81111AW, Agilent, USA), AO/BTO capacitor, and digital oscilloscope (TDS684C, Tektronix, USA) were serially connected. A 500-ns-wide square pulse was used for capacitor charging, and the time-resolved capacitor charging current (i_C) was monitored using an oscilloscope with 50 Ω internal impedance. Figure 5.11 shows the time-transient i_C of the 8-nm-thick AO/BTO capacitor with 3-17 V input pulse voltages. The i_C trends in the charging (0≤t<500 ns) and discharging (t≥500 ns) periods are consistent with the typical step responses of the serial RC circuit, which is given by

$$i_C = \frac{V}{R} \cdot e^{-\frac{t}{R \cdot C}} \tag{5.2}$$

From this measurement, the capacitor's stored and released charges (Q_c and Q_d) during the charging and discharging periods can be obtained by integrating the i_C with the time. Especially, when the i_C converges to zero at the end of the pulse, the serial resistance component can be ignored in the capacitor charge analysis, as follows:

$$\int_0^{t_f} i_C(t)dt = (-RC) \cdot [i(t_f) - i(0)] = C \cdot V = Q \tag{5.3}$$

The charge measurement method from this pulse charging system was verified using a non-ferroelectric $ZrO_2/AO/ZrO_2$ (ZAZ) thin-film capacitor.

The differential capacitance of the ZAZ capacitor was measured using an impedance analyzer (HP4194A, Hewlett-Packard, USA) at the 10 and 100 kHz AC frequencies (Figure 5.12 inset). Figure 5.12 shows the amount of charges of the ZAZ thin-film capacitor at different applied voltages measured from a pulse charging system, and an impedance analyzer confirming the validity of the pulse measurements.

Figures 5.13a and b show the variations of the Q_c and Q_d values of the BTO single layer and the 8-nm-thick AO/BTO bi-layer capacitor. The Q_c-V curves in both cases can be divided into two distinguishable charging stages. In the lower-voltage region, the Q_c-V curves showed a gradual increase following the linear capacitor charging behavior ($dQ/dV \sim$ constant, which means a linear capacitance), which approximately corresponds to a linear dielectric response by a background dielectric constant of the BTO films. When V was increased to ~5 and ~6.5 V for the BTO and the 8-nm-thick AO/BTO, respectively, an abrupt change in the slopes of the Q_c-V curves and a nonlinear capacitor charging behavior was observed in both cases. By contrast, the increment of the slope was not shown in both capacitors over the whole voltage range when negative polarity pulses were applied (Figure 5.14), which is consistent with the results shown in Figure 5.7. Considering the initial direction of Ps in the BTO films, it can be concluded that the nonlinear charging stages are closely related with the switching dynamics of Ps in the BTO layer. While the BTO single-layer capacitor showed a much

smaller Q_d across the high-voltage region, which must be related with FE polarization switching, the Q_d of the 8-nm-thick AO/BTO bi-layer capacitor closely follows the Q_c up to 14 V, suggesting that the FE switching in this case was efficiently suppressed. This is in stark contrast to the fluent FE switching of this capacitor with a 9.5 V coercive voltage in Figures 5.6a.

To examine the influence of polarization switching on the nonlinear charging behavior, the residual charge (Q_{res}, the red symbol in Figures 5.13, which is approximately proportional to the permanent change of Ps in the BTO layer, was calculated by integrating i_C with respect to the time from 0 to 1 μs. It is clearly shown that the starting voltages of Q_c and Q_{res} deviating from the linear behavior are identical in the BTO single-layer capacitor, meaning that FE polarization switching induced the nonlinear capacitor charging behaviors. In these cases, the available charge through the pulse charging-discharging process is identical to Q_d ($Q_d = Q_c - Q_{res}$), which is much smaller than Q_c due to the charge loss related with polarization switching. Unlike the BTO single-layer capacitor, the Q_{res} of the AO/BTO capacitor remained at ~zero even in the nonlinear-charging region (up to ~14 V). Under this circumstance, the compensation of the ferroelectric-bound charge is interfered with by the AO layer, which induced a strong depolarization field across the FE layer.[20] Therefore, the depolarization field leads to the restoration of the initial Ps configuration when the voltage pulse is removed. From this operation, all the stored charges can be reversibly available during

the discharging process. This behavior shares a common aspect of the domain wall ping-pong reported by Jiang et al.[28] In that work, a sol-gel-process-derived polycrystalline PZT film was adopted, and the reverse domain was nucleated from a fully poled film using a short pulse with a bias opposite the poling direction. The pulse duration was carefully controlled to prevent the reverse domain from becoming stabilized by reaching the opposite electrode. Therefore, when the pulse was removed, the penetrating reverse domain was retracted, which was accompanied by a very-high-charge motion related with Ps. In this work, the large involvement of the polarization charge of the FE layer is identical to the previous case, but reverse domain formation was not introduced. This is probably due to the high quality of the epitaxial BTO film (reverse-domain nucleation usually starts from a defect position at the interface) with the appropriate preference of Ps from the pristine state. Although such assertion can hardly be proven directly, the highly-well-matching charging/discharging behavior with the theoretical model on the NC effect shown below strongly suggests that the AO/BTO layer in this work showed the genuine NC effect under appropriately controlled conditions.

Nevertheless, a sufficiently high voltage (>14 V) allowed charge compensation in Ps by tunneling through the thin AO layer even during such a short time period. Under this condition, part of the Qs is dissipated as FE switching charges (Q_{res}). From the Q_{res} curve, the critical voltage for the

charge injection (coercive voltage for the case of the BTO single layer) under the pulse charging condition could be estimated, and their specific values were ~5 and ~14 V for the BTO and 8-nm-thick AO/BTO capacitors. Compared to the results of the P-V and AC capacitance measurements, the charge compensation in the pulse charging condition is largely mitigated by the limited time for the charge injection. The 5- and 10-nm-thick AO/BTO capacitors exhibited similar results (i.e., a high Q_d), where the pulse voltages for inducing a significant Q_{res} were ~9.5 and ~18 V, respectively.
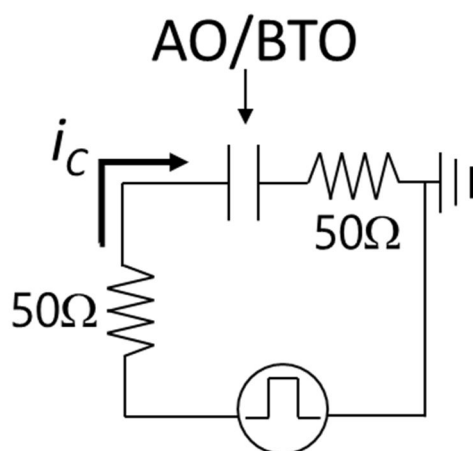
Figure 5.10 Schematic circuit diagram of the pulse charging system.
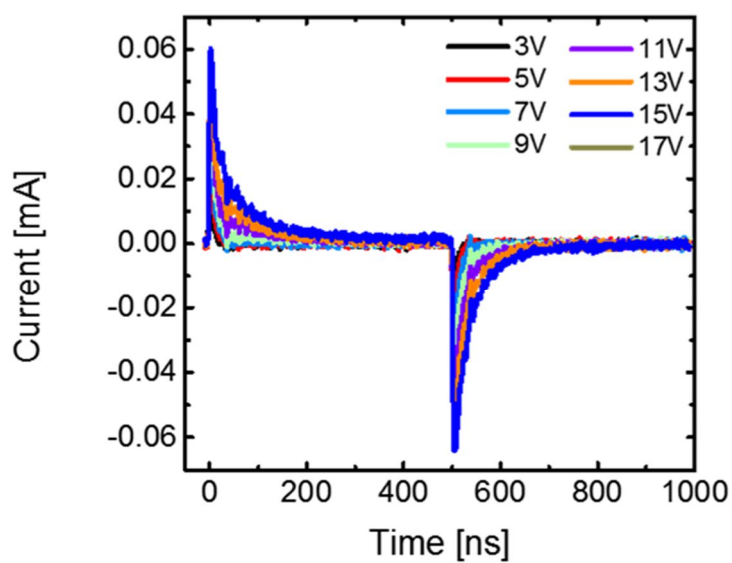
Figure 5.11 Capacitor charging current of the 8-nm-thick AO/BTO capacitor with various pulse voltages.
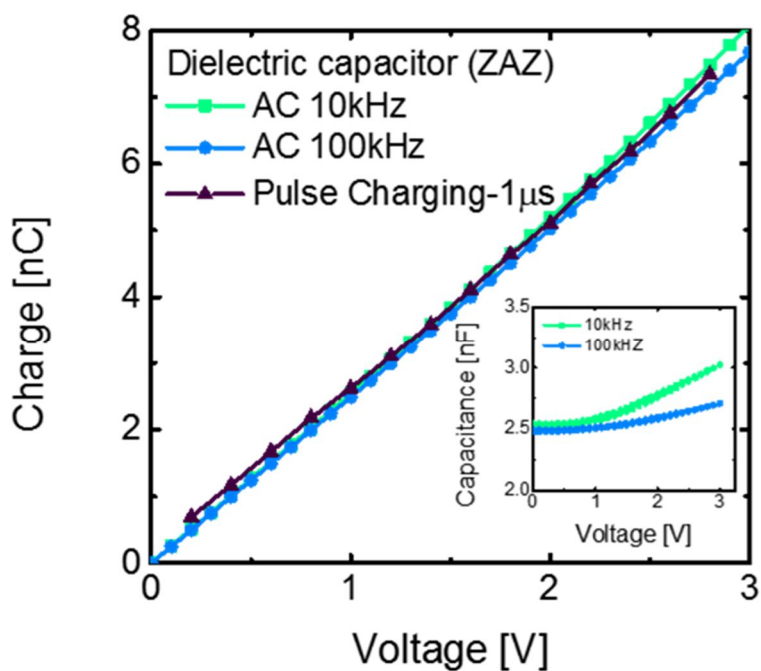
Figure 5.12 Capacitor charge-voltage curve of the ZAZ capacitor measured
by pulse charging system and through AC capacitance measurement with 10
and 100 kHz frequencies.
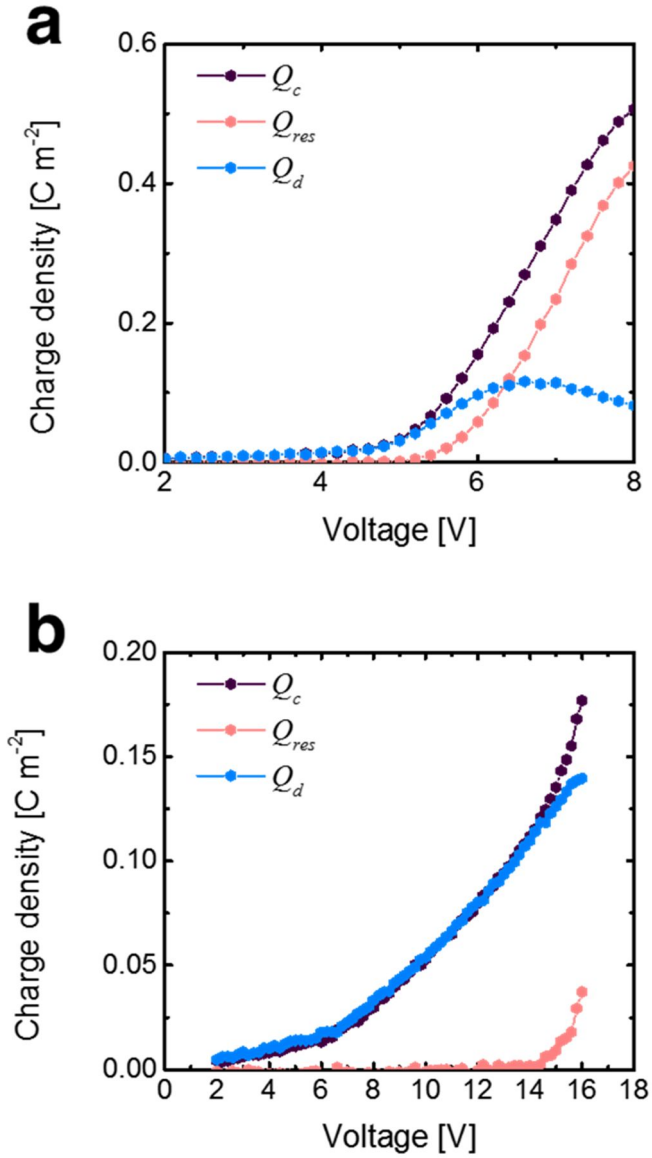
Figure 5.13 Stored charge density (Q_c), residual charge density (Q_{res}), and released charge density (Q_d) of the (a) BTO and (b) 8-nm-thick AO/BTO capacitors measured by pulse charging system with various pulse voltages.
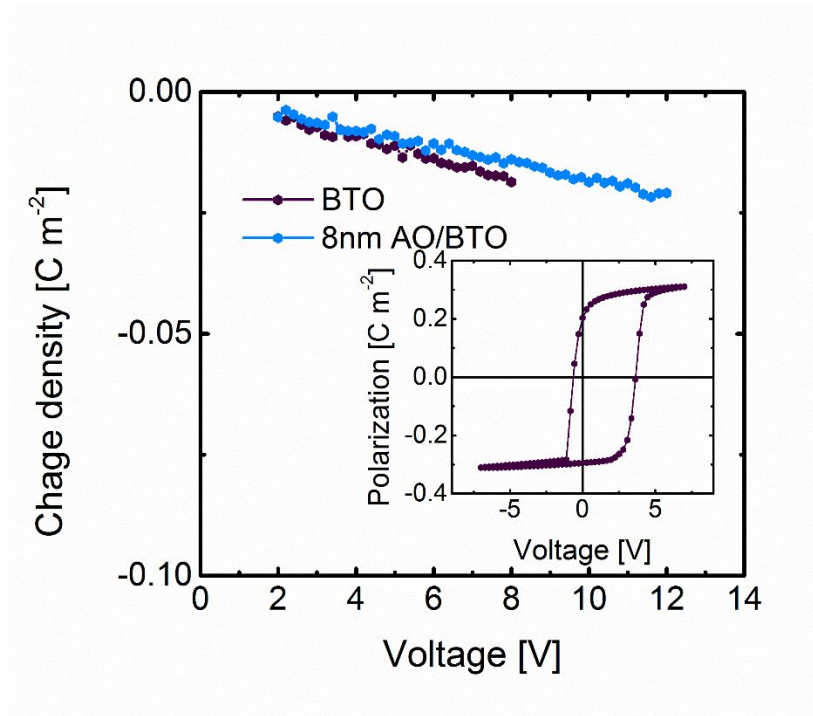
Figure 5.14 Released charge density of the BTO and 8-nm-thick AO/BTO capacitors under a negative pulse voltage. The inset figure is the polarization-voltage characteristic of the BTO capacitor reproduced from Figure 5.6.

Next, the voltage-induced charging and discharging behaviors are compared with the theory based on the LD model. The Q_d of each capacitor was also plotted as a function of the pulse voltage in Figure 5.15. In all the AO/BTO capacitors, the nonlinear capacitor discharging (and charging) stages (steep-slope regions) are clearly observed. The Ps-E equation of the FE layer in the DE/FE structure with the epitaxial strain considered can be written as follows (from equation 5.1):

$$
\begin{aligned}
E_{ext,FE} &= 2(\alpha + \eta_3)P_s + 4(\beta + \eta_{33})P_s^3 + 6\gamma P_s^5 - \frac{\sigma_i - P_s}{\varepsilon_0 \cdot l_f} \cdot \left(\frac{\varepsilon_b}{l_f} + \frac{\varepsilon_d}{l_d} \right)^{-1} \\
&= 2(\alpha + \eta_3)P_s + 4(\beta + \eta_{33})P_s^3 + 6\gamma P_s^5 - E_{dep}
\end{aligned}
\tag{5.4}
$$

Where, $E_{ext,FE}$ is the effective external field across the FE layer, which is assumed as constant over the FE layer. The last term in equation 5.4 corresponds to the depolarization field being induced by the uncompensated Ps in the FE layer. From this relation, the total electric field of the FE layer can be determined as the sum of the external electric field and the depolarization field ($E_{ext,FE}+E_{dep}$). It is noteworthy that the uncompensated polarization charge also induced an additional field into the DE layer. The Q-V relation can be derived using equation 5.5 with the continuum theory and Kirchhoff's voltage law, as in the following steps:

$$
\begin{aligned}
D(P_s) = D_{DE} = D_{FE} &= P_s + \varepsilon_0 \varepsilon_b (E_{ext,FE} + E_{dep}) \\
&= P_s + \varepsilon_0 \varepsilon_b (2(\alpha + \eta_3)P_s + 4(\beta + \eta_{33})P_s^3 + 6\gamma P_s^5)
\end{aligned}
\tag{5.5}
$$

$$V(P_s) = l_f E_{ext,\text{FE}} + l_d E_{ext,\text{DE}} = \left(l_f + \varepsilon_b \frac{l_d}{\varepsilon_d} \right) E_{ext,\text{FE}}$$

$$= \left(l_f + \varepsilon_b \frac{l_d}{\varepsilon_d} \right) \left[2(\alpha + \eta_3)P_s + 4(\beta + \eta_{33})P_s^3 + 6\gamma P_s^5 - \frac{\sigma_i - P_s}{\varepsilon_0 \cdot l_f} \cdot \left(\frac{\varepsilon_b}{l_f} + \frac{\varepsilon_d}{l_d} \right)^{-1} \right]$$

(5.6)

where D and V are the displacement and total applied voltage, respectively; and V(Ps) is an odd polynomial function of Ps with all positive coefficients. Therefore, an inverse function of V(Ps) can be defined in the entire range of V (equation 5.6). By combining equation 5.5 and the inverse function of equation 5.6, the D(V) can be determined for a DE/FE bi-layer structure. Assuming a constant imprint voltage (Vim) for a given DE/FE system (i.e., Vim≠f(V)), the Q-V relation can be defined as follows:

$$Q(V) = D(V - V_{im}) - D(V = 0) \tag{5.7}$$

The dashed lines in Figure 5.15a and the solid line in Figure 5.15b show the simulated Q-V curves using equation 5.7. The specific l_d values of each AO/BTO capacitor were taken from l_{AO}* with ε_d=8.9. Each simulation was performed assuming the invariant σ_i and V_{im} over the pulse voltage, with the specific σ_i values being -0.13, -0.15, and -0.17 C/m^2, and the V_{im} values being 4, 4.5, and 4.7 V for the AO thicknesses of 5, 8, and 10 nm, respectively. As shown in Figure 5.15, it was confirmed that the model well described the reversible charging behaviors of all the AO/BTO capacitors. To

142

examine the NC effects of the AO/BTO capacitor, the AO single-layer charging curves of each thickness were also calculated using $l_{AO}*$, and the results are plotted in Figure 5.15b (dash-dot lines). For comparison with the experimental results, the calculated curves were laterally shifted and represented as tangent lines to the Q-V curves of the AO/BTO structure. By definition, the slope of the charging curve corresponds to the differential capacitance (dQ/dV) of capacitor materials. In this regard, it is clearly seen in Figure 5.15a and b that the capacitances of the AO/BTO capacitors are higher than those of the AO single layers within a certain voltage range. The capacitance values deduced from the slopes are summarized in the Figure 5.16 inset, where the capacitance values of each AO layer were appended for comparison. These results experimentally and directly demonstrated the possibility of producing capacitance enhancement effects (i.e., NC effects) in the DE/FE systems under pulse charging conditions. By contrast, the nonlinearly boosted charging stage was not observed in the Q-V curves calculated from the AC capacitance, as shown in Figure 5.16. This indicates the variation in σ_i at the AO-BTO interface, which can be accelerated by the high leakage current of the AO layer due to the NC effects of the BTO layer. The details of such influence of the σ_i variation on the FE performance (hysteresis) have been reported elsewhere.[19,20] In short, the injected charge can induce polarization switching in the FE layer by compensating the polarization charge. Under this condition, the stable operation of the NC

effects is hindered in the DE/FE structure.

To prove the aforementioned correlation between the NC effects and charge injection (leakage current), the time dependency of the NC effect in the AO/BTO capacitor was investigated. With increasing pulse time, it is supposed that a larger charge amount can transfer to the interface at the same applied voltage. In this regard, the voltage at which charge loss occurs should appear at a lower voltage with increasing pulse length. This was indeed the case as shown in Figure 5.17; the Q_d-V of the 8-nm-thick AO/BTO capacitor curves at the 5 and 50 μs pulse lengths clearly showed charge loss at ~13 and ~11 V, respectively, whereas the 0.5 μs (500 ns) case endured up to 15 V. These results actually explain why the observation of the NC effect in the AO/BTO capacitor was hindered in the capacitance measurement with the almost-static mode.

From these results, the qualitative model of the time-dependent NC effect in the DE/FE structure can be established as follows: (i) the NC effect in the DE/FE structure should follow the theoretical prediction from ref. 20 and equation 5.4; (ii) the change of the interface charge state precludes stable NC operation and can permanently alter the polarization state of the FE layer; and (iii) this change of the interface charge state mainly occurs through a charge injection from the electrode to the DE/FE interface, which can be regarded as a leakage current (and total amount of interface charge is

proportional to the stress time). Thus, a short measurement time is required to directly observe the NC effects, where a short measurement time does not allow sufficient interfacial charge change. Nonetheless, the precise time scale is dependent on the specific materials and structural parameters of the DE/FE capacitor. Figure 5.18 shows a schematic diagram of the pulse time dependency of the NC effect in the DE/FE structure (upper panel: short pulse, which is effective for NC operation; lower panel: long pulse, which is ineffective for NC operation). The polarization switching driven by charge injection is normally considered a spatially inhomogeneous process, as depicted in Figure 5.18. Whether the domain switching in AO/BTO follows plate-like growth (2D growth, FE-dominant) or needle-like growth (1D growth, DE-dominant) is still unclear,[29] but no matter what the detailed FE switching mechanism is, such charge-injection-induced FE switching suppresses the possibility of the absolute value of P being approximately zero, which is the prerequisite for the NC effect. The slight lateral shift in the Q_d-V curves in Figure 4a towards the low-voltage region is believed to be related with the reduction in V_{im} by the redistribution or migration of the charged defects under a high-bias condition.[30-32]
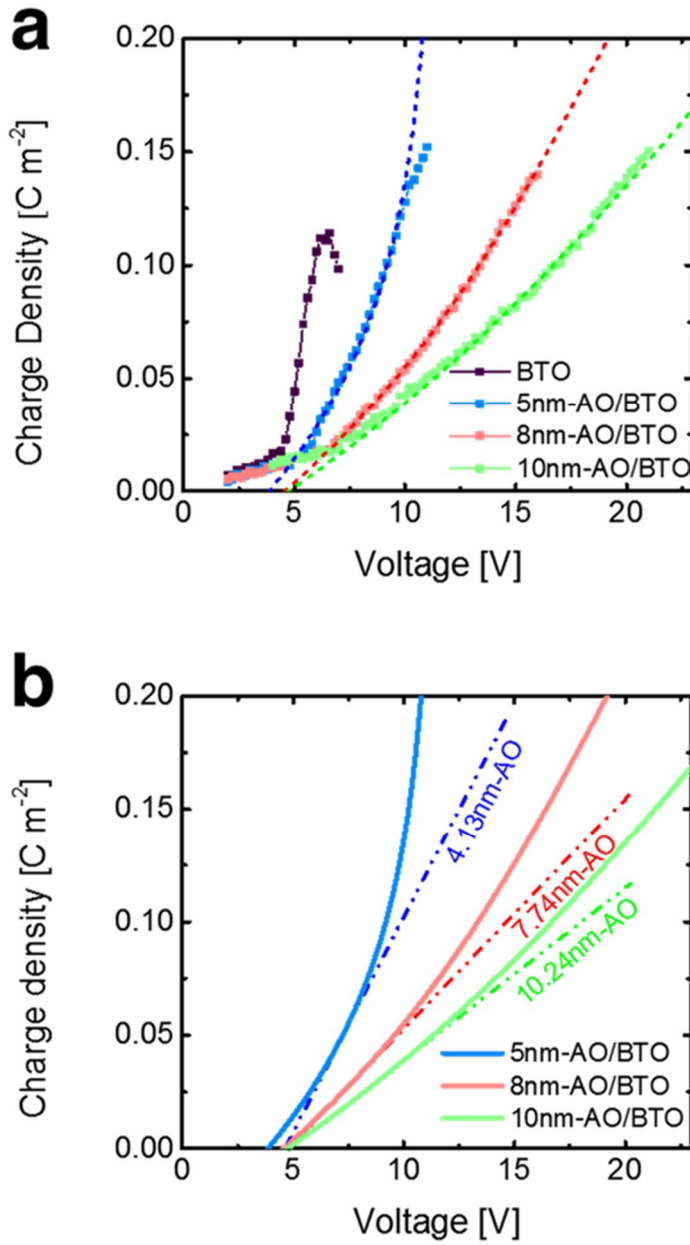
Figure 5.15 (a)-(b) Released charge density-voltage curves of the BTO and

AO/BTO capacitors. The dashed lines in (a) and the solid lines in (b) are the

theoretical results. The dash-dot lines in (b) are the calculated charge density-

voltage curve of the AO single layer.
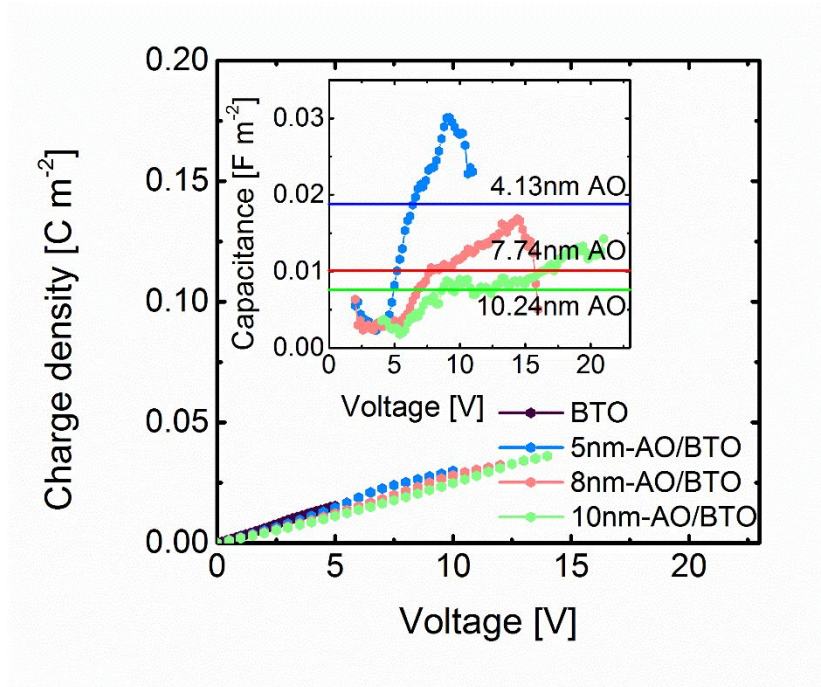
Figure 5.16 Charge density-voltage curves of the BTO and AO/BTO capacitors calculated using the AC capacitance data. The inset figure shows the capacitance (dQ/dV)-voltage relation of the AO/BTO capacitor from the pulse charging measurements.
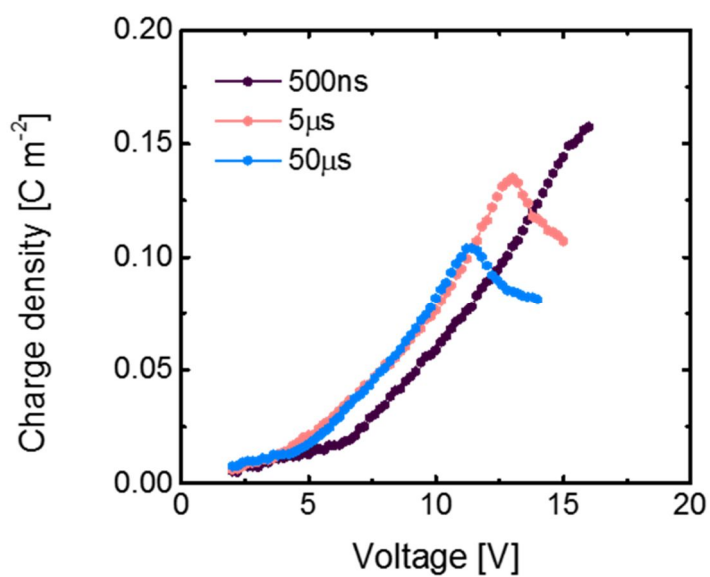
Figure 5.17 Released charge density-voltage characteristics of the 8-nm-thick AO/BTO capacitor with 500 ns, 5 μs, and 50 μs pulse widths.
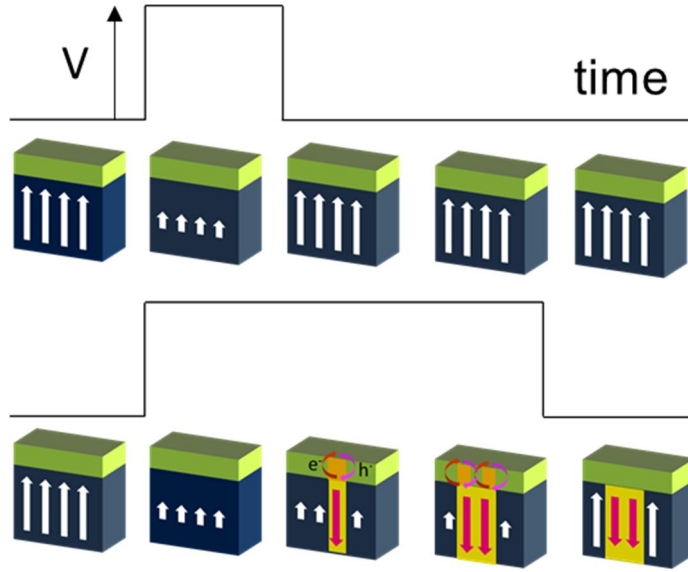
Figure 5.18 Schematic diagram of the pulse width dependency of the NC effects and the polarization switching behaviors in the DE/FE bi-layer structure.

The stability of NC operation was further confirmed by applying a series of pulses with different voltages in the 8-nm-thick AO/BTO capacitor. As shown in Figure 5.19a, the Q_d values from the +8 to the +12 V pulses were almost constant up to 1,000 pulses (500 ns pulse length), which indicates that stable NC operation can be achieved under such short and relatively weak pulse condition. A pulse voltage of +16 V, however, induced progressive polarization switching (charge injection), which can be confirmed by the upsurge of the non-zero Q_{res} value, as shown in Figure 5.19b. Hence, the Q_d value of +16 V progressively decreased with the increasing pulse number, and becomes lower than that of the +14 V pulse

case when the pulse number becomes higher than ~200. Unexpectedly, the Q_d and Q_{res} values of the +14 V pulse slightly increased at the initial stage, and the +14 V Q_d value did not show a noticeable change even when the Q_{res} value became almost identical to the +16 V pulse case at pulse > ~200. This phenomenon is believed to be related with the depoling effects during the long interval (~1 sec) between the pulses. For the case of +14 V, the partly switched domains recovered their original configuration during the interval because the switched domains were not fully stabilized due to the insufficient charge injection. For the case of +16 V, however, the already-well-stabilized switched domains remained switched during the same period, and permanent Q_d loss occurred. This can be more evidently understood from the variation of Q_c with the switching cycles shown for +12, +14, and +16 V in Figure 5.19b (right vertical axis). The initially very high Q_c for the +16 V case was due to the involvement of permanent polarization switching, which cannot be fully recovered during the subsequent cycles, resulting in the loss of the charging effect.

The hysteretic behavior in the Q_d-V curves of the 8-nm-thick AO/BTO capacitor was also investigated by applying stepwise pulse trains (pulse length at each voltage: 500 ns), as shown in the Figure 5.20a inset picture. The directions of the Q_d-V curves are indicated by the numbered arrows in the figure. Up to the ±14 V pulse, there were negligible changes in the Q_d-V curve, and as such, no hysteresis was observed, which is consistent with the

above results. At the ±16 V pulse, hysteresis started to be shown mainly within the positive-voltage region, due to partial switching, which also increased the absolute amount of Q_d in the negative-bias region. As the pulse voltage increased to ±18 V, a clearly hysteretic curve was shown, suggesting that FE switching occurred. Figure 5.20b shows the variation in the Q_{res}, which is consistent with the charge-injection-induced FE switching model. Based on the relation between Q_d-V and Q_{res}-V in Figures 5.20a and b, it was confirmed that the excessive charge injection at the sufficiently high voltage induced the hysteresis behavior and eliminated the NC effects in the AO/BTO capacitor. In addition, the initial charging state could not be recovered after applying a -18 V pulse. This phenomenon is believed to be attributable to the damage of the AO layer due to the high leakage current level or the space charge redistribution within the BTO layer.
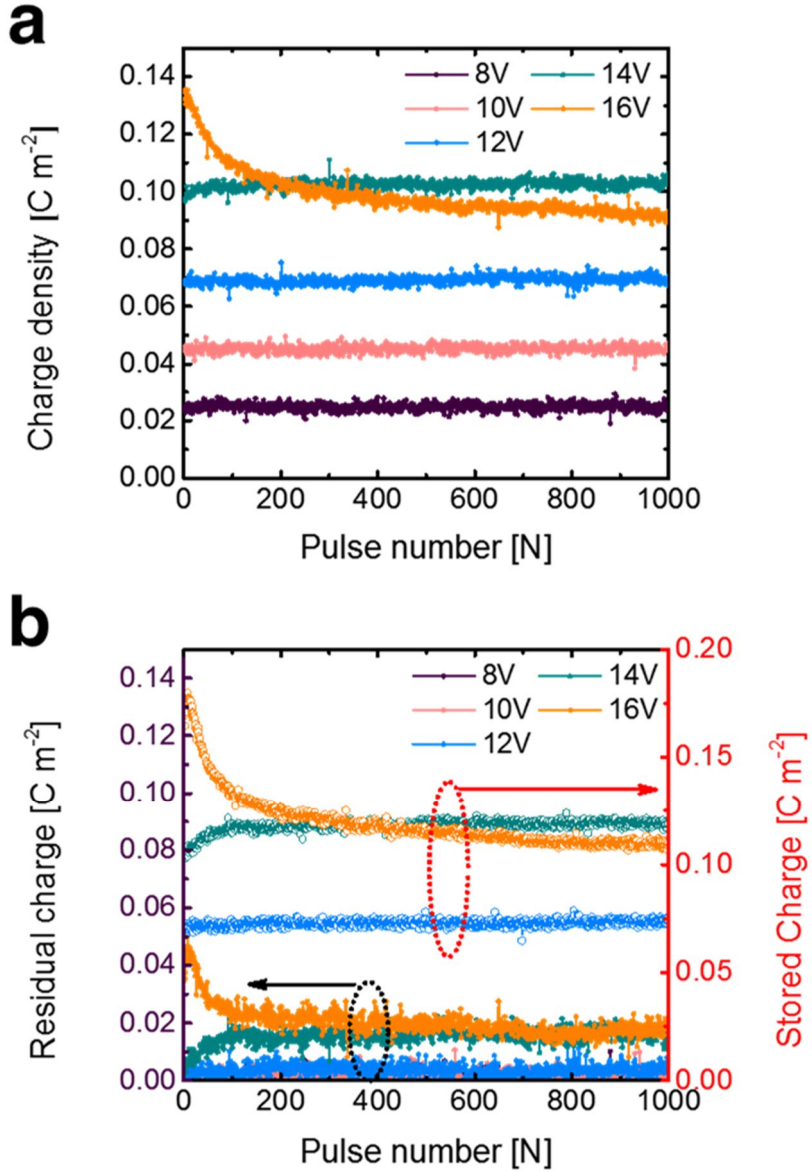
Figure 5.19 (a) Released charge density, (b) residual charge density (left vertical axis), and stored charge density (right vertical axis) of the 8-nm-thick AO/BTO capacitor as a function of the pulse numbers with the pulse voltage as a parameter.
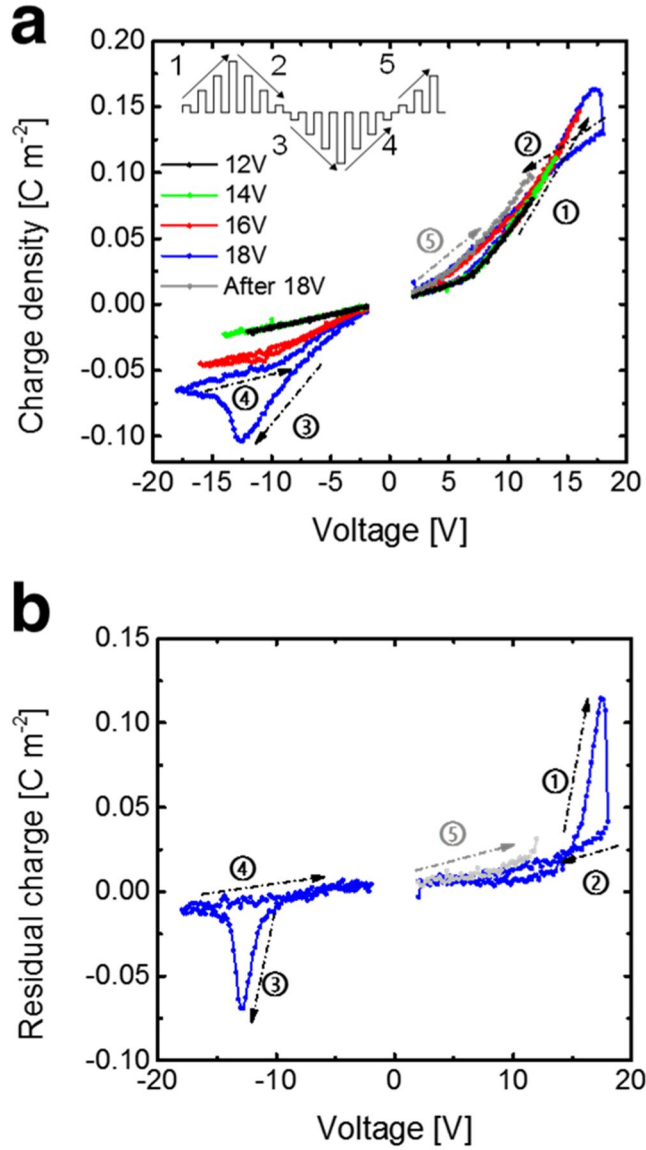
Figure 5.20. (a) Released charge density of the 8-nm-thick AO/BTO capacitor measured using a stepwise increasing and decreasing pulse train, as shown the inset figure with various pulse voltages. (b) Residual charge density of the 8-nm-thick AO/BTO capacitor from the stepwise pulse train with a ±18 V pulse voltage

5.4. Summary

In summary, the conditions for the emergence of genuine NC effects or hysteretic P-V behaviors in the AO/BTO capacitors were examined through a time-varying pulse switching method. While the NC effects in the AO/BTO capacitor have been theoretically expected, a direct proof has hardly been obtained due to the lack of a precise understanding of the influence of the measurement method on the subtle effect.[20] In this study, a nanosecond-scale pulse charging system was adopted, and the capacitance boosting from the AO/BTO capacitors compared with the single-layer AO film was directly observed. This is a direct support for the NC operation of the FE BTO layer in the DE/FE bi-layer structure. The measured NC effects were well consistent with the theoretical model based on the fundamental LD theory, but the charge injection, mainly driven by the leakage of the DE layer, diminished the NC effects and induced the hysteretic behavior during the capacitor charging/discharging. For this reason, the NC effect in the DE/FE structure exhibited time dependency, which can be explained by the leakage current of the DE layer. These competitive dynamics between the NC effects and the hysteresis in the AO/BTO capacitor can be extended to understand the hysteric behavior in the NCFET device. The time scale of transfer characteristic measurement in the previous NCFET studies[14,15] is comparable to that of the AC capacitance measurement in this study. Hence, it is evident that hysteresis was observed in the transfer curve of the NCFET

due to the gate leakage in the base MOSFET device. Especially in the previous work by Jo et al.,[14] the oscilloscope channel, which is located between the FE capacitor and the MOSFET gate for monitoring the internal voltage, could also work as an additional source of charge injection into the intervening metal layer, which can fluently stabilize the switched polarization. The nanosecond NC effects in the FE/DE bi-layer with such short electric pulses are beneficial for applications such as the capacitive layer of dynamic random access memory (DRAM), for which a high operation speed is beneficial whereas non-volatility is not required.[33] It should be noted that the capacitor area that was used in this study was in the order of $\sim 10^3$ μm^2, and that the electric pulse length required to charge/discharge a capacitor should linearly decrease with the decreasing capacitor area. For the actual DRAM capacitor with an effective capacitor area of ~ 1 μm^2, therefore, the estimated charging time should be <1 ns. It is believed that this study shed light on a new methodology that can store a high charge in a limited capacitor area by effectively preventing the injection of carriers that can frustrate the NC effect.

5.5. Bibliography

1. C. S. Hwang, *Adv. Electron. Mater.* **1**, 1400056 (2015).

2. S. K. Kim, S. W. Lee, J. H. Han, B. Lee, S. Han and C. S. Hwang, *Adv. Funct. Mater.* **20**, 2989-3003 (2010).

3. S. Salahuddin and S. Datta, *Nano Lett.* **8**, 405-410 (2008).

4. A. I. Khan, K. Chatterjee, B. Wang, S. Drapcho, L. You, C. Serrao, S. R. Bakaul, R. Ramesh and S. Salahuddin, *Nat. Mater.* **14**, 182-186 (2015).

5. S. Kasamatsu, S. Watanabe, C. S. Hwang and S. Han, *Adv. Mater.* **28**, 335-340 (2016).

6. A. I. Khan, D. Bhowmik, P Yu, S. J. Kim, X. Pan, R. Ramesh, S. Salahuddin, *Appl. Phys. Lett.* **99**, 113501 (2011).

7. W. Gao, A. I. Khan, X. Marti, C. Nelson, C. Serrao, J. Ravichandran, R. Ramesh and S. Salahuddin, *Nano Lett.* **14**, 5814-5819 (2014).

8. D. J. R. Appleby, N. K. Ponon, K. S. K. Kwa, B. Zou, P. K. Petrov, T. Wang, N. M. Alford and A. O'Neill, *Nano Lett.* **14**, 3864-3868 (2014).

9. V. V. Zhirnov and R. K. Cavin, *Nat. Nano.* **3**, 77-78 (2008).

10. W. Shu-Yau, *IEEE Trans. Elect. Dev.* **21**, 499-504 (1974).

11. M. Bibes, *Nat. Mater.* **11**, 354-357 (2012).

12. J. W. Reiner, A. M. Kolpak, Y. Segal, K. F. Garrity, S. Ismail-Beigi, C. H. Ahn and F. J. Walker, *Adv. Mater.* **22**, 2919-2938 (2010).

13. C. Dubourdieu, J. Bruley, T. M. Arruda, A. Posadas, J. Jordan-Sweet, M. M. Frank, E. Cartier, D. J. Frank, S. V. Kalinin, A. A. Demkov and V. Narayanan, *Nat. Nano.* **8**, 748-754 (2013).

14. J. Jo, W. Y. Choi, J. –D. Park, J. W. Shim, H. -Y. Yu and C. Shin, *Nano Lett.* **15**, 4553-4556 (2015).

15. A. I. Khan, K. Chatterjee, J. P. Duarte, Z. Lu, A. Sachid, S. Khandelwal, R. Ramesh, C. Hu and S. Salahuddin, *IEEE Elect. Dev. Lett.* **37**, 111-114 (2016).

16. S. J. Song, Y. J. Kim, M. H. Park, Y. H. Lee, H. J. Kim, T. Moon, K. D. Kim, J. -H. Choi, Z. Chen, A. Jiang and C. S. Hwang, *Sci. Rep.* **6**, 20825 (2016).

17. A. Cano and D. Jiménez, *Appl. Phys. Lett.* **97**, 133509 (2010).

18. A. M. Bratkovsky and A. P. Levanyuk, *Appl. Phys. Lett.* **89**, 253108 (2006).

19. Y. J. Kim, M. H. Park, W. Jeon, H. J. Kim, T. Moon, Y. H. Lee, K. D. Kim, S. D. Hyun and C. S. Hwang, *J. Appl. Phys.* **118**, 224105 (2015).

20. Y. J. Kim, M. H. Park, Y. H. Lee, H. J. Kim, W. Jeon, T. Moon, K. D. Kim, D. S. Jeong, H. Yamada and C. S. Hwang, *Sci. Rep.* **6**, 19039 (2016).

21. A. Q. Jiang, H. J. Lee, G. H. Kim and C. S. Hwang, *Adv. Mater.* **21**, 2870-2875 (2009).

22. D. Lee, A. Yoon, S. Y. Jang, J. G. Yoon, J. S. Chung, M. Kim, J. F. Scott and T. W. Noh, *Phys. Rev. Lett.* **107**, 057602 (2011).

23. H. Lee, T. H. Kim, J. J. Patzner, H. Lu, J. -W. Lee, H. Zhou, W. Chang, M. K. Mahanthappa, E. Y. Tsymbal, A. Gruverman and C. -B. Eom, *Nano Lett.* **Article ASAP,** DOI:10.1021/acs.nanolett.5b05188 (2016).

24. X. Ren, *Nat. Mater.* **3**, 91-94 (2004).

25. K. J. Choi, M. Biegalski, Y. L. Li, A. Sharan, J. Schubert, R. Uecker, P. Reiche, Y. B. Chen, X. Q. Pan, V. Gopalan, L. -Q. Chen, D. G. Schlom and C. B. Eom, *Science* **306**, 1005-1009 (2004).

26. X. Lu, H. Li and W. J. Cao, *Appl. Phys.* **114**, 224106 (2013).

27. T. Yamada, *J. Appl. Phys.* **43**, 328-338 (1972).

28. A. Q. Jiang, X. J. Meng, D. W. Zhang, M. H. Park, S. Yoo, Y. J. Kim, J. F. Scott and C. S. Hwang, *Sci. Rep.* **5**, 14618 (2015).

29. T. H. Kim, S. H. Baek, S. M. Yang, Y. S. Kim, B. C. Jeon, D. Lee, J. -S. Chung, C. -B. Eom, J. -G. Yoon and T. W. Noh, *Appl. Phys. Lett.* **99**, 012905 (2011).

30. Y. A. Genenko and D. C. Lupascu, *Phys. Rev. B* **75**, 184107 (2007).

31. C. M. Folkman, S. H. Baek, C. T. Nelson, H. W. Jang, T. Tybell, X. Q. Pan, and C. B. Eom, *Appl. Phys. Lett.* **96**, 052903 (2010).

32. S. -H. Kim, D. -J. Kim, J. Hong, S. K. Streiffer and A. I. Kingon, *J. Mater. Res.* **14**, 1371-1377 (1999).

33. J. A. Mandelman, R. H. Dennard, G. B. Bronner, J. K. DeBrosse, R. Divakaruni, Y. Li and C. J. Radens, *IBM J. Res. Dev.* **46**, 187-212 (2002).

6. Conclusion

Enhancement of capacitance by negative capacitance (NC) effect in a dielectric/ferroelectric (DE/FE) stacked film is gaining a greater interest as a feasible solution to miniaturize capacitors and field effect transistors for future semiconductor devices. Since its model was first suggested, several experimental proofs on the capacitance boost of DE/FE stacked films were reported. However, the previously reported theoretical background of this intriguing effect holds a self-contradictory problem. Therefore, this work suggests an alternative model to describe the negative capacitance effect in a DE/FE system quantitatively. This work adopted a modified formalism to incorporate the depolarization effect to describe the energy of the general DE/FE system. The model predicted that the $Al_2O_3/BaTiO_3$ (AO/BTO) system shows the capacitance boost effect with no FE-like hysteresis behavior. However, the involvement of the trapped charges at the DE/FE interface, originating from the very high field across the thin AO layer when the BTO layer played a role as the NC layer, can frustrate, the NC effect in the AO/BTO system. Under this circumstance, the highly stored charge by the NC effect of the BTO during the charging period could not be retrieved during the discharging process because integral part of the polarization charge was retained within the system as a remanent polarization.

Next, the polarization switching behavior of AO/Pb(Zr,Ti)O$_3$ (PZT) bi-layer capacitors had been studied by comparing the experimental results and theoretical model. From the theory, the paraelectric-like NC state was expected above 3nm thick AO layer in AO/150nm-PZT bi-layer system. However, the experimental results clearly showed the FE hysteresis without any sign of NC effects. This result emerged from the tunnel switch behavior of AO layer. which means that the charge exchange occurred between the electrode and AO/PZT interface trap sites by FN tunneling through thin AO layer during domain switching in PZT layer. And the detailed mechanism of tunnel switch operation was identified by the potential distribution analysis in bi-layer structure based on the modified NC theory. This interface trapping is relevant for hysterical polarization switching and the disappearance of NC effects in AO/PZT system. Nonetheless, if the charge trapping is perfectly eliminated in DE/FE system, a stable NC operation could be obtained.

However, suppressing the charge tunneling is quite difficult because the field across the thin dielectric layer must be extremely high when the ferroelectric layer is under the NC state. For a general measurement condition, the time span is long enough to induce the sufficient charge tunneling, and the tunnel switching can occur mostly in DE/FE systems. This in turn implies that if the measurements can be performed within a time regime much shorter than the time for the sufficient charge tunneling, the genuine NC effect without being

interfered by the accompanying FE hysteresis effect might be observed. In this work, therefore, the short pulse-type measurements were systematically performed for the AO/BTO capacitor. From theses experiment, it was clearly demonstrated that the reversibly drivable charge of the AO/BTO bilayer was enhanced compared with that of the AO single layer over a wide voltage region. This is a direct demonstration of the NC effect from the ferroelectric layer, and the result was quantitatively matched with the theoretical expectation. And, it is believed that this study shed light on the new methodology which can store high charge in a limited capacitor area.

Abstract (in Korean)

커패시터는 대다수의 전자 소자의 중요 구성 요소로서, 높은 커패시턴스가 필수적으로 요구되고 있다. 이러한 높은 정전 용량을 얻기 위해서, 커패시터의 면적을 키우거나, 커패시터의 유전막의 두께를 줄이거나, 고유전율을 가지는 물질을 커패시터 유전체로 이용하는 것이 일반적인 방법으로 통용되고 있다. 하지만, 소자의 미세화가 진행 됨에 따라 기존의 방법으로 차세대 소자에서 요구되는 커패시턴스를 확보하는 데에 있어서 어려움에 직면하고 있다. 따라서, 차세대 소자에 적합한 고커패시턴스를 가지는 커패시터의 개발에 있어서, 기존의 틀을 벗어난 근본적으로 새로운 접근방법이 요구되고 있다.

이에, 강유전체에서 보이는 음의 커패시턴스 (NC) 현상이 고커패시턴스 커패시터 소자 개발 난제를 해결할 수 있다는 가능성이 제시되었다. 하지만 강유전체의 NC 현상은 오로지 강유전체가 불안정한 에너지 상태를 가지는 지점에서 관찰된다는 점으로 일반적인 조건 하에서는 NC현상을 응용할 수 없다는 제약을 가지고 있다. 최근 연구들에서, 강유전체와 상유전체를 직접적으로 적층한 구조에서 두 층 사이의 charge coupling에 의해 강유전체의 NC 영역이 안정화 된다는 결과를 보고하였고, 실험적으로 특수한 상유전체/강유전체 이종 에피택셜 구조에서 NC 현상이 안정적으로 발현되는 것을 증명하였다. 지금까지의 NC에 대한 이론적인

연구에서는, 강유전체/상유전체 적층 구조에서 보이는 NC 현상을 강유전체의 자유에너지를 표현하는 Landau-Khalatnikov (LK) 식을 이용하여, 각층의 에너지를 선형적으로 합한 상태를 바탕으로 구성하여 왔다. 하지만 이러한 이론적인 모델은 실제 NC 현상을 대변하기에는 여러가지 문제가 존재하였다. 또한, 실험적으로는 특수한 구조의 적층 박막에서만 NC 현상이 발견되며, 일반적인 상유전체/강유전체 적층 박막에서의 NC 현상은 보고된 적이 없다.

따라서, 본 연구에서는 강유전체/상유전체 적층구조에서 보이는 NC현상을 강유전체의 depolarization 이론을 적용하여 기존 이론적 모델의 오류를 개선한 새로운 이론적 모델을 제안하였다. 새로운 모델은 Landau-Devonshire (LD) 이론으로부터 강유전체 층의 분극이 상유전체 층에 의해 불완전하게 보상되는 상황일 때 강유전체의 에너지 상태를 수식적으로 유도하였다. 이렇게 상유전체층에 의해 분극의 전하량이 완전히 상쇄가 되지 않는 불완전한 보상 상황에서 강유전체 층으로 depolarization 전계가 발생하여 강유전체가 강유전성을 잃어버리며, NC영역으로 안정화 되며, 이와 반대되는 전계가 상유전체 층에도 인가되는 것을 확인 하였다. 이런 상황에서는 외부 전계에 대해서 상유전체 층의 전계가 더 크게 걸리는 전압 증폭 현상이 발생하는 것을 알 수 있었으며, 결론적으로 전체 구조의 커패시턴스가 단일 층의 커패시턴스보다 커지는 현상이 관측될 것이라 예상된다.

164

본 이론은 또한 일반적인 강유전체/상유전체 적층구조에서 NC 현상이 저해 받는 요인에 대해서도 분석을 진행하였다. NC 동작 시 전압 증폭 현상에 의해 상유전체 층의 막대한 전계가 걸리게 되고 상유전체 층을 통하여 강유전체/상유전체 계면으로 전하가 주입되는 상황이 발생하게 된다. 이렇게 주입된 전하는 강유전체 분극을 보상하게 되고 depolarization 전계 및 상유전체 전계를 감소시켜 결론적으로 NC현상을 억제하게 된다.

다음으로, Al_2O_3/$Pb(Zr,Ti)O_3$ (AO/PZT) 커패시터의 분극-전압 특성을 이론적 NC 모델을 이용하여 분석을 진행하였다. 실험에 사용한 AO 박막의 두께는 2 에서 10nm 로 변화 시켰고, PZT 층의 두께는 150nm 로 고정하였다. 열역학적 NC 모델에 따르면, 3nm 두께에서 AO/PZT 구조가 강유전체와 유사한 에너지에서 상유전체와 유사한 에너지로 전이 되는 것을 확인 하였다. 이러한 상유전체와 유사한 에너지 상태에서는 시스템의 변화 없이는 강유전체처럼 영구적인 분극 변화가 발생할 수 없으며, NC 현상이 나타나게 된다. 하지만 실제 실험 결과에서는 극명한 분극 이력 곡선이 관측 되었고, 이는 AO층의 막대한 전계에 의해 AO/PZT 계면의 전자가 주입되기 때문으로 밝혀졌다.

따라서, 이러한 전자 주입을 막고 직접적인 NC현상 관측을 위해서 나노초의 펄스를 이용하여 커패시터를 충전하는 방법을 통해 NC 현상을 분석하였다. 전자 주입은 상유전체를 통해서

흐르는 누설전류를 통해 이루어 진다. 따라서, 기존의 측정 방식은 수 밀리 초에서 수초로 매우 길기 때문에 이러한 누설전류에 의한 계면 전하 주입이 많을 수 밖에 없어 NC 현상을 관측하기 힘들게 된다. 반면 측정 시간을 극단적으로 줄이게 되면, 전하 주입을 획기적으로 줄일 수 있기 때문에 나노초의 펄스를 이용한 측정에서 NC 현상을 직접적으로 관찰할 가능성을 제기 되었다. 실제 $Al_2O_3/BaTiO_3$ (AO/BTO) 커패시터에서 펄스로 충전하였을 때 특정 전압 상황에서 전체 구조의 커패시턴스가 AO 단일층의 커패시턴스에 비해 커지는 NC현상에서 비롯된 커패시턴스 증폭 현상이 관측 되었다. 또한 펄스 시간이 길어짐에 따라 높은 전압에서 커패시턴스 증폭 현상이 점차 사라지는 결과를 얻었다. 이 결과는 일반적인 강유전체/상유전체 구조에서 안정적인 NC 구동은 특정 조건하에서만 가능하다는 것을 의미한다. 물론, 정적인 상황에서의 NC 현상의 응용은 제약이 있지만, 빠른 속도로 동작하는 소자로 적용에 있어서는 여전히 NC현상이 유용할 것이라 전망 된다.

주요어: 음의 커패시턴스 (정전용량), 커패시턴스 증가, 전압 증폭, 강유전체, 분극, 탈분극, 전자 주입, 터널링

학번: 2012-31277

김 유 진